Modeling, simulation and analysis of mechanochemical patterns in active tissues

Submitted in partial fulfillment of the requirements

of the degree of

Doctor of Philosophy

by

Supriya Bajpai

Supervisors:

Dr. Mandar M. Inamdar (IIT Bombay)

Dr. Raghunath Chelakkot (IIT Bombay)

Dr. Prabhakar Ranganathan (Monash University)

INDIAN INSTITUTE OF TECHNOLOGY BOMBAY, INDIA

and

MONASH UNIVERSITY, AUSTRALIA

The course of this study for this award was developed jointly by Monash University, Australia and Indian Institute of Technology Bombay, India and was given academic recognition by each of them. The programme was administrated by The IITB-Monash Research Academy

2021

Copyright notice

Acknowledgements

I wish to record a deep sense of gratitude to my supervisor Dr. Mandar M. Inamdar, Dr. Prabhakar Ranganathan and Dr. Raghunath Chelakkot for his valuable guidance and constant support at all stages of my Ph.D study and related research. I am greatly indebted to my supervisors for all the time and energy that they have patiently spent to teach me the fundamentals of computational biology, physics, mechanics and analytical tools and techniques that have been helpful for carrying out this work. I thank IITB-Monash Research Academy for financial support and computing facilities at MonARCH cluster, Monash University. My sincere thanks to my parents and husband who helped me in completing this work.

Abstract

A key challenge in biology is to understand how spatiotemporal patterns and structures arise during the development of an organism. An initial aggregate of spatially uniform cells develops and forms the differentiated structures of a fully developed organism. On the one hand, contact-dependent cell-cell signaling is responsible for generating a large number of complex, self-organized, spatial patterns in the distribution of the signaling molecules. On the other hand, the motility of cells coupled with their polarity can independently lead to collective motion patterns that depend on mechanical parameters influencing tissue deformation, such as cellular elasticity, cell-cell adhesion and active forces generated by actin and myosin dynamics. Moreover, it is getting increasingly clear that the spatiotemporal patterns of cell shape and size in the tissues, for example, in cancerous and sensory epithelium, are also governed by feedback between chemical signaling and cell mechanics. However, a clear quantitative picture of how these two aspects of tissue dynamics, i.e., signaling and mechanics, lead to pattern and form is still emerging.

Although modeling efforts have, thus far, treated cell motility and mechanics and cell-cell signaling separately, experiments in recent years suggest that these processes could be tightly coupled. Hence, in the present thesis, we first study how the dynamics of cell polarity and migration influence the spatiotemporal patterning of signaling molecules such as Delta and Notch. These signaling interactions can occur only between cells that are in physical contact, either directly at the junctions of adjacent cells or through cellular protrusional contacts. We present a vertex model which accounts for contact-dependent signaling between adjacent cells and between non-adjacent neighbors through long protrusional contacts that occur along the orientation of cell polarization. We observe a rich variety of spatiotemporal patterns of signaling molecules that are influenced by polarity dynamics of the cells, relative strengths of adjacent and non-adjacent signaling interactions, range of polarized interaction, signaling activation threshold, relative time scales of signaling and polarity orientation, and cell motility. We then extend this vertex model framework to include a simple feedback mechanism between cell-cell adhesion and the expression of signaling molecules in cells. We use this model to explore the origin and diverse manifestation of chemical and cell morphological patterns in the tissues. We systematically quantify different aspects of resulting cellular morphologies as a function of

the coupling parameters between Delta-Notch signaling and cell-cell adhesion. Overall, by using a basic vertex model connected to simple chemical reactions, we show that even elementary coupling between chemical signaling and cell mechanics can give rise to a wide variety of hitherto unexplored mechanochemical patterns in epithelial tissues. Though we focus on Delta-Notch signaling in the current work, our framework can easily be extended to explore the mechanochemistry of other contact-based signaling pathways.

Contents

List of Figures

Chapter 1

Introduction

How the cells of a multicellular organism create chemical and mechanical developmental patterns during morphogenesis by modifying and adjusting their shape, size, polarity, migration, signaling, differentiation potential, proliferation, and death is an open question [54, 111]. Morphogenesis involves complex mechanochemical processes that bring diverse cell populations together to build complex structures such as heart, lungs, and limbs [52, 94]. Starting from a simple homogeneous monolayer of cells or an aggregate of homogeneous mesenchymal stem cells, different organs develop their shape and size by controlling the spatial distribution of cells during embryonic development [111, 117].

Understanding tissue morphogenesis requires the integration of various processes across different scales. These range from the processes that take place at an intracellular level involving genes and protein (signaling) networks and mechanical components, such as molecular motors, to the processes at the extracellular level in which cells respond to signaling cues [54]. On the one hand, signaling proteins/molecules interact within the same cell, with different cells, or with the extracellular matrix to form chemical patterns in the tissues, thus forming the chemical basis of morphogenesis. These signaling proteins interact to form complex signaling networks or pathways and direct the embryonic cells to their final fate or cell type in order to establish their future identity. On the other hand, mechanical forces cause changes in cell size, shape, movement and death of cells and form the mechanical basis of morphogenesis [20, 42, 188]. The integration of these two categories of processes result in large-scale deformation, shape changes, and chemical patterning in the tissues.

1.1 Chemical basis of morphogenesis

Four basic types of signaling pathways are reported in multicellular organisms that plays central role in controlling all the development activities during organism development: juxtracrine (signaling by direct contact) [216], autocrine signaling [127, 223], paracrine signaling [233] and endocrine signaling [49]. The signaling pathways are composed of a large number of molecules/proteins that interact with various other signaling pathways to form complex signaling networks [21]. Many receptors and signal-transducers interact and integrate to form signaling networks that regulate biochemical signaling within and between the cells that governs the cell fate determination and information flow in the tissue [30]. To establish the intra-cellular and inter-cellular communication and to transfer the information of extra-cellular matrix to the cell nucleus, multiple signaling pathways have been reported in various multicellular organisms [14, 132]. Fgf [119], Hedgehog [212], Wnt [144], TGF-β [142] and Delta-Notch [103] are the few examples of signaling pathways and signaling molecules that are responsible for cell communication.

Delta-Notch signaling pathway is one of the most important among signaling pathways (Figure 1.1). This pathway is considered ideal for mediating precise patterning signals, as the Notch receptor and Delta ligand both are trans-membrane and act as a switch to toggle cell fates on or off [179]. Notch signaling is a conserved signaling pathway that is central to the development, morphogenesis, and differentiation process in organisms and is present in almost all animals [30, 116]. The disruption of Notch signaling result in several cancers such as leukemia [268], pancreatic cancer [173, 274], lung cancer [83, 84], skin cancer [163, 184] as well as developmental defects [34, 166],and diabetes [3]. Notch signaling also acts as both a tumor suppressor and tumor-promoting factor in several types of cancers such as lung cancer, lymphoid neoplasm, breast cancer, skin cancer and colorectal cancer [186]. An in-depth understanding of Delta-Notch signaling is thus required to understand the development process and cancer pathogenesis. It can be further applied to understand targeted cellular differentiation into desired cell types [132].

Notch and its ligand family DSL (Delta, Serrate, LAG-2) are trans-membrane proteins [63]. For signaling to take place, the cells expressing the ligands must be in contact with the Notch expressing cell. Notch signaling pathway depends on the contact between

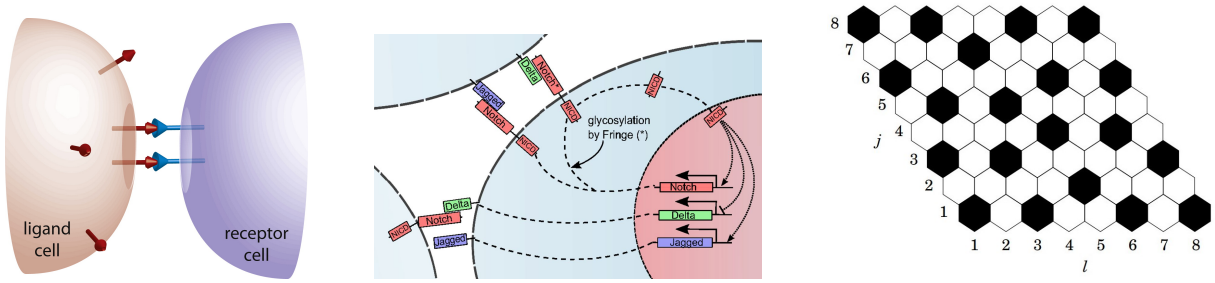

(a) (b) (c)

Figure 1.1: (a) Schematic of a juxtacrine signaling system. Receptors of one cell (blue cell) interact with ligands on the membrane of a neighboring cell (red cell). Ligands are present on the membrane surface of the ligand cell and interact with receptors that reside at the contact area between the cells. The figure is taken from Yaron *et al.* [272]. (b) Schematic of the intracellular and intercellular Delta-Notch signaling pathway. Notch, the trans-membrane receptor of one cell, binds to Delta, the trans-membrane ligands belonging to the neighboring cell. This interaction cleaves the Notch receptor to release the intracellular Notch domain. The intracellular Notch domain migrates to the nucleus and regulates the transcription of many genes. This regulation leads to the activation of Notch and Jagged and inhibition of Delta. The figure is taken from Boareto *et al.* [28]. (c) Figure showing the steady-state checkerboard pattern of primary and secondary fates in a monolayer of hexagonal cells, generated through lateral inhibition mechanism. Black colour shows the cells with primary fate, and white cells show the secondary fate. The figure is taken from Collier *et al.* [47]

two neighboring cells or non-neigbouring cells and does not require any other mediator to transmit the signal. After a ligand present on the surface of one cell is linked to the receptor present on the membrane of the other cell, the intracellular domain of the receptor is cleaved off and it reaches the nucleus where it directly regulates gene expression [129]. However, a complex regulation mechanism is required to secure the wide range of events driven by Notch signaling.

The Delta-Notch kinetics have previously been modeled in a number of ways. The cellular contacts during signaling could either be local and between the nearest neighbors [1, 104, 121] or they could be long-ranged and mediated by protrusions such as filopodia [44, 65, 182, 210, 212]. Protrusion-based signaling through Notch pathway is quite common during morphogenesis [44, 182]. Similar long-ranged signaling is also seen, for example, in Sonic hedgehog pathway (Shh) during limb patterning in vertebrates [212].

The short-range signaling via lateral inhibition, in which the immediate neighbouring cells in a tissue attain a different fate results in a self-organised checker-board pattern [47]. More complex patterns such as bristle patterns in *Drosophila notum* and stripe patterns in zebrafish can be produced by protrusion-mediated long-range signaling with protrusion directionality and signaling efficiency [99, 255]. Moreover, the patterning dynamics can be sped up by the inclusion of the mutual inactivation of Delta-Notch along with the dynamics of lateral inhibition [226, 227].

1.2 Mechanical basis of morphogenesis

Cell mechanics and motility forms the mechanical basis of morphogenesis that governs cell geometry, morphology and overall tissue dynamics. During morphogenesis, the cells in the tissue actively migrate and rearrange themselves to ensure the formation of proper shape and size of the organs [151]. This behaviour is regulated by the cell elastic and active forces and the coupling between neighbouring cells [22, 70]. In tissues, the cells are mechanically coupled to their neighbouring cells via adhesion molecules along the cell membranes, and exert forces on each other and their environment [4]. These interactions are complex and lead to morphogenetic deformations of tissues during development, and are crucial in setting up the shape of the organism. The actin cytoskeleton is responsible for generating

surface and line tensions that act along the cell membranes, and are balanced by cell–cell adhesion and cell–extracellular matrix adhesion. The actin cytoskeleton, which is a network of polar, semiflexible protein filaments is essential for driving cell motility [25]. The main forces that govern cell motility are the internal forces caused by the cytoskeleton (mainly actin, myosin, and adhesion molecules) and the subcellular structures (lamellipodia and filopodia). As the cells in the tissue are connected to each other via adherens junctions that are composed of mainly cadherins and contractile actin-myosin, the collective effect of the motility of each cell leads to collective cell migration [10, 75, 225]. The cells also have polarity, i.e., a differentiation between top-bottom or front-rear, and show polarized behaviour. Depending on the type of front-rear polarity dynamics, the cells can have different types of motility behavior. Cells can either exhibit random walk or can move in an aligned manner depending upon the polarity dynamics. Cell polarity and thus motility can be governed by biochemical signals or signaling pathways.

The law of mechanics are essential to understand the physics of morphogenesis [270] since the forces acting in the tissue that cause deformation must be balanced. Since the inertial forces in tissues are much smaller as compared to the friction forces, internal and external forces acting on the tissue are effectively balanced by viscous or friction forces [23]. A tissue deforms due to the internal forces (that is generated from various activities within the cell) and external forces act on the tissue either from the surrounding tissues or from external forces such as fluid flows and gravitation. As a result, cells deform and topological rearrangements of the bonds that joins the cells takes place.

A large number discrete cell-based models have been used to provide insight into cellular processes within epithelia, including cell motility, adhesion, and mitosis, among many developmental processes [26, 73]. Some of the commonly used models are fixed lattice cellular automata [67], cellular Potts model [91], off-lattice centre dynamics [213, 252] and vertex dynamics models [8, 70]. To model the sub-cellular complex interactions, there is a requirement of a discrete cell population model that can incorporate motion of the cells via governing equations of motion and cell-cell interactions due to intercellular signalling and mechanical adhesion, and is relatively difficult to incorporate in continuum models due to the essential discrete nature of the problem. To be physically realistic, such models also have the control mechanisms for cell shape and cell volume. Vertex model (VM) given by Honda and Eguchi [114] and further modified by Farhadifar et

al. [70] have the ability to incorporate all these cellular activities with conceptual and implementation ease. The vertex models can also be modified to incorporate new cell properties, cell birth, cell death, cell rearrangement processes, cell-cell signaling processes, mechanical or chemical feedback and are also suited to the modelling of differential cell-cell adhesion [73, 74]. In vertex dynamics model, each cell is modelled as a polygon (or polyhedron in three dimensions), having vertices and edges. The boundaries of polygon represent the cell's membrane. The effective mechanical force is experienced by the cell vertex and is given by the gradient of a work function with respect to its position. In the basic vertex model, the combined forces on any of the cell vertex are due to cell area elasticity, actin-myosin bundles (cell perimeter contractility) and adhesion molecules (line tension) [70]. In addition to these forces cells also exhibit polarized motility.

1.3 Mechanochemical basis of morphogenesis

Biochemical patterning as well as mechanical processes work in coordination to shape cells and tissues [30]. Besides biochemical signaling, cell and tissue mechanics is crucial to understand many outstanding questions in morphology, for example how gastrulation happens and how different organs are shaped and sized [42, 188]. The mechanochemical approach is a natural extension of the ideas suggested originally by Turing [117].

Coupling between collective cell migration, cell mechanics, and cell-cell signaling is observed in many biological processes such as wound healing, cancer metastasis, branching morphogenesis and embryonic development [41, 85, 134]. This coupling is also observed in the case of Delta-Notch signaling. For example, in endothelial cells exhibiting Delta-Notch kinetics, the expression of Dll4 (Delta) is significantly enhanced at the tips of the migrating epithelium during angiogenesis [206]. Evidence suggests that Notch is involved in controlling cell-cell adhesion in *Drosophila* eye cells [16]. Notch signaling is linked to the adhesion force between cells expressing Notch receptors and Delta ligand [2]. Also, Delta increase is associated with the motility and spreading of individual keratinocytes [41] and stimulated lamellipodia formation [145]. Furthermore, Delta-induced activation of Notch is linked with the application of mechanical force [89, 169]. Thus there are good indications that spatiotemporal chemical patterns of molecules due to contact-based signaling are

associated with cell-cell signaling kinetics, tissue mechanics, cell polarisation dynamics, and cell motility.

The chemical patterns due to contact-based signaling are interpreted using models generally with a simplifying assumption that the tissue morphology is fixed and does not alter during the patterning process [44, 47, 99, 226, 227]. This assumption may not always be correct since cell migration and cell division can dynamically modify the connectivity among cells. Hence, in order to maintain a regular pattern, the signaling pathway requires some feedback mechanisms to coordinate with cell migration and dynamic tissue topology. For example, it is known that FGF and Notch signaling pathways play a crucial role in cell fate decisions and cell migration during gastrulation in *Xenopus* [119]. During somitogenesis in zebrafish (Figure 1.2), it is observed that Delta-Notch signaling is accompanied by cellular movements in the course of segmentation clock generation [113, 141]. Similarly, it is reported that somitogenesis in chick embryos involves a complex interplay of individual cell movements and dynamic cell rearrangements [161]. Such large scale cellular movements and rearrangements of different types of cells are also observed during germ-layer formation in zebrafish [217, 264]. Computational studies show that cell migration plays a vital role in Delta-Notch patterning in zebrafish [249, 251]. Canonical Notch signaling is known to increase cell-cell adhesion by inducing the expression and activation of cell adhesion molecules such as integrins [109, 176, 214]. Notch also controls cell-cell adhesion in *Drosophila* eye cell [16]. A number of studies suggest that Delta-Notch expression levels in cells is coupled to the adhesion molecules and thus adhesion forces [2, 71, 266]. During the feather branching of chicks, periodic activation of Notch signaling drives the differential cell adhesion and coordinated adjustment of cell shape and adhesion orchestrates feather branching, which is regulated by Notch signaling [40].

It has been observed that healthy tissues typically consist of cells of the same type resulting in overall homogeneity in their shape and size [87, 199] (Figure 1.3a). In contrast, diseased cells and tumor cells are pleomorphic, exhibiting large variations in shape and size within the same tissue [60, 87, 202] (Figure 1.3b). Thus, cell size heterogeneity can indicate underlying pathology [87]. Various types of sensory epithelia also exhibit heterogeneity both in their cell morphology and in their spatial pattern [242]. For example, the olfactory epithelium (OE), which is located inside the nasal cavity of mammals, is responsible for odor perception. It is characterized by alternating mosaic patterns formed by smaller

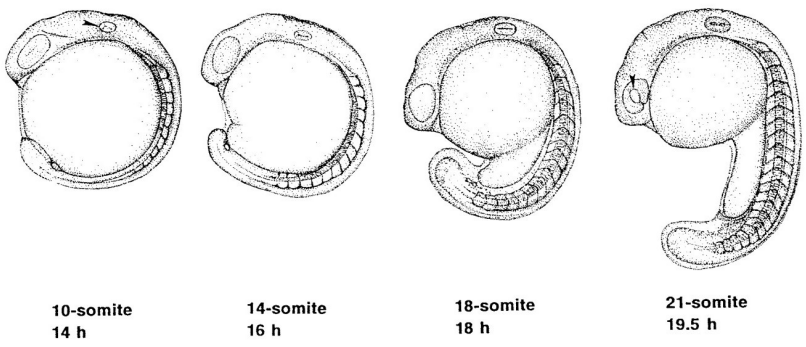

Figure 1.2: Sketches showing the development stages of the zebrafish embryo and formation of somites. Somites are paired blocks of mesoderm that form along the head-to-tail axis in vertebrates during the embryonic stage of somitogenesis. The figure is taken from Kimmel *et al.* [126].

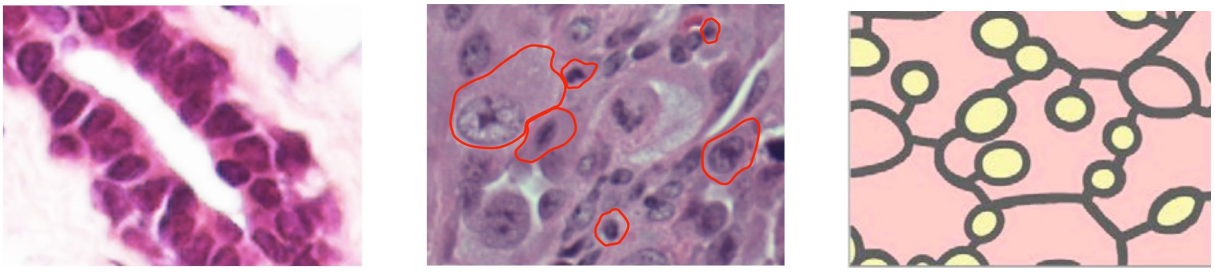

(a) (b) (c)

Figure 1.3: (a) The figure shows the uniform cell size in healthy mouse mammary epithelium. The uniformity in cell size is characteristic of epithelial tissues. The figure is taken from Ginzberg *et al.* [87]. (b) The figure shows a pleomorphic mammary tumor that exhibits a large variation in cell size. The cell size heterogeneity visually characterizes a pleomorphic tumor. It is shown by outlining (red) the borders of cells of varying sizes. The figure is taken from Ginzberg *et al.* [87]. (c) Cellular rearrangements in the developing mouse olfactory epithelium. Schematic showing larger size supporting cells (pink) surrounding smaller size olfactory cells (yellow). The figure is taken from Katsunuma *et al.* [124].

olfactory cells separated by the adjacent larger sensory supporting cells [51, 232, 242] (Figure 1.3c). Such mosaic patterns are also observed in the auditory epithelium [243, 244] that is found in the ear canal. Differential cell adhesions, mediated by integrins and cadherins/catenins, play a critical role in dictating cell morphology [243, 244]. Expression and modification of these adhesion molecules are linked with cell growth, intercellular signaling, cell differentiation, and apoptosis [112]. There are several evidences that Notch signaling controls cell-cell adhesion by modifying cell adhesion molecules [16, 40, 109, 176, 214, 214].

As discussed above, the movement characteristics can control the signaling patterns in the tissues. However, the migration pattern of cells in the tissue strongly depends on mechanical properties and cell polarisation dynamics [23]. In addition to this, it is also observed that intercellular signaling influences cell and tissue morphology by modifying the cell-cell adhesion of the cells. Hence it is important to understand the connection between signaling patterns, cell polarisation, migration dynamics and cells/tissue mechanics.

A few theoretical models investigate the potential mechanisms underlying the various signaling patterns observed as a result of contact-based signaling [45, 99, 250]. However, very few theoretical works are available that examine the link between tissue mechanics, cell polarisation dynamics, cell motility, and cell signaling. To test the influence of factors mentioned above on the signaling patterns, we use the well-established vertex model [70, 73, 74], with several crucial additions and modifications.

In Chapter 3, first, we overlay the contact-based signaling kinetics to the vertex model with both junctional contacts (short-ranged) as well as protrusional contacts (long-ranged signaling) [44, 47, 99]. Then, we couple the cell mechanics with cell-cell signaling by coupling the intrinsic cell polarities with the orientation of protrusional contacts. We then systematically study the effect of two different cases of polarisation dynamics (random rotational diffusion and polarity alignment with the nearest neighbors) on the resulting signaling patterns. Furthermore, we examine how activation thresholds affect chemical patterns in long-range signaling. As a result of these new changes to the model, we obtain a wide range of complex patterns ranging from spotted motifs to diffuse patterns with random rotational diffusion-dominated polarity. Moreover, for neighbor-aligned polarity dynamics, we observe stripe-like signaling patterns. We also quantify the spatio-temporal

characteristics of the patterns using the number, distribution, and anisotropy of the cluster of the signaling patterns. In summary, we show that cell polarity dynamics greatly influence the richness of molecular signaling patterns arising from contact-based signaling.

In Chapter 4, we test the influence of cell motility on the formation of signaling patterns using the new coupled model discussed in Chapter 3. We also include cell motility in every cell, which is oriented towards intrinsic cell polarity, and investigate the role of cell migration and tissue mechanics on the resulting signaling patterns due to dynamically evolving cell-cell contacts. Upon addition of motility, we observe that the cell-cell contacts evolve dynamically. The cellular structure keeps dynamically shifting in space with time, but the signaling molecule patterns are maintained. By the dynamic correlation function, we quantitatively analyze the spatial and temporal characteristics of chemical patterns.

In Chapter 5, we develop a simple mechanochemical vertex model of the tissue based on Delta-Notch signaling. The expression levels of Notch and Delta in the cells are linked with the tension along their shared edges which in turn influence both cell morphologies and topological transitions in tissue. We systematically study the range of chemical and morphological patterns in the tissue due to this mechanochemical process.

Chapter 2

Literature Review

In the previous chapter, we had discussed the background of the problem that would be dealt with in the thesis. In this chapter, we expand more on those ideas and put our work in the context of the literature that currently exists in the field.

Until a couple of decades ago, cells, which are the building blocks of life, were predominantly thought of as miniature-scale chemical factories. However, advancements in the methods of molecular biology and biophysics, and development of new physical and engineering experimental techniques, since, have made this notion obsolete. We now know with certainty that it is not only the biochemical reactions, but also the physical processes and mechanical forces, which play a huge role in deciding cell functionality and fate. In multicellular organisms, cells are generally organized into collectives called tissues [207]. Broadly speaking there are four types of animal tissues: (i) connective tissue, (ii) muscle tissue, (iii) nervous tissue and (iv) epithelial tissue.

Epithelial tissues consists of groups of tightly connected cells and form a protective covering for blood-vessels and various organs. Epithelial tissues can form a monolayer of cells that are attached to each other by bonds called cadherins and to the underlying substrate with bonds called integrins [5]. Epithelial tissues have clear functions during many important biological processes such as morphogenesis. The morphogenesis of epithelial tissues is widely observed during the early stages of development [269].

Morphogenesis means the origin of form and involves the study of how organisms get their shape in response to their designed function [102, 117, 136, 178]. Morphogenesis is dominantly used in the context of early embryo development. However, it is also appro-

priate in contexts as diverse as protein folding, the formation of virions, shaping of plants, form-finding in engineering structures, and emergence of geological landforms. Although biochemistry plays a significant role in driving morphogenesis in living structures, it is mechanics that is ultimately responsible for giving rise to its ultimate form in response to a function [95]. During the organ development, on the one hand chemical pre-patterning takes place to provide the positional information and on the other hand, cell mechanics and movement tries to deform the tissue and organize the cells to form mechanical patterns to regulate the shape and size of the organ [76]. The following sections review cell signaling, cell mechanics and motility and different models that have been proposed to study the mechanochemical patterning observed during morphogenesis.

2.1 Chemical basis of morphogenesis

Starting from nearly homogeneous population of cells, different areas of a tissue develop strikingly different patterns or structures [76, 265]. The formation of a morphological pattern is generally assumed to result from a primary pattern of morphogen concentrations [265]. Such primary spatial patterns are formed from an aggregate of uniform cells due to cell differentiation process in which cells acquire different fate depending on their spatial position [76]. Tissues establish self-organizing chemical patterns due to chemical and mechanical interactions between cells [250, 251]. A large number of self-organising, regular, spatio-temporal patterns in tissues have been documented in various organisms. These include, for example, bristle patterns on the *Drosophila* notum [44, 120], spotted skin patterns on pearl danio fish [65] and striped skin patterns on zebrafish [101].

Beginning as early as 1744, study of morphogenesis has a long history. Abraham Trembley (1744) discovered that the freshwater polyp hydra has the ability to regenerate head and foot from sections cut from the hydra body [247]. Such findings raised questions about how such spatial patterning occurs and how the organism development can resume even after severe perturbations such as the organism being cut into pieces. It was postulated that the morphogenetic gradients specifies positional information, raising the question of how such gradients are formed and how they regulate the development. In the early part of the 20th century D'Arcy Thompson made, then revolutionary, discovery

based on his observations that mechanical forces that shape the foams or soap films are also at work in morphogenesis of living organism [241]. Later, Turing (1952) made a key contribution and discovered that the spatial concentration patterns can be generated, starting from nearly uniform initial distribution, by interaction of two substances with different diffusion rates [248]. He derived the now named Turing equation from an analysis of spatial destabilization created by concentration waves of certain wavelengths. The theory is based on short range activation and long range inhibition. Reaction and diffusion processes involving activators and inhibitors can result in a large variety of the so called Turing patterns in the tissues [92, 156, 248]. Later on, studies in insects and worms, and more recently in vertebrates and animal tissues have revealed an evolutionarily conserved mechanism that is based on lateral inhibition [12, 43, 48, 107]. Lateral inibition is a cell-cell interaction in which a cell leading to achieve a particular fate inhibits its neighbours or other cells in contact from attaining the same fate [90, 106]. For example, it is observed that during development of nervous system, the neural cells inhibit the neigbouring cells from developing the neural fate. In this way, the neighbour cells are compelled to attain different fate [48].

Cell signaling is the process by which information is transmitted from one cell to the other and ultimately to the nucleus, resulting in changes in gene expression [98]. Four types of signaling pathways are found in multicellular organisms that play a central role in controlling all the important activities during organism development: paracrine signaling, endocrine signaling, autocrine signaling, and juxtracrine signaling [223]. Paracrine signaling occurs when cells communicate with neighbouring cells through signaling molecules. The signaling molecules diffuse over short distances relatively quickly which alters the function of neighbouring cells [233]. In the endocrine signaling process, the signaling molecules are secreted from specialized endocrine cells and are transported through the bloodstream to act on distant target cells in the body [49]. During autocrine signaling, a cell secretes an extracellular mediator that binds to receptors within the same cell to initiate signaling [127]. Juxtracrine signaling takes place via lateral inhibition, which is a cell interaction mechanism where a cell with a particular fate inhibits the other cells in contact from achieving the same fate [216]. In embryos and adults, a number of genes and proteins are involved in lateral inhibition signaling [138, 216, 222]. Recently, a transcriptional regulator TAZ was also identified as a mediator of lateral inhibition in zebrafish and

is involved in directing cell fate [271]. More commonly, in several multi-cellular organisms such as flies, worms, fish and other vertebrates, signaling takes place by the lateral inhibition of Notch ligand and Delta receptor, which are trans-membrane proteins that reside on the cell surface [47, 50]. The Notch ligands and Delta receptor are transmembrane proteins and are members of the DSL (Delta/Serrate/LAG-2) family of proteins [63]. Various investigations indicate that a large number of self-organised spatial patterns can be generated through juxtacrine signaling (contact dependent signaling) that occurs through contacts either between cells or between cells and the extra-cellular matrix (ECM) [11].

The Notch signaling pathway, which is one of the key juxtacrine process, plays a crucial role in organism development, physiology and diseases such as cancer [29, 103]. During the adult and embryonic life, proper regulation of the Notch signaling pathway is essential for development, homeostasis and differentiation of tissues [30, 221]. The deregulation of Notch signaling can also lead to various diseases and disorders, for example leukemia [268], solid cancers including breast cancer, glioblastoma (a form of brain tumor), pancreatic cancer [173, 274], lung cancer [83, 84] and skin cancer [163, 184]. Notch1 was identified as an oncogene in leukemia and it is also found to have tumor suppressive function [143, 147, 201]. Thus, Notch signaling is hoped to prove to be a valuable target for the treating a wide range of cancers [82, 263].

While the Notch signaling pathway is the most prominent juxtacrine developmental signaling pathway, others such as Epidermal Growth Factor Receptor (EGFR) and Hedgehog (HH) pathways are also important for morphogenesis [44, 194, 223]. The cellular contacts during signaling could either be local and between the nearest neighours [1, 104, 121] or they could be long-ranged and mediated by protrusions such as filopodia [44, 65, 182, 210, 212]. Although protrusion-based signaling through Notch pathway is quite common during morphogenesis [44, 182], similar long-ranged signaling is also seen, for example, in Sonic Hedgehog (Shh) during limb patterning in vertebrates [212].

Researchers have tried to model the Delta-Notch signaling kinetics with short range or nearest neigbour signaling (via junctional contact) as well as long range signaling (via protrisional or filopodial contacts). One of the earliest mathematical models for the lateral inibition was developed by Collier et al. [47]. They constructed a simple and generalized mathematical model for short-range signaling via contact-mediated lateral

inhibition. The model consists of differential equations for two variables — Notch and Delta in each cell – that evolve with time.The model proposed that the activation of Notch decreases the ability to produce Delta which amplified the differences of these molecules between neighbouring cells. The model generated a self-organised checker-board pattern with wide range of initial and boundary conditions [47]. Later, another research group reported a quantitative time-lapse microscopy platform to analyze Notch–Delta signaling dynamics [227]. They measured the combined cis–trans input– output relationship in the Notch–Delta system. A striking difference between the responses of Notch to trans- and cis-Delta was reported. The response to trans-Delta was observed to be graded and the response to cis-Delta was sharp and independent of trans-Delta. They also developed a simple mathematical model and showed that the Delta-Notch patterns emerge from the mutual inactivation of Notch and Delta proteins in the same cell [227]. They also showed that cis interaction optimizes the system in the formation of fine-grained pattern [226]. Recently, several papers showed that the developmental patterns also involve Notch signaling via protrusional contacts, for example in bristle patterns on the *Drosophila* notum [45, 120], spotted patterns on skin of pearl danio fish [65] and striped patterns on the skin of zebrafish [101]. Two theory-based papers explored the range of patterns that can potentially be formed by taking into account the long range protrusinal contacts [99, 255]. Hadjivasiliou et al. [99] developed a model with junctional as well as protrusion-mediated contacts of lateral signaling and showed that when signaling kinetics is allowed to differ at junctional and protrusion-mediated contacts, lateral activation and lateral inhibition are promoted in cells. Complex variety of Delta-Notch patterns were generated using the model, as observed in typical reaction-diffusion systems. Different patterns arose when changes in signaling kinetics, length and distribution of protrusions were also included [99].

Cell communication using the juxtacrine mode has been studied in the case of lateral inhibition. A few recent studies indicate that juxtacrine signals can also produce the opposite phenomenon known as lateral induction [209, 224]. Lateral induction is a process by which neighbouring cells attain the same fate in an aggregate of initially equivalent cells. Owen et al. [190] used mathematical modeling to show that lateral induction, in combination with lateral inhibition, provides a mechanism that generates spatial patterns with wavelengths of many cell lengths.

Mechanical basis of morphogenesis

Cell mechanics, motility and cell adhesion combine to drive morphogenetic events, cell geometry and tissue deformation to establish the proper shape and size of the organs [151]. Cells are considered active system or engines, operating away from thermal equilibrium and convert chemical energy into cell motion [118]. Cells in tissues are connected to their neighbouring cells along the cell membrane by adhesion molecules such as cadherins and have contractile acto-myosin cortex which together give rise to adhesion and tension [183, 218, 253]. The internal forces within cells are generated by the actin cytoskeleton (a network of polar, semiflexible protein filaments), acto-myosin cortex, adhesion molecules, and also subcellular structures such as lamellipodia and filopodia which are responsible for inducing motility in cells [10, 75, 225]. Cadherins, in particular, play a key role in many aspects of cell interactions, regulation, and signaling during embryonic development and morphogenesis in general [97, 198, 200]. Gradients of cadherin expression levels often produce macroscopic cell sorting through collective and relative movements [275]. A difference in adhesiveness and contractile properties between genetically heterogeneous cells determines cell shape, size, and cellular pattern, as reported in sensory epithelia of the ear, nose, and eye [203, 242, 243]. In the sensory epithelium, one can find different cell sizes and cellular patterns with different characteristics. Olfactory epithelium (OE) is a sensory epithelium inside the nasal cavity of mammals that is responsible for the perception of odors, and consists of olfactory cells, supporting cells, and basal cells [124]. A mosaic pattern of small olfactory cells and large supporting cells is observed in the olfactory epithelium [51, 232]. Sensory cells in the ear are known as auditory hair cells. The auditory epithelium (inner ears in mammals) have mechanosensory and non-sensory supporting cells. They are formed by an alternate arrangement (mosaic pattern) of hair cells staggered in rows and separated by supporting cells in a checkerboard pattern [243, 244]. Studies show that adhesion molecules (nectins, and cadherins) are essential for the mosaic cell patterns in sensory organs. These adhesion molecules interact with each other leading to differential adhesivity of cells for the formation of such complex cellular patterns in sensory epithelia [242].

The differential adhesivity in cells give rise to a number of different behaviours in

cells and tissues in addition to mosaic cell patterning in sensory organs, for example, cell sorting, tissue segregation [9, 237, 275] and apoptosis [195, 240]. The differential adhesion hypothesis (DAH) [77, 230, 231, 245] for cell-cell interactions explains the physics behind liquid-like tissue segregation, mutual envelopment, and cell sorting behaviours of cells and tissues during embryonic development. The tissues with motile cells and varying degree of cell adhesion rearrange spontaneously to minimize their adhesive free energy. Brodland et al. [33] explained how cell surface energies are interpreted in terms of interfacial cell tensions and computed the equivalent cell surface tension in accordance with the various subcellular components of forces [32]. They proposed a modified theory for spontaneous rearrangement of cells in tissues named Differential Interfacial Tension Hypothesis (DITH) [32]. In this theory, all cytoskeletal components and cell adhesion mechanisms were systematically accounted for. In the paper, the authors outlined all the conditions for the cell and tissue rearrangements such as mixing, sorting, and formation of checkerboard patterns in heterogeneous aggregates of cells, and separation, partial or total engulfment, and dissociation of tissues. Finite element-based computer simulations involving two or more cell types confirm these conditions [32]. Graner and Glazier performed simulations using a large-Q Potts model for cell sorting phenomenon in a mixture of two different types of cells with differential cell adhesion [91]. They showed that long-distance cell movement leads to the sorting of cells with rounded clusters in two phases. The first phase observed was a faster boundary-driven low-cohesive cell layer around the aggregate, followed by a slower internal rearrangement that was boundary independent [91]. Belmonte et al. [18] proposed a self-propelled particle model to study cell sorting phenomenon in organisms. They evaluated the effect of intrinsic motility in cells and differential adhesion with fluctuations to explain various rearrangement processes in cells and tissues and showed that the ability of cells to follow their neighbours actively significantly reduces the time scales of segregation.

As the cells in a tissue are coupled to their neighbours, the cells rearrange themselves and move actively and collectively in response to the elastic (passive) and active forces. Many cells show polarized behaviour due to the polarity [35, 228]. Cellular polarity arises from cellular asymmetry, resulting from the asymmetry of the molecular composition on either side of the cell, which defines a polarity axis along which cellular processes are regulated. Thus, cell polarity is an inherent property in most cells [158]. The active forces

can lead to different types of polarity in cells and thus depending on the polarity dynamics, the cells can show different types of motility behaviour. The cells can walk randomly or in an aligned manner [24, 235, 259, 260] and are modelled as active Brownian particles. Active Brownian particles, are idealized micro-movers that are self propelled in a specific direction and are driven out of thermodynamic equilibrium [208]. Vicsek et al. [259] presented a simple model to investigate the development of self-ordered motion of particles that was motivated by biological interactions in collectively moving organisms [154]. In this model each biological unit or particle had a constant velocity magnitude and its velocity direction at each step was assumed to have an average direction of motion of the neighbouring particles with some random perturbation. A kinetic phase transition was observed from zero collective velocity to finite collective flocking by spontaneously breaking rotational symmetry [259]. In other model, Martin et al. [159] presented a computational analysis of collective motion resulting from interactions involving excluded volume interactions, self-propulsion, and velocity-alignment of active particles. The model was an extension of the active Brownian particles model, in which the self-propelled particles align with the direction of their neighbours. The authors observed the flocking behaviour of particles in a low-density regime, and the behaviour was dominated by the strength of velocity-alignment interactions. Depending on the system parameters, either finite-sized polar clusters or amorphous, highly fluctuating, lane-like or band-like structures were formed [159]. Biochemical signaling plays a governing role in deciding the polarity dynamics of the cells which otherwise is depicted in terms of empirical rules in these models [53, 164]

A large number of models have been developed for tissues to provide insight into morphogenesis due to cellular processes that includes cell motility, cell adhesion, apoptosis and other developmental processes. The mechanisms and mechanics of deformation of epithelial monolayer have been extensively studied by vertex dynamics models [73, 74]. Recognized more than 100 years ago by D'Arcy Thompson, tissues show remarkable similarity with foams. Mathematically, this analogy is implemented in the so-called vertex models in which a planar epithelial monolayer is represented by polygonal tessellation. In the most basic version of the vertex model, the cells (face) and cell-cell connections (edges) are, respectively, provided with mechanical stiffness and line tensions, that model contractility of acto-myosin fibers [70, 180]. The tissue thus represented can respond to

mechanical stimuli by the movement of vertices (hence vertex model) – the cells can also change their connectivity by neighbor exchanges [8]. This vanilla vertex model can be made richer by including cell division and death, and autonomous forcing from cell cytoskeleton and junctions, for instance. Moreover, it is also possible to include variables (such as acto-myosin and morphogen concentrations) on each cell. Their dynamics can have two-way coupling with the underlying tissue mechanics (mechanochemistry), thus leading to patterns of cellular flow, deformation, and chemical concentration. The planar vertex model can also be allowed to have out-of-plane movements to form 3D spatial structures and patterns. The 2D and 3D vertex models have been successful in providing keen insights into various vital morphogenetic events such as germband elongation and pupal wing formation in Drosophila and zebrafish epiboly [115, 254].

To understand how physical cellular properties and proliferation determine cell-packing geometries, Farhadifar et al. [70] used a vertex model for the epithelial junctional network in which cell packing geometries correspond to stable and stationary network configurations. The model takes into account cell elasticity and junctional forces arising from cortical contractility and adhesion. By numerically simulating proliferation, they generated different network morphologies that depend on physical parameters. These networks differ in polygon class distribution, cell area variation, and the rate of T1 and T2 transitions during growth and estimated parameter values by quantifying network deformations caused by laser ablating individual cell boundaries [70].

Bi et al. [23] provided a framework to understand collective solid-to-liquid transitions that have been observed in embryonic development. They used self-propelled Voronoi model to capture polarized cell motility and cell-cell interactions in a tissue monolayer and showed that the tissue exhibits a jamming transition from a solid-like state to a fluid-like state that is controlled by three parameters: the single-cell motile speed, the persistence time of single-cell tracks, and a target shape index that characterizes the competition between cell-cell adhesion and cortical tension [23]. Glazier et al. [88] used the extended large-Q Potts model to show that differential adhesion with fluctuations can explain a wide range of cellular rearrangement, for example, in checkerboard patterning, cell sorting, dispersal, and position reversal [88]. The vertex models can also be systematically coarse-grained by quantifying the contributions to tissue deformations from cell elongation, neighbor exchanges, and cell division [69]. The resulting multi-scale analysis gives

insights into the emergent mechanics and thermodynamics of the tissue, and the contribution to deformation from various components provides cues about the effective forcing and energetics that drive morphogenesis. In order to understand tissue morphogenesis during development, Popovic et al. [196] proposed a continuum hydrodynamic model for describing the shear flow in developing epithelia. The model includes hydrodynamic fields related to cell elongation and tissue shear flow due to topological rearrangements of a cell. The authors investigated the rheological behaviour associated with memory effects on the tissue. Depending on different boundary conditions on the tissue, active stress generation and topological rearrangements were identified as the two processes that were responsible for producing different cellular and tissue shape changes.

Mechanochemical morphogenesis

Coupling between collective cell migration, cell mechanics, and cell-cell signaling is observed in many biological processes such as wound healing, cancer metastasis, branching morphogenesis and embryonic development [41, 85, 134]. Specifically, this coupling is observed in the case of Delta-Notch signaling. For example, in endothelial cells exhibiting Delta-Notch kinetics, the expression of Dll4 (Delta) is significantly enhanced at the tips of the migrating epithelium during angiogenesis [206]. Riahi et al [206] used time-lapse microscopy on the tissue and computational modelling to show that the leader cell dynamics in the moving tissue monolayer is regulated by Notch1–Dll4 signaling mediated via lateral inhibition through both Notch1 and cell stresses. Mechanical stress also inhibits the expression of Dll4 and formation of the leader. It is also known that a Delta increase is associated with the motility and spreading of individual keratinocytes [41] and stimulates lamellipodia formation [145]. Furthermore, Delta-induced activation of Notch is linked with the application of mechanical force [89, 169]. Thus there are good indications that spatiotemporal chemical patterns of molecules due to contact-based signaling are associated with cell-cell signaling kinetics, tissue mechanics, cell polarisation dynamics, and cell motility.

The chemical patterns due to contact-based signaling are interpreted using models generally with a simplifying assumption that the tissue morphology is fixed and does not

alter during the patterning process [44, 47, 99, 226, 227]. This assumption may not always be correct since cell migration and cell division can dynamically modify the connectivity among cells. Hence, in order to maintain a regular pattern, the signaling pathway requires some feedback mechanisms to coordinate with cell migration and dynamic tissue topology. For example, it is known that FGF and Notch signaling pathways play a crucial role in cell fate decisions and cell migration during gastrulation in *Xenopus* [119]. In zebrafish and chick embroyos, cells moving randomly in posterior presomitic mesoderm (PSM) plays an important role in axis elongation [19, 133]. Mobility gradient in cells along the anterior-posterior (AP) axis of the PSM was observed with more mobility in posterior PSM than anterior, using high-resolution time-lapse imaging [57, 153]. The mean square displacement of the cell trajectories showed that diffusive motion of cells and the direction of cell protrusions which is representative of the direction of cell movement was also randomly distributed. Simultaneously, it was observed that cell motion in the PSM was regulated by a gradient in FGF signaling with high FGF signals in posterior area [19, 57, 133]. During somitogenesis in zebrafish, it is observed that Delta-Notch signaling is accompanied by cellular movements in the course of segmentation clock generation [113, 141]. Similarly, it is reported that somitogenesis in chick embryos involves a complex interplay of individual cell movements and dynamic cell rearrangements [161]. Such large scale cellular movements and rearrangements of different types of cells are also observed during germ-layer formation in zebrafish [217, 264].

Computational studies show that cell migration plays a vital role in Delta-Notch patterning in zebrafish [249]. Numerical modelling also shows that during somitogenesis, the synchronization of the segmentation clock is sustained and promoted by randomly moving cells [251], which in turn promotes the flow of information across the tissue by cell mixing and destabilizing the regular patterns [250]. In such a case, the ratio of time scales of cell migration and cell-cell signaling is crucial for patterning and information transfer between the moving cells [249].

The cellular protrusions responsible for signaling in cells are known to be highly dynamic and polarized [44]. However, the cell mechanics in the tissue strongly depends on mechanical properties and cell polarisation dynamics [23]. Cell growth, migration and remodelling are the important processes controlling morphogenesis. All these processes are known to be governed by cell forces that are also influenced by cell–cell adhesion molecules.

Transmission of force through cell membranes is attributed to adherens junctions, which provide a physical connection between the actomyosin cytoskeleton and transmembrane proteins of the cadherin superfamily (E-cadherin, N-cadherin and P-cadherin) [31, 78, 149, 273]. Hence it is important to understand the connection between signaling patterns and cell polarisation and migration dynamics.

In addition to above disscusion, several studies have demonstrated that the signaling in cells, especially the Delta-Notch signaling is responsible for upregulating or downregulating the adhesion molecules such as nectins, cadherins and integrins. As a result, differentiated cells display differential cell adhesion properties [109, 176, 214]. Periodic activation of Notch signaling regulates the differential cell adhesion between cells, and the coordinated modification between cell shape and cell adhesion organise branching of the feather in chicks [40]. Studies show that Notch is also involved in controlling cell-cell adhesion [2, 193] in different tissues such as *Drosophila* cell eye [16], stem cell clustering [266] and hematopoietic stem cells [205]. Podgorski et al. [195] adopted a computational approach to understand how the interaction between lateral inhibition, differential adhesion and programmed cell death can lead to mosaic patterns, observed in the auditory sensory epithelium of chicks formed by primary and supporting secondary cells. Boareto et al. [27] developed a mathematical model to study the interaction between Notch signaling and epithelial-mesenchymal transition (EMT), and examined the effect of Wnt and TGFb (EMT-inducing signals) on Jagged and Delta ligands. They integrated the Notch-Delta-Jagged signalling with the EMT circuit to assess the influence of cell-cell communication on EMT. They used Notch-Delta-Jagged nearest neighbour interaction between cells. Notch signalling acts as an intercellular switch that leads to different fates adoption of neighbouring cells—Sender cell (low Notch, high Delta) and Receiver cell (high Notch, low Delta), resulting in a checkerboard pattern (lateral inhibition). Notch-Jagged signalling establishes an intercellular feedback loop that directs neighbouring cells to follow same fates (high Notch, high Jagged), leading to the same fate throughout the tissue (lateral induction). Thus, it behaves as a three-way switch and adopts three fates— Sender, Receiver and hybrid Sender/Receiver. Their work showed that increasing Delta/Jagged ligands activates Notch signalling, resulting in EMT. Furthermore, they also explored the significance of Notch-Delta and Notch-Jagged in inducing EMT by Notch-EMT coupled dynamics in the epithelial tissue. It was observed that when Notch-Jagged signalling dom-

inates, mixed E/M or M cells tend to cluster together; and when Notch-Delta signalling dominates, cells segregate.

As discussed above, cell polarity, cell movement characteristics, cell mechanics, and cell-cell signaling control and coordinate with each other during mechanochemical pattern formation in the tissues. It is also evident from the studies that the signaling dynamics control the adhesive molecules connecting cells in the tissue and hence modulate the intercellular forces. These signaling actions thus drive the differential cell adhesion between patterned cells. Hence it is important to understand the connection between signaling patterns, cell polarisation, migration dynamics and the parameters controlling cell mechanics such as cell-cell adhesion in order to get a clearer picture of how pattering and deformations occur during tissue morphogenesis.

2.2 Thesis outline

The subject matter of the thesis is presented in the following five chapters,

- ✓ Chapter-3 elucidates the role of cell polarity dynamics in pattern formation due to contact dependent signaling. We propose a protrusional contact based long distance signaling model to explore the role of junctional and protrusional contact on the signaling pattern formation. We also explore the role of model parameters and polarity dynamics on the formation of signaling patterns.

- ✓ Chapter 4 elucidates the influence of cell motility in the patterns formed by signaling molecules. For every cell, we include cell motility that is oriented along cell polarity and investigate the role of cell migration and tissue mechanics on the resulting signaling patterns due to dynamically evolving cell-cell contacts.

- ✓ Chapter-5 elucidates the influence of signaling proteins on cell-cell adhesion. We propose a simple extension of the proposed model by coupling signaling molecule dynamics to cell-cell adhesion parameter and explore the collective formation of chemical and cell morphological patterns in the tissue.

- ✓ Chapter-6 summarises the work done in the present thesis with final concluding

remarks and a list of potential future problems that are natural extensions of the current work.

Chapter 3

Role of cell polarity dynamics in pattern formation due to contact dependent signaling

3.1 Introduction

Intercellular signaling, cell mechanics and motility are important for morphogenesis during the development of organism. Cell mechanics and movement influences cell-cell signaling by rearranging the neighboring cells and actively migrating [113, 141, 161, 249, 251]. Although some of existing theoretical models investigate the potential mechanisms that could result in a variety of patterns due to contact-based signaling, to the best of our knowledge, there are no theoretical studies and coupled model yet that attempt to include the role of tissue mechanics and cell polarisation dynamics influencing cell-cell signaling. However, as discussed in detail, in literature review, these factors are expected to be important in dictating orientation, range and topology of cellular contacts in the tissue and hence could be critical for the origin and maintenance of the chemical patterns. To test the influence of above mentioned factors in the patterns formed by signaling molecules, we study the system using the well-established vertex model [70, 73, 74], with several crucial additions. First, we overlay the lateral inhibition based signaling kinetics to the vertex model. We consider both short-ranged as well as long-ranged signaling kinetics, to account for junctional and protrusional contacts [44, 47, 99]. We also study the effect

of the activation threshold for long-range signaling on the chemical patterns. Second, we couple the orientation of protrusional contacts with the underlying cell polarities and study the effect of polarisation dynamics on the generated patterns. We specifically look at two cases of polarity dynamics: (i) random rotational diffusion and (ii) polarity alignment with the nearest neighbors.

Based on these new inclusions to the model, in addition to the standard checker-board patterns for signaling molecules, we obtain a large number of intricate patterns ranging from well-defined spotted motifs to diffuse patterns. Moreover, for neighbor aligned polarity dynamics, we see striped patterns of signaling molecules. We systematically quantify the spatio-temporal characteristics of the chemical patterns by obtaining the number of clusters, cluster size distribution and cluster anisotropy of the signaling molecules. Overall, we show that the dynamics of cell polarity greatly influences the richness of molecular patterns arising from contact-based signaling.

3.2 Methods and Model

In our paper, the mechanics of the tissue is implemented using a vertex model [22, 23, 70, 73], in which the tissue is represented as a monolayer formed of polygonal cells having vertices and edges (for implementation details, see Appendix A). The mechanical forces within the tissue arise from area elasticity and boundary contractility of individual cells and the forces at cell-cell contacts from acto-myosin contractility and E-cadherin adhesivity. The mechanical contribution from these sources can be expressed using a energy function of the form,

$$U = \sum_{\alpha=1}^{\mathcal{N}} [K_\alpha (A_\alpha - A_{\alpha,0})^2 + \Gamma_\alpha L_\alpha^2] + \sum_{\text{edges:}\gamma\beta} \Lambda_{\gamma\beta} l_{\gamma\beta}, \tag{3.1}$$

where, $\mathcal{N}$ is the total number of cells in the monolayer and K_α, A_α, $A_{\alpha,0}$, Γ_α, and L_α are the area stiffness, current area, preferred area, boundary contractility and perimeter, respectively, of cell α. $\Lambda_{\gamma\beta}$ is the contractility of the junction of length $l_{\gamma\beta}$ shared by cells γ and β. The contributions from these different forcing terms is converted in effective

force acting on any vertex i as

$$\mathbf{F}_i^{\text{elastic}} = -\frac{\partial U}{\partial \mathbf{r}_i}, \tag{3.2}$$

where $\mathbf{r}_i$ is the position vector for vertex i [74]. In many epithelial tissues, cells are known to be front-rear polarised and in many cases also have self-propelled motility. The motility is assumed to act in the direction of cell polarity. Hence, in addition to the elastic forces, for a given vertex i, we add a motile force [23, 234] of the form

$$\mathbf{F}_i^{\text{active}} = \eta v_0 \frac{1}{n_i} \sum_{\beta} \hat{\mathbf{p}}_\beta, \tag{3.3}$$

where n_i is the number of cells β that contain vertex i, $\hat{\mathbf{p}}_\beta$ is the polarity unit vector for cell β, η is the viscous drag acting on the vertex and v_0 is the motility of a single cell. The total force on vertex i, which is a combination of the elastic and active force, is balanced by the external viscous force. The resulting dynamical equation of evolution for the vertex position is

$$\eta \frac{d\mathbf{r}_i}{dt} = \mathbf{F}_i^{\text{elastic}} + \mathbf{F}_i^{\text{active}}. \tag{3.4}$$

As is common for vertex models, T1 transitions are also included in our formalism and facilitate fluidisation of the tissue.

We model the polarity of every cell to have a tendency to orient with respect to the director ($\pm\mathbf{p}$) of its nearest neighbors while also undergoing rotational diffusion [17, 23, 36, 100, 170]. This rule can be expressed with the following equation:

$$\frac{d\theta_\alpha}{dt} = \xi \sum_{\beta} \sin 2(\theta_\beta - \theta_\alpha) + \zeta_\alpha, \tag{3.5}$$

where θ_α denotes the orientation angle of cell polarity, $\hat{\mathbf{p}}_\alpha = \cos\theta_\alpha \hat{\mathbf{e}}_x + \sin\theta_\alpha \hat{\mathbf{e}}_y$. Here, ξ is the strength of the polarity alignment of a given cell α with respect to that of its

connected neighbors β and ζ_α is the rotational Gaussian white noise which follows

$$\begin{aligned} \langle \zeta_\alpha(t) \rangle &= 0 \\ \langle \zeta_\alpha(t)\zeta_\alpha(t') \rangle &= 2D_r\delta(t-t'), \text{ and .} \end{aligned} \tag{3.6}$$

where, D_r is the rotational diffusivity. In order to study pattern formation of molecules due to contact-based, cell-cell signaling, we now overlay the signaling kinetics on the mechanical vertex model. As discussed earlier, we use Delta-Notch signaling, which is based on contact based lateral inhibition, as our model system [44, 47, 99]. In this formalism, the Delta-Notch kinetics of the cells is modelled by keeping track of Notch and Delta concentration N_α and D_α, respectively, in each cell α. It is known that while Notch concentration in a given cell α is enhanced by the Delta concentration of the cells in contact, the Delta generation of that cell is suppressed by Notch concentration. This signaling dynamics is mathematically represented as follows

$$\frac{dN_\alpha}{dt} = R_N \frac{\bar{D}_\alpha^2}{a + \bar{D}_\alpha^2} - \mu N_\alpha, \tag{3.7a}$$

$$\frac{dD_\alpha}{dt} = R_D \frac{1}{b + N_\alpha^2} - \rho D_\alpha, \tag{3.7b}$$

$$\bar{D}_\alpha = \frac{1}{2}[\beta_j \bar{D}_j^\alpha + \beta_p \bar{D}_p^\alpha], \tag{3.7c}$$

where $R_N|\mu$ and $R_D|\rho$ are, respectively, the production | decay rates of Notch and Delta. Here, $\bar{D}_\alpha$ denotes the mean Delta generation in the cells that are in direct contact with cell α through cell-cell junctions and cellular protrusions. It was pointed out by Collier et al. [47] that the power h of Notch (N^k) and k of Delta (D^h), and the parameters a and b in Eqs.3.7a and 3.7b are responsible for the existence, precise values, and steady-state stability of Delta-Notch expression levels. Increasing the values of h and k and/or ρ and μ

speeds up the emergence of the final pattern [47]. We take the values of these parameters ($h = k = 2$) from the work of Collier et al. [47]. With this choice, the steady state is reached neither too early or too late. β_j and β_p correspond to the contact weights for nearest neighbor and protrusional contacts, respectively, such that $\beta_j + \beta_p = 1$. We define

$$\bar{D}_j^\alpha = \frac{1}{n_j} \sum_{\gamma \in n_j} D_\gamma \text{ and} \tag{3.8a}$$

$$\bar{D}_p^\alpha = \frac{1}{n_p} \sum_{\gamma \in n_p} D_\gamma, \tag{3.8b}$$

where n_j and n_p are the number of cells in contact with cell α, respectively, via cell-cell junctions and protrusions. The nearest neighbors of the cell α constitute n_j and the non-adjacent neighbors constitute n_p. Delta and Notch molecules are known to be asymmetrically distributed in the cells [258] but in order to keep our model simple we assume that the system does not have any asymmetry or noise or spatial dependence in terms of distribution of Delta or Notch molecules associated with cell division.

There are various readouts for the front-rear polarity of cells such as, the gradient of small GTPase molecules within the cells, gradient in the strength of focal adhesions, and the orientation of golgi with respect to cell nuclei, to name just a few, and signaling pathways such as MAPK are involved in cell polarisation [59, 137]. A free cell typically has motility along the direction of polarity via lamellipodia protrusions at the front. In many cases, filopodial protrusions are also formed at the front and the rear of the cells to aid various aspects of cell migration. Because of this connection between cell polarity, cell motility and filopodial protrusions, in our model we assume that the orientation of cell protrusions is the same as that of cell polarity $\hat{\mathbf{p}}$ as defined above. Below we outline the procedure followed to obtain the n_p cells that contact cell α through protrusions.

The coupling between the mechanical vertex model and the signaling kinetics is made by identifying that the protrusions of cells are indicative of polarity and motility of the cells [37, 171]. In that spirit, cell protrusions are modelled by assuming a protrusional

length l extending along the orientation of cell polarization, $\hat{\mathbf{p}}_\alpha$ and $-\hat{\mathbf{p}}_\alpha$ [99]. We assume that the cellular protrusions lie in a interval of $[-\Delta\theta, \Delta\theta]$ around the directions $\hat{\mathbf{p}}_\alpha$ and $-\hat{\mathbf{p}}_\alpha$. We choose the protrusion length l of cell protrusion [44]. As there is strong experimental evidence of Delta-Notch signaling arising from contact between filopodia of cells [44, 182, 210, 212], we focus exclusively on this mode of long range signaling in our paper. Hence, we assume that signaling takes place when the protrusion of a given cell makes contact with the protrusion of other cells within an annulus of thickness Δl around the protrusion length l of the protrusion. Effectively, protrusions of two cells can potentially contact with each other for signaling only if the distance between the centers of the cells is within the interval $[2l - \Delta l, 2l]$. We term this as the separation criterion. However, the extent of cellular protrusions overlap depends on the relative positions of cell pairs, polarity of each cell and the angular sweep of protrusions $2\Delta\theta$ (Figure 3.1). For example, if $\Delta\theta = \pi/2$, then any pair of cells that satisfy the separation criterion will be in large protrusional overlap with each other. Similarly, if $\Delta\theta$ is small, then any pair of cells satisfying the separation criterion would have relatively small protrusional overlaps, and that too for only certain relative positions and polarity orientations (Figs. 3.1bc).

The signaling between the contacting cells is believed to have an activation threshold [44] that, for example, could depend on the extent of the overlap [96, 108, 219]. The exact protrusional overlap between the pair of cells can be calculated using geometry. However, since in our model we couple the protrusion orientation with the cell polarity which constantly evolves in time (Eq. 3.5), for computational convenience we use a simpler criteria for overlap that also includes the signaling activation threshold T in a coarse-grained fashion. In our model, we define

$$w^{\alpha\beta} = \max\Big[\frac{1}{2}((\hat{\mathbf{p}}_\alpha \cdot \hat{\mathbf{r}}_{\alpha\beta})^2 + (\hat{\mathbf{p}}_\beta \cdot \hat{\mathbf{r}}_{\alpha\beta})^2),\ \sin^2\Delta\theta\Big]. \tag{3.9}$$

Only if $w^{\alpha\beta} \geq T$ and the cell separation criterion is satisfied there exists protrusional contact between the cell pair α, β. Here, $\hat{\mathbf{r}}_{\alpha\beta}$ is the unit vector from the center of cell α to the center of cell β (Figure 3.1c). The threshold criteria excludes, in a coarse-grained manner, unfavourable configurations from forming signaling contacts.

The different parameters used in our model are non-dimensionalised as discussed in Table B.1 (Appendix B). We implemented the model in CHASTE by modifying and

extending the CHASTE library (written in C++). The modified and extended CHASTE codes are provided in Appendix B.

3.3 Results

As described in Section 3.2, there are different factors that interact with each other to control the fate of Delta-Notch pattern formation. Some of these are the relative contributions from junctional and protrusional contacts (β_j/β_p), Delta-Notch signaling rates ($\rho \approx \mu \approx R_D \approx R_N$), polarity orientation time-scales, ($1/D_r, 1/\xi$), length and overlap margin of protrusions ($l, \Delta l$), angular range of protrusions ($\Delta\theta$), and neighbor exchange time-scales (L_c/v_0), where L_c is the characteristic length scale of the system given by the cell size (Figure 3.1a). For example, in the case, when $\Delta\theta$ is large, the contact between any pair of cells only depends on the spacing between the cells. Hence, the pattern formation is expected to be predominantly dictated by the relative time-scales L_c/v_0 over which the cells move away from each other and $1/\rho$. On the other hand, when $\Delta\theta$ is small, even if the spacing between the cells does not change (e.g., when $v_0 \approx 0$) the pattern formation from protrusional contacts should still be influenced by the time-scales for polarity changes $1/D_r$ when compared with the signaling time-scales $1/\rho$. In this section, we systematically explore, how these different chemical and mechanical factors decide the spatio-temporal dynamics of signaling patterns. In Sec. 3.3A-C, we study the role of mechanochemical parameters on signaling patterns when cell motility is low. The effect of cell motility on signaling patterns is explicitly investigated in Chapter 4. The mechanical parameters for the vertex model were chosen such that the tissue remained in the solid-like regime (Section 3.3.1-3.3.4; Appendix B) or in the fluid-like regime (Chapter 4) [22, 23]. The dynamical parameters were chosen such that the signaling time-scales allowed for the chemical patterns to form, but the polarity and motility time-scales could also allow the patterns to remain dynamic.

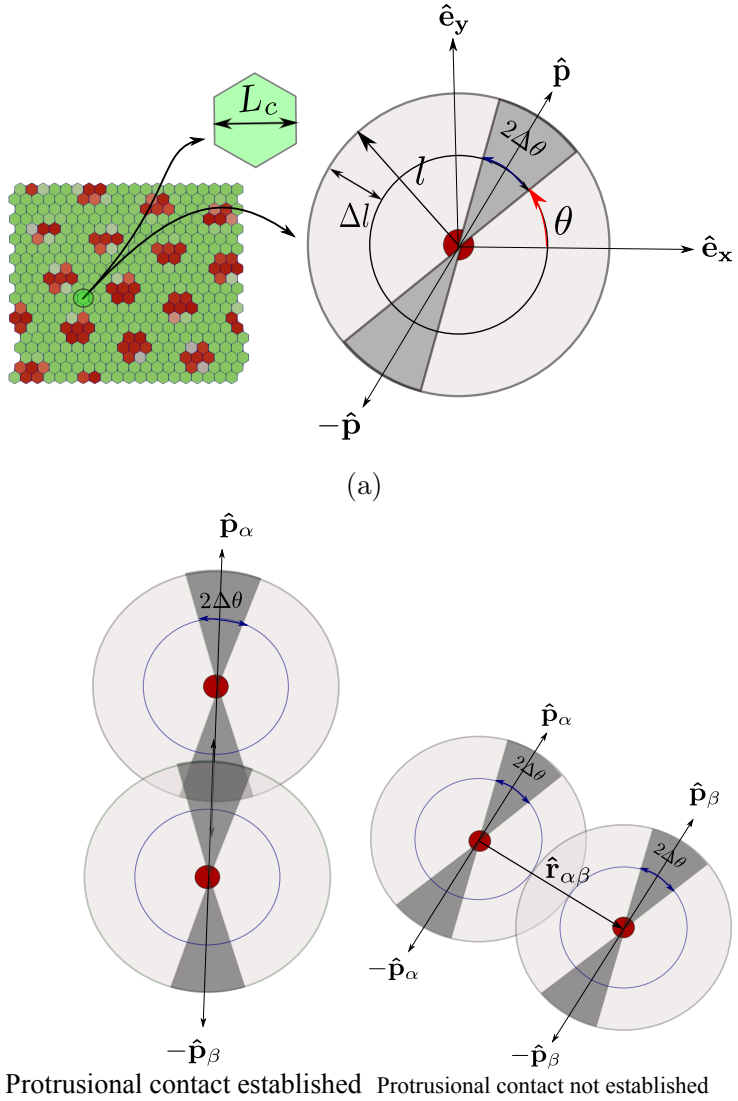

Figure 3.1: Schematic showing protrusion along cell polarization and contact interactions with neighbors. (a) Single cell with polarisation $\hat{\mathbf{p}} = \cos\theta\mathbf{e}_x + \sin\theta\mathbf{e}_y$ and protrusions along $\hat{\mathbf{p}}$ and $-\hat{\mathbf{p}}$. Length of protrusions is l and its angular spread is $2\Delta\theta$ around θ and $\theta + \pi$. The red and green color cells are Delta and Notch cells respectively. (b) Cellular protrusions of two cells overlapping each other. The likelihood of contact for two cells is high if their cell polarization vectors are coaxial or the angular range of protrusion is high. (c) The centers of two cells that are within range $[(2l - \Delta l), 2l]$ of one another but the protrusions do not touch.

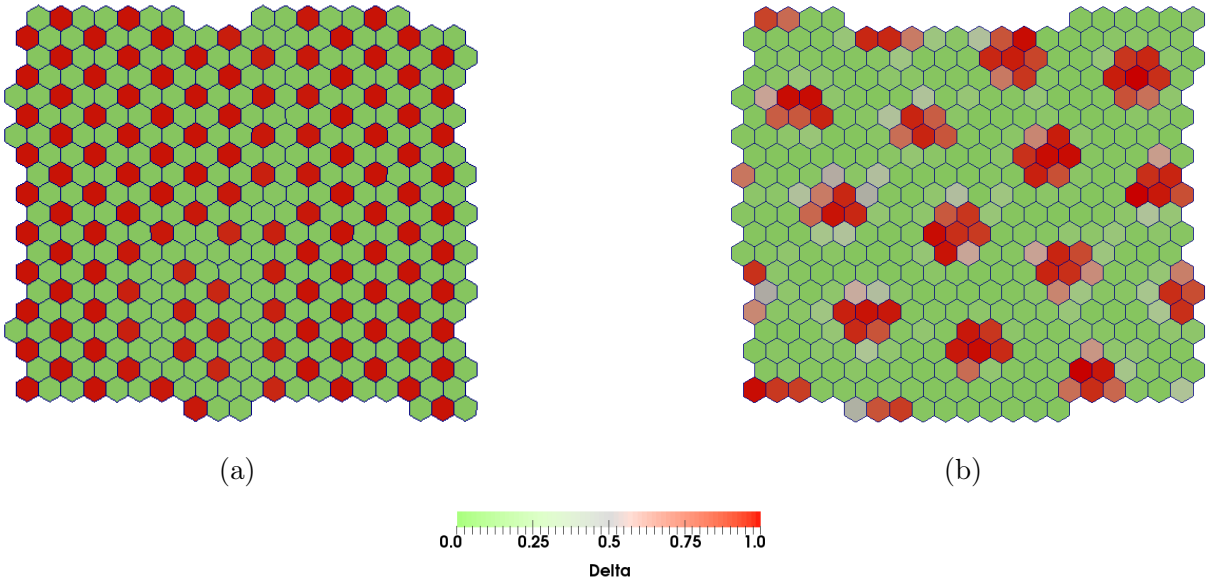

Figure 3.2: Delta (red)-Notch (green) signaling patterns formed by contact mediated signaling via (a) junctional contacts $\beta_j \gg \beta_p$ and (b) protrusional contacts $\beta_p \gg \beta_j$. The final time point of the simulations after steady pattern has emerged is shown for both the cases. The results in (a) and (b) confirm the findings in Refs. [47, 99], respectively.

3.3.1 Role of contact ratio (β_j/β_p) from junctional and protrusion-mediated contacts

The strength of Delta–Notch signaling at junctional and protrusional contacts is captured by β_j and β_p, respectively. The contact ratio β_j/β_p is critical for deciding signaling pattern in this model. When the contact ratio is large $\beta_j/\beta_p \gg 1$ checker board pattern emerges since the signaling is dominated by the junctional contacts as in the classic model by Collier et al. [47] (Figure 3.2a; Movie 1 in Appendix B). On the other hand, consider the case of small contact ratio $\beta_j/\beta_p \ll 1$ with $\Delta\theta = \pi/2$ (Figure 3.2b; Movie 2 in Appendix B). Here, the dominant mode of signaling is through cell protrusions. Moreover, for $\Delta\theta = \pi/2$, the cell-cell signaling is isotropic and occurs for any pair of cells that satisfy the separation criterion. The signaling pattern in this case is similar to the checkerboard pattern observed for large contact ratio. However, the pattern shows a new length scale corresponding to the size of protrusions ($2l \approx 3$ cell-lengths) [99]. Thus the nature of pattern formation in contact based signaling is influenced by the relative strengths of junctional and protrusional contacts.

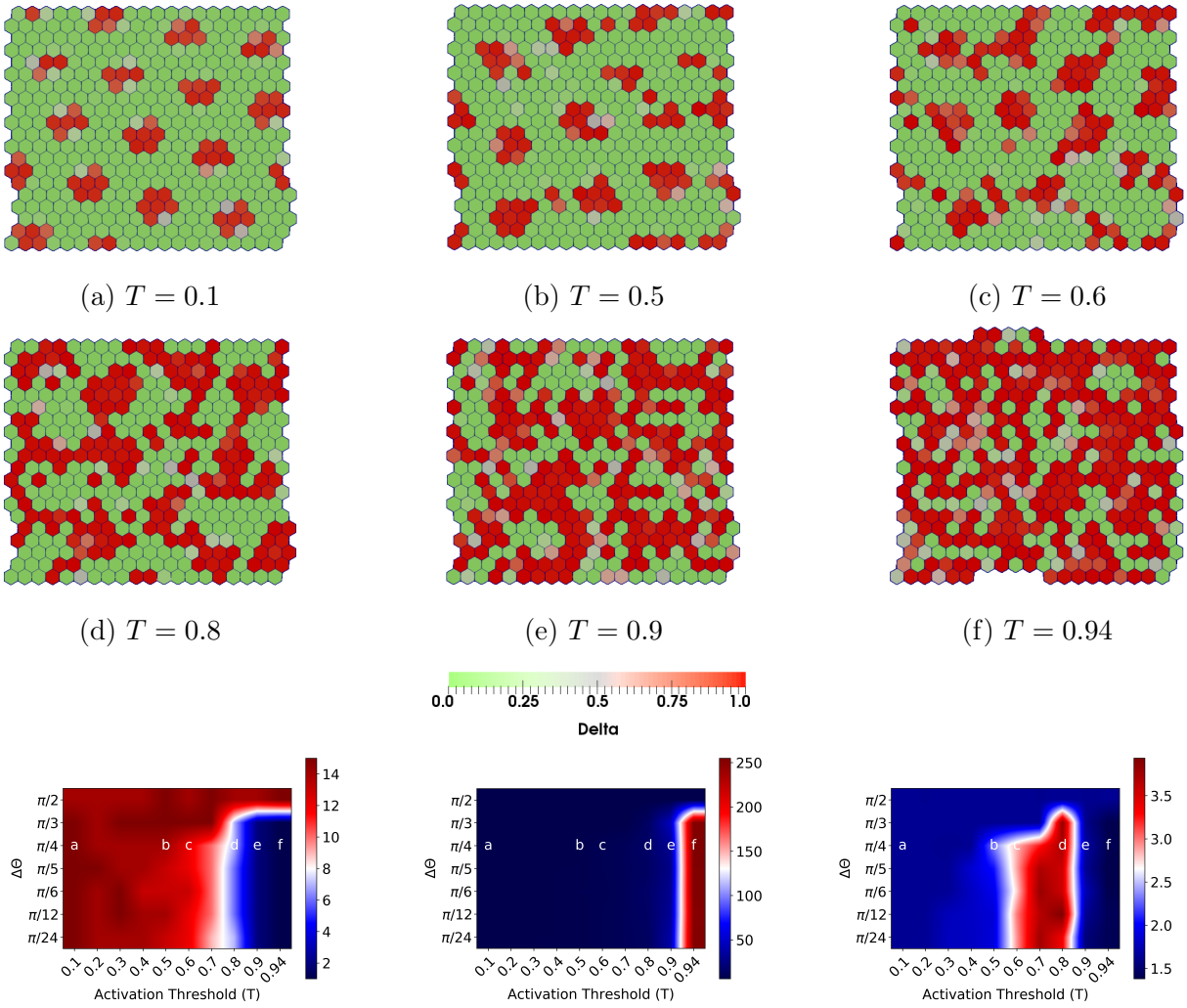

(a) $T = 0.1$ (b) $T = 0.5$ (c) $T = 0.6$

(d) $T = 0.8$ (e) $T = 0.9$ (f) $T = 0.94$

(g) Number of clusters (h) Cluster size (i) Shape ratio

Figure 3.3: Role of angular range of protrusions $\Delta\theta$ and activation threshold T on pattern formation. (a-f) Steady-state Delta(red)-Notch(green) patterns obtained with $R_N = R_D = \rho = \mu = 1$, $D_r = 10^{-3}$, $\beta_j/\beta_p = 10^{-2}$, $\Delta\theta = \pi/4$, $v_0 = 3.1 \times 10^{-4}$, and $\Lambda = -13.77$, $\xi = 0$ and varying $T \in [0.1, 0.5, 0.6, 0.8, 0.9, 0.94]$. (g,h) Phase diagrams for the median number of clusters and the median cluster size (median number of Delta cells per cluster) (see Appendix B) in a confluent tissue as a function of $\Delta\theta$ and T. Large value of cluster number with small cluster size indicates many isolated small Delta patches, whereas a small number of clusters with large cluster size indicates connected regions of Delta expression. (i) Phase diagram for the median shape ratio of Delta clusters in a confluent tissue as a function of $\Delta\theta$ and activation threshold T (see Appendix B). Lower and higher values of this quantity indicate dominant presence of circular and elongated patches, respectively.

3.3.2 Role of angular range of protrusions ($\Delta\theta$) and activation threshold (T)

As discussed in Sec. 3.2, long-range signaling can be achieved by protrusional contacts. As described there, the orientation of protrusion for any cell α is decided by the direction of cell polarization $\pm\hat{\mathbf{p}}_\alpha$. In this section, we consider the case where the cell polarization is governed by the random rotational diffusion only ($\xi = 0$). The signaling dynamics additionally depend on the length and overlap range of protrusion (l, Δl), the angular range of the protrusions $\Delta\theta$ and activation threshold (T). We now systematically study the effect of $\Delta\theta$ and T on signaling patterns by varying only these two while keeping all other model parameters fixed (Figure 3.3; Movie 2-7 in Appendix B). The protrusions are more polarized if $\Delta\theta$ is small and not polarized at all if $\Delta\theta = \pi/2$, i.e., the protrusions can grow in all directions.

We keep $\Delta\theta = \pi/4$ and explore how the steady-state signaling patterns evolve with the activation threshold T. When T is relatively small, we see isolated, ordered patterns of sharp isotropic spots of Delta expression, similar to the ones already discussed in Sec. 3.3.1 (Figure 3.2b). Upon increase in T, there is a decrease in Delta-Notch signaling (Eq. 3.9) that results in reduction of Notch in cells and hence a general increase in Delta levels (Eq. 3.9). Moreover, the Delta cell patches also gets relatively anisotropic. As a result, the Delta expression patterns start getting less structured, more elongated, and increasingly connected. This effect becomes most pervasive at the largest threshold value.

We now quantify different aspects of Delta patterns that are observed for various combinations of $\Delta\theta$ and T. To get insights into the connectivity of the Delta patches, we compute the median number of Delta clusters and median size (number of Delta cells per cluster) of isolated Delta clusters. We define one cluster of Delta cells as the group of connected cells, each with Delta concentration $D > D_{\text{critical}}$ (see Appendix B). To also get insight into the geometry of these patches, we then quantify their shape ratio (see Appendix B). In Figures 3.3g, 3.3h and 3.3i, respectively, we represent the median number of clusters, median size of the clusters and their median shape ratio, calculated over space, time and simulation runs, as functions of $\Delta\theta$ and T (see Appendix B). By observing these phase-diagrams together we can see that, for lower values of T the Delta

expression patterns are isolated in small isotropic clusters (Figures. 3.3ab). However, upon increase in T, the clusters keep getting smaller in numbers, i.e, larger in size, and become increasingly elongated for lower values of $\Delta\theta$ (Figs. 3.3cd). For largest values of T, the clusters remain bigger but become more isotropic due to increasing connectivity of Delta regions (Figure 3.3ef). For large values of $\Delta\theta$, however, the clusters always remain small and isotropic, as discussed in Sec. 3.3.1.

We note that, when $\Delta\theta = \pi/4$ and $T \leq 0.5$, from Eq. 3.9, $w_{\alpha\beta} \geq T$, due to which the results in Figure 3.3a ($T = 0.1$) and Figure 3.3b ($T = 0.5$) should ideally be identical. However, due to small round-off errors during computing, at these values of T and $\Delta\theta$ the condition $w_{\alpha\beta} \geq T$ is always satisfied for $T = 0.1$ but not for $T = 0.5$. Consequently, there are a few differences between Figs 3a and 3b. This small numerical deviation would be the expected at the critical transition point when $\sin^2 \Delta\theta = T$.

We also point out that, for large values of T, the Delta patterns depend on protrusion orientations ($\hat{\mathbf{p}}$), which evolve on time-scales set by D_r^{-1}. When D_r is zero, we get a static but well-formed Delta pattern (Appendix B Movie-23). When D_r is non-zero but small compared to signaling rates (Eq. 3.7), we get well-formed but fluctuating Delta patterns (Appendix B Movie-4). However, when D_r becomes large, the protrusional contacts evolve too fast for signaling to take effect, because of which the patterns are underdeveloped as Delta levels remain low and fluctuating (Appendix B Movie 24). Hence, in this section, we chose D_r that was small compared to signaling rates to get well-formed but dynamic Delta patterns (also see Appendix B).

We thus find that a rich array of Delta-Notch patterns are observed due to an interplay between the angular range of protrusions and the threshold for signaling due to protrusional contacts. We also provide an effective way of quantifying the nature of these patterns.

3.3.3 Role of coupling strength ratio (ξ/D_r) on pattern formation

In our model, the dynamics of cell polarity has two components (Eq. 3.5). The first component tends to align the polarity of any cell with that of its nearest neighbors with rate ξ and attempts to bring about global alignment of polarity in the tissue [160]. The

second component D_r brings about rotational diffusion of cell polarity, thus creating an overall disorder in tissue polarity. As studied in the previous section, for the case of polarity alignment rate $\xi = 0$, the cell polarities dictate the local dynamics of protrusional contacts (Eq. 3.9) and hence the Delta-Notch patterns. However, since ξ influences the global alignment of cell polarity, in this section we study the role of the coupling strength ratio ξ/D_r on Delta-Notch pattern formation.

We fix $T = 0.5, D_r = 0.1, \Delta\theta = \pi/4$ and vary the value of ξ from $0 - 0.25$. The progressively changing patterns for increasing magnitude of ξ/D_r are shown in (Figs. 3.4a-f) and (Appendix B Movies 8-13). As expected, when ξ is relatively small, D_r dominates and the cell polarity is spatially disordered, thus resulting in isotropic circular patterns of Delta expression (also see Figure 3.3a). However, when ξ becomes comparable to D_r, the spatial disorder of cell polarity decreases and local regions of polarity alignment with an effective direction are created. Since protrusions are oriented along the polarity of cells in our model, the cell-cell contacts predominantly occur along the effective polarity orientation and very little in the perpendicular direction. As a result, the signaling is diminished along the perpendicular direction resulting in reduction of Notch levels along that direction. The lowering of Notch concentration, in turn, results in greater expression of Delta, thus leading to formation of elongated Delta domains. Consequently, we see Delta expression emerging in stripe-like patterns that are oriented perpendicular to the overall direction of cell polarity in the ordered region. In the region with disordered polarity, we still observe circular regions of Delta expression (Figs. 4c and 4f). As expected, the thickness of stripes and the diameter of the circular spots are roughly equal to twice the protrusion length ($2l \approx 3$ cell lengths). As a result of Eq. 3.7-3.9, if two cells touch each other, one becomes a Delta cell and the other a Notch cell. In any cell α, the orientation of protrusion is determined by the direction of polarization $\pm\hat{\mathbf{p}}_\alpha$ and the length of the protrusion is l. Therefore, the nearest interaction between two cells via protrusion is $l - \Delta l$ in both directions. As a result, the distance between two notch cells will become $2(l - \Delta l)$, and we observe the spotted delta pattern of diameter approximately $2l$. A similar trend is also observed with the stripes pattern. Upon further increase in ξ, the cell polarities align globally, thus resulting exclusively in stripe-like patterns of Delta expression. However, the presence of D_r leads to modification of the global polarity alignment causing the patterns to reorient over longer time-scales (see Appendix B Movies 8-13).

As we had done in the previous section, we now quantify the median number of clusters, median cluster size and median shape-ratio of the Delta patterns using phase-diagrams obtained as a function of $\Delta\theta$ and ξ/D_r (Figs. 4g-i, also see Appendix B). As expected, for large values of $\Delta\theta$, we mostly observe patterns of isolated, circular clusters, irrespective of the magnitude of ξ/D_r, since the cell protrusional contacts are mostly isotropic. However, for lower values of $\Delta\theta$, an increase in ξ/D_r, which results in cell polarity ordering, leads to the formation of uniformly oriented and continuous Delta stripes.

We also performed simulations for parameters used in (Figure 3.5; Movie 16-22 in Appendix B) when $T = 0.94$. Since both T and D_r are large, the amount of switching of cell contacts due to fluctuations is naturally very high. As a result, the patterns are either not formed or are more dynamic (see Appendix B Movies 16-18). It could be observed that only when the alignment term ξ dominates over D_r, the fluctuations in polarity and hence in protrusion alignment are reduced. The system is then able to generate and maintain Delta patterns (Appendix B Movies 19-22).

We thus find that polarity dynamics can have a strong influence on the nature of Delta-Notch signaling patterns.

3.3.4 Role of D_r and T in Delta pattern formation

At lower values of threshold T, the differences in the patterns formed by static and rotationally diffusing filopodia are negligible since, in this case, the protrusional contacts between the nearby cells are mostly independent of filopodia orientation ($\hat{\mathbf{p}}$) for intermediate to high values of $\Delta\theta$ (Eq. 3.9). However, for higher values of T, the nature of Delta patterns depend on filopodia orientations and the relative positions of cells (Eq. 3.9). In this case, when D_r is zero, the final patterns are static and seem to depend only on the initial orientations of filopodia (Movie 23, for $D_r = 0$, $\Delta\theta = \pi/4$, $T = 0.6$, and initial orientation randomly chosen from $[-\pi, \pi]$). When D_r is non-zero but relatively small compared to the Delta-Notch signaling rates (Eq. 3.7), the system remains established in a particular configuration of orientation network of protrusional connections for a sufficient duration of time to establish Delta levels and patterns. However, due to the

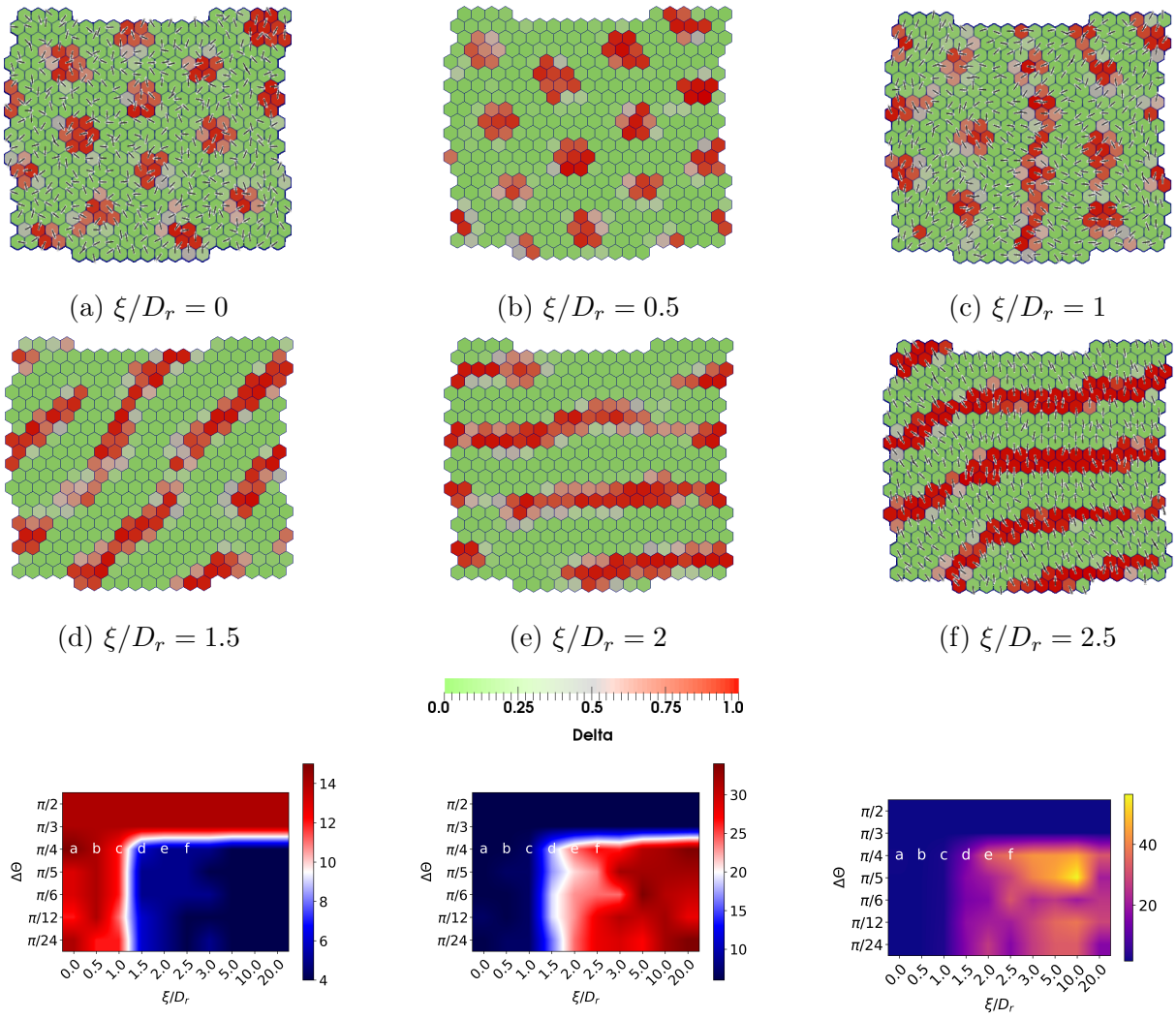

(a) $\xi/D_r = 0$ (b) $\xi/D_r = 0.5$ (c) $\xi/D_r = 1$

(d) $\xi/D_r = 1.5$ (e) $\xi/D_r = 2$ (f) $\xi/D_r = 2.5$

(g) Number of clusters (h) Cluster size (i) Shape ratio

Figure 3.4: Screenshots showing the steady state Delta(red)-Notch(green) patterns formed with polarized cells with varying coupling strength ratio (ξ/D_r) and angular range of protrusions ($\Delta\theta$). The fixed parameters are $R_N = R_D = \rho = \mu = 1$, $\Lambda = -13.77$, $D_r = 0.1$, $v_0 = 3.1 \times 10^{-4}$, ${}^{\beta_j}/_{\beta_p} = 0.01$, $T = 0.5$, and $\Delta\theta = \pi/4$. The patterns (a-f) are obtained by varying coupling strength ratio $\xi/D_r \in [0, 0.5, 1.0, 1.5, 2.0, 2.5]$. The lines in each cell indicate the nematic orientation of cell polarity. No arrows are shown due to the equivalence of $\pm\hat{\mathbf{p}}$ in our model for cell motility (Eq. 3.5) and protrusional signaling (Eq. 3.8). (g,h) Phase diagrams for the median number of clusters and median cluster size in a confluent tissue (see Appendix B) as a function $\Delta\theta$ and ξ/D_r. (h) Phase diagram for median shape ratio in a confluent tissue as a function of $\Delta\theta$ and ξ/D_r (see Appendix B). Large number of Delta clusters with small cluster size and low shape ratio indicate the dominance of isolated circular patterns, wheres low number of clusters with big cluster size and high shape ratio point towards stripe-like patterns.

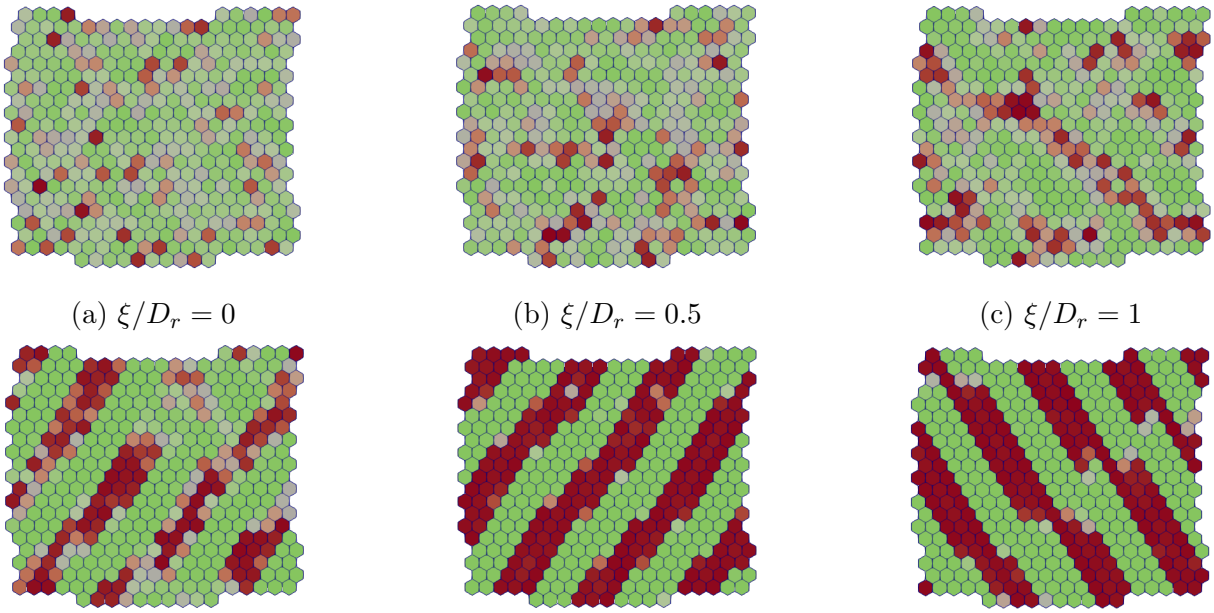

(a) $\xi/D_r = 0$ (b) $\xi/D_r = 0.5$ (c) $\xi/D_r = 1$

(d) $\xi/D_r = 1.5$ (e) $\xi/D_r = 2$ (f) $\xi/D_r = 2.5$

Figure 3.5: Screenshots showing the steady state Delta (red)-Notch (green) patterns formed with polarized cells with varying coupling strength ratio (ξ/D_r), angular range of protrusions ($\Delta\theta$) and $T = 0.94$. The fixed parameters are $R_N = R_D = \rho = \mu = 1$, $\Lambda = -13.77$, $D_r = 0.1$, $v_0 = 3.1 \times 10^{-4}$, $\frac{\beta_j}{\beta_p} = 0.01$ and $\Delta\theta = \pi/4$. The patterns (a-f) are obtained by varying coupling strength ratio $\xi/D_r \in [0, 0.5, 1.0, 1.5, 2.0, 2.5]$.

non-zero value of D_r, the orientations evolve and hence form newer protrusional connection network, thus leading to dynamical patterns (Movie 4, for $D_r = 10^{-3}$, $T = 0.6$ and $\Delta\theta = \pi/4$). Finally, when D_r becomes large when compared to the signaling rates, the protrusional contact network evolves much faster due to which the system does not get sufficient time to establish Delta levels and patterns. Consequently, the overall Delta levels remain low and time-varying, and the patterns not as anisotropic as for the case $D_r = 0$ (Movie 24, for $D_r = 1$, $T = 0.6$ and $\Delta\theta = \pi/4$). Thus, Delta patterns depend on threshold T, $\Delta\theta$, and the relative time-scales for orientational changes and signaling.

3.4 Discussion

In this study, we report a rich variety of Delta-Notch patterns that depend on the nature of cell-cell contacts, signaling threshold, polarity dynamics and tissue mechanics. The classic model by Collier et al. [47] exhibits checkerboard pattern for Delta-Notch expression. We show that this pattern modifies to a spot-like pattern due to long-range contacts with essentially a change in the length-scale that arises due to linear protrusion range. However, the modification in the angular range of protrusional contacts elicits local contact anisotropy and hence results in more elongated Delta patterns. We further showed that the signaling threshold is also important in dictating the connectivity of Delta clusters. Moreover, we systematically quantified the nature of these patterns by measuring the number of Delta cells cluster, cluster size and calculating the shape of individual clusters. We see that by changing the polarity dynamics by increasing the signaling ratio ξ/D_r, the cell directors ($\pm\mathbf{p}$) become globally aligned thus leading to the formation of stripe-like patterns.

Our model with protrusional contacts indeed shows patterns of Delta-Notch that look similar to that formed by the EMT related molecules in Boareto et al. [27] and it is indeed tempting to draw parallels. However, this similarity seems superficial on account of the following important aspects. (1) Unlike in that paper in which the signalling is governed by nearest neighbour interactions, in our work in this context, the signalling is long range due to protrusional contacts. (2) In Boareto et al, while there are two interconnected modules: Notch-Delta-Jagged (lateral induction and inhibition) and EMT

circuit, in our work we only have Delta-Notch (lateral inhibition) chemical kinetics. (3) As opposed to a static lattice in Boareto et al, we have a dynamic lattice in our model. That said, it is possible that the effective behavior of our model could be mapped to that of the model by Boareto et al. However, it is not clear if that's the case in the current scenario.

Chapter 4

Role of cell motility in pattern formation due to contact dependent signaling

Collective cell movement is a fundamental and intricate process essential for the morphogenesis of organ systems in multicellular organisms—the cells in the tissue move in sheets or clusters of closely associated cells. Collective cell migration is known to occur in a large number of development processes. Rather than migrate individually, cells migrate collectively, for example, wound healing [157], gastrulation [267], and cancer metastasis [80]. During tissue remodeling, collective motion keeps the tissue together and enables mobile cells to move immobile cells along to maintain an even distribution of cells within the tissue. Furthermore, it has been found that the movement patterns of such cell clusters differ significantly from the movement pattern of the individual cells within [257]. In *drosophila*, collective cell movement occurs during border cell migration and tracheal development [175]. In vertebrates, collective cell migration takes place during gastrulation, neural crest cell development, vascular sprout, and pronephros development [56, 238, 256]. In aquatic animals, collective cell movement is observed during the sensory lateral line development [86]. The myosin molecular motors in the cytoskeleton produces motile forces or active forces which are transmitted via junctional contacts that drives the cell motion. Cytoskeletal structures and the actin proteins generate tension at the cell level that gives rise to active stress [6].

Cell motility, tissue mechanics, and intercellular signaling play a crucial role during morphogenesis. For example, during somitogenesis in *chick* embryos, it is observed that cell movement and dynamic cell rearrangements take place [161]. Similarly, during

somitogenesis in *zebrafish*, Delta-Notch signaling occurs at the same time as cellular movement during the segmentation process [113, 141]. Somites are segmented axial structures in vertebrate embryos that develop into the ribs, vertebral column, skeletal muscles, and subcutaneous tissues. During the vertebrate developmental phase, somites develop from the anterior of the presomitic mesoderm (PSM) [123, 187, 197].

Several studies support the fact that the cell movement in tissues controls the signaling patterns. In some existing theoretical models, mechanisms that could lead to different patterns due to contact-based signaling are examined [45, 47, 99, 226, 250, 251], but no research has been conducted to integrate tissue mechanics, cell polarization dynamics, and cell motility simultaneously. These factors are expected to play a role in determining the orientation, range, and arrangement of cellular contacts. They may therefore play a crucial role in the formation and maintenance of signaling molecules pattern. We investigate the role of cell motility that ultimately leads to the collective movement of cells on the patterns formed by signaling molecules. For model details, see Chapter 3, which includes the cell mechanics and polarity dynamics. In addition to cell mechanics, cell polarity, and cell-cell signaling, we also For every cell, we also incorporate cell motility in each cell that orients in the direction of cell polarity. We observe that the cell-cell contacts evolve dynamically, but the patterns formed by signaling molecules are maintained. We also quantify the spatio-temporal characteristics of the patterns by dynamic correlation function.

4.1 Effect of motility on pattern formation

In the previous chapter, we have studied the role of protrusion spread, signaling threshold and polarity dynamics on the formation of Delta-Notch patterns in tissues. In our model, the polarity dynamics influences the signaling via modification of protrusional contacts. However, as discussed earlier, cell polarity is also connected with cell migration, which in conjunction with cell shape index can control tissue fluidization through cell neighbor exchanges (see Appendix B) and thus influence the signaling pattern. Hence, we provide cells with larger values of motility v_0 and adjust cell line tension Λ such that the cell-shape index $p_0 = -\frac{\Lambda}{4\Gamma\sqrt{A_0}} \approx 3.85 > 3.8$, that is required for tissue fluidization for $v_0 =$

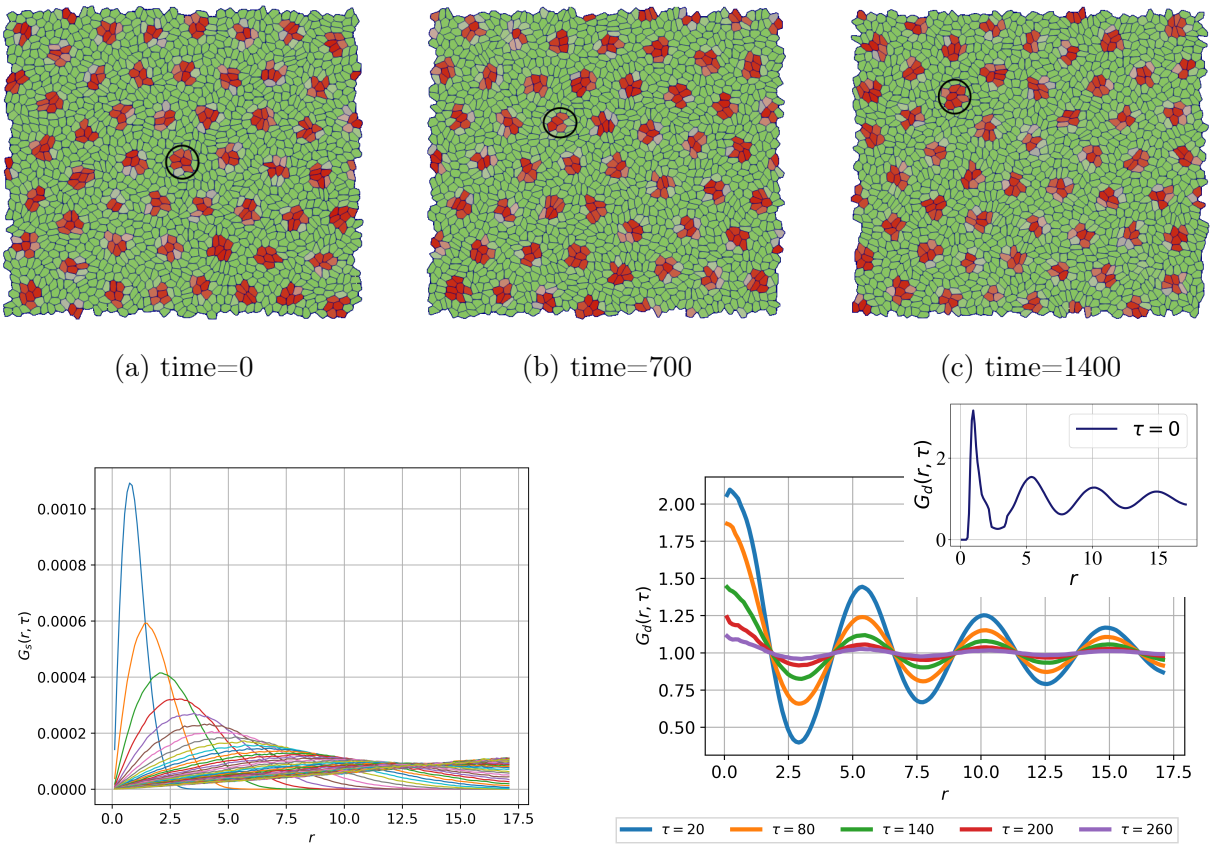

(a) time=0 (b) time=700 (c) time=1400

(d) (e)

Figure 4.1: Screenshots and plots showing the effect of cell motility and tissue mechanics on Delta-Notch pattern formation. The parameters used for the simulations are $R_N = R_D = \rho = \mu = 10$, $\Lambda = -14.32$, $D_r = 0.001$, $\xi = 0$, $\Delta\theta = \pi/2$, $T = 0.1$ and $v_0 = 0.31$. The shape parameter for the cells $p_0 > 3.82$, the so called fluidization threshold. (a)-(c) The spot-like Delta patterns keep re-arranging in space as a function of time. The circles correspond to manual tracking of the cluster shown in panels. (d) Plot of the Delta-Delta correlation function $G_s(r,\tau)$ shows the cell movement as a function of time. (e) Plot of the Delta-Delta correlation function $G_d(r,\tau)$ shows clear spatial pattern with a length scale of approximately 5 cell lengths. Although the shape of the function $G_d(r,\tau)$ does not change with τ, its amplitude decreases, thus indicating that the dynamic nature of the patterns.

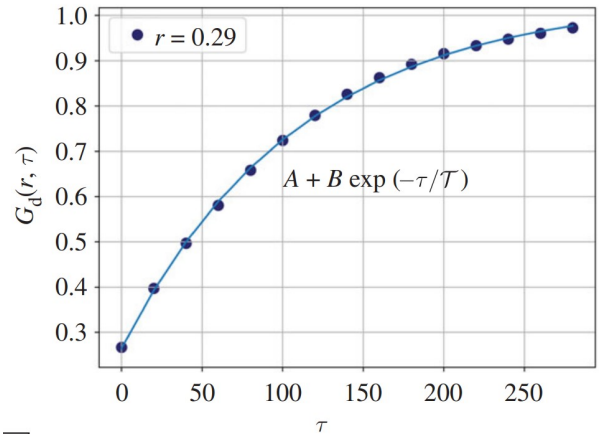

Figure 4.2: The magnitude of $G_d(r,\tau)$ as a function of τ for $r \approx 2.9$ is plotted as a function of time for the simulation parameters: $R_N = R_D = \rho = \mu = 10$, $\Lambda = -14.32$, $D_r = 0.001$, $\xi = 0$, $\Delta\theta = \pi/2$, $T = 0.1$ and $v_0 = 0.31$. An exponentially saturating function of the form $A + B\exp(-t/\mathcal{T})$ fits well to these values with $\mathcal{T} \approx 100$ and provides the time-scale for pattern re-arrangement.

0 [22, 23, 229]. First, we study the effect of uncorrelated cell movement on pattern formation by fixing $\xi = 0$, $v_0 = 0.31$, and $D_r = 0.001$ at different values of T. If the signaling rates are small, then the neighbor exchanges between the cells are too fast as compared to the signaling time-scales. As a result, we do not observe Delta-Notch patterns as for the static cell network. However, upon increasing the signaling rates by ten-fold, we recover back the circular, isolated patterns seen earlier.

In chapter 3, v_0 was almost zero but here we use $v_0 = 0.31$, much higher value to model motility. Interestingly, the patterns are now no longer static but keep spatially rearranging. The movement of the Delta patterns mainly depends on the dynamics of the cluster of Delta expressing cells, which in turn is dictated by the collective cell migration patterns that are governed by the underlying tissue mechanics and polarity dynamics of individual cells (Figures. 4.1a-c; Movies 14 and 15 in Appendix B). In the case where a particular cluster of Delta cells breaks apart, a new group of Delta expressing cells is created by the entry of new cells into a pre-exisiting nuclei of Delta expressing cells. On the other hand, there are cases where the entire group of Delta expressing cells migrates as a whole in which case the Delta patterns also take the same trajectory as the complete cluster. A combination of cellular movements and chemical patterns leads to an emergent time-scale for the spatial rearrangement of Delta clusters.

To quantify the spatio-temporal dynamics of these patterns, we calculate the Delta-Delta self and distinct parts $G_s(r,\tau)$ and $G_d(r,\tau)$, of the radial distribution function:

$$G_s(r,\tau) = \frac{1}{\kappa\mathcal{N}} \sum_{\alpha} \sum_{\substack{\alpha \\ r<|\mathbf{r}_{\alpha\alpha}|\leq r+\Delta r}} \langle D_\alpha(t) D_\alpha(t+\tau)\rangle_t, \tag{4.1}$$

$$G_d(r,\tau) = \frac{1}{\kappa\mathcal{N}} \sum_{\alpha} \sum_{\substack{\beta\neq\alpha \\ r<|\mathbf{r}_{\alpha\beta}|\leq r+\Delta r}} \langle D_\alpha(t) D_\beta(t+\tau)\rangle_t, \tag{4.2}$$

where, the normalization factor,

$$\kappa = \frac{1}{\mathcal{N}(\mathcal{N}-1)} \sum_{\alpha} \sum_{\alpha\neq\beta} \langle D_\alpha(t) D_\beta(t+\tau)\rangle_t$$

The idea behind the distinct part of the Delta-Delta radial distribution function (distinct part) function is to capture for every cell α at a given time t how much its Delta expression correlates with the Delta levels of every other cell β that is present within a particular distance $r < |\mathbf{r}_\beta - \mathbf{r}_\alpha| \leq r + \Delta r$ at time $t + \tau$. The plots of $G_d(r,\tau)$ as a function of r for different time-lags τ at $\Delta\theta = \pi/2$ and $T = 0.1$ are shown in Figure. 4.1d. The plot for each value of τ was obtained from the average of $G_d(r,\tau)$ over three set of simulations, each with 1600 cells. The initial configuration of polarity $\hat{\mathbf{p}}$ for individual cells was generated from uniform random orientation in the range $[-\pi,\pi]$ and uniform random concentration of Delta and Notch in the range $(0,1)$ for a given combination of simulation parameters. When $\tau = 0$, we see a decaying oscillatory pattern in space that is indicative of periodic Delta expression with the distance between the centers of neighboring Delta region of approximate 5 cells. For increasing values of τ, we see that the shape of $G_d(r,\tau)$ remains invariant, but the amplitude of the function decreases, thus indicating that the patterns are not stationary but diffuse in space. To quantify the rearrangement time-scale of the Delta patterns, we plot the amplitudes of the radial distribution function $G_d(r,\tau)$ corresponding to its first minima $r \approx 2.5$ as a function of time-lag τ (Figure. 4.2). After

fitting an expression of the form $A + B\exp(-\tau/\mathcal{T})$, the pattern re-arrangement time-scale $\mathcal{T} \approx 90$ emerges. We note that $\mathcal{T}$ is much greater than either the time-scale for signaling, ($\tau_s = 1/\mu \approx 0.1$) or that for cellular rearrangements ($\tau_r = L_c/v_0 \approx 3$) and is very likely an emergent time-scale. Such emergent features are common in active systems, but require a more detailed analysis that is beyond the scope of the current work [155, 185, 191]. We also run the simulation and plot the corresponding $G_d(r,\tau)$ function at $\Delta\theta = \pi/4$ $T = 0.9$ and $T = 0.94$. We observe that the correlation decays very fast as we increase the activation threshold and it becomes completely uncorrelated at higher values of activation threshold (Figure. 4.3).

The self-part of Delta-Delta radial distribution function captures for every α at a given time t how much does its Delta expression correlate with itself when it has moved a distance of $r < |\mathbf{r}_\beta - \mathbf{r}_\alpha| \leq r + \Delta r$ at time $t + \tau$. The plot of $G_s(r,\tau)$ as a function of r for different time-lags τ at $\Delta\theta = \pi/2$ and $T = 0.1$ are shown in Figure. 4.1e. The initial configuration for the simulation is same as described above. For increasing values of τ, we see that the amplitude peak of $G_s(r,\tau)$ decreases and shifts in space with time delay, thus indicating that the Delta cells are constantly moving.

We also study the effect of cell movement on pattern formation when the alignment strength ratio ξ/D_r is relatively high with $\xi = 0.25$, $v_0 = 0.31$, and $D_r = 0.1$. In this case, we see that stripe-like patterns of Delta expression are seen similar to the case when $v_0 = 10^{-4}$ (Figure. 4.4; Movies 14 and 15 in Appendix B). However, the patterns are more dynamic and, as opposed to the formation and breaking of clusters in the case of spot-like patterns when $\xi = 0$, we see that the stripes break and merge to continuously change their alignment.

Thus, we observe that the polarity and motility dynamics of cells, along with tissue mechanics, influence the signaling patterns and hence the spatio-temporal levels of Delta and Notch expression.

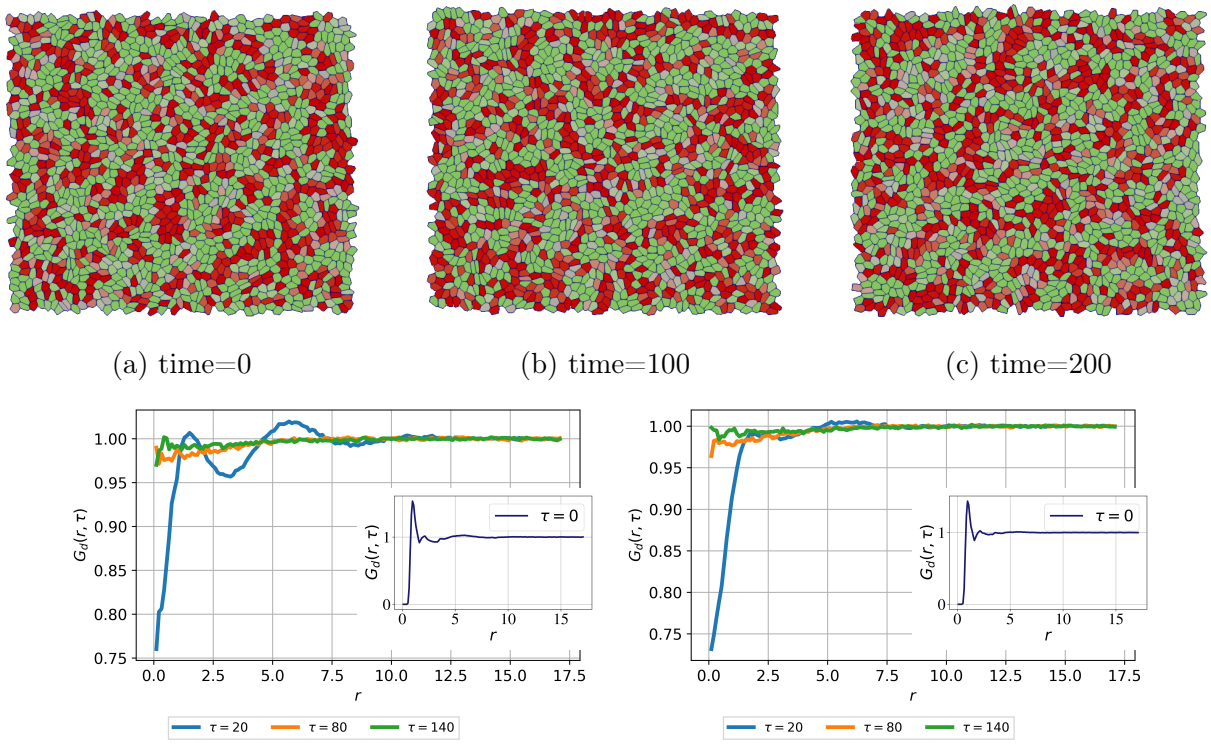

Figure 4.3: Screenshots and plots showing the effect of cell motility and tissue mechanics on Delta-Notch pattern formation. The parameters used for the simulations are $R_N = R_D = \rho = \mu = 10$, $\Lambda = -14.32$, $D_r = 0.001$, $\xi = 0$, $\Delta\theta = \pi/4$, $T = 0.9$ and $v_0 = 0.31$. The shape parameter for the cells $p_0 > 3.82$, the so called fluidization threshold. (a)-(c) At $T = 0.9$, the Delta patterns keep re-arranging in space as a function of time. (d,e) Plot of the Delta-Delta correlation function $G_d(r,\tau)$ at (d) $T = 0.9$ and (e) $T = 0.94$ shows clear spatial pattern with a length scale of approximately 5 cell lengths. Although the shape of the function $G_d(r,\tau)$ does not change with τ, its amplitude decreases, thus indicating that the dynamic nature of the patterns.

4.2 Discussion

In this chapter, we studied the effect of cell motility and tissue mechanics on the contact dependent signaling patterns. We observed that when the cells have motility and shape index beyond the fluidization threshold, the cells can rapidly change their connectivity due to which their signaling contacts are also modified. As a result, the expression patterns for Delta-Notch no longer remain static. Their dynamics is decided by the dynamics of the formation and breaking of Delta clusters, which in turn are governed by the motility patterns of the cells. When the polarity diffusion dominates, we see the formation of moving spot-like patterns, which we systematically quantified using the spatio-temporal radial correlation function for Delta expression. On the other hand, when the polarity alignment term dominates, we saw that stripe-like patterns arise. However, unlike for the static case, the stripes keep modifying their alignment by splitting and then merging with the other stripes – this dynamics being governed by cellular movements.

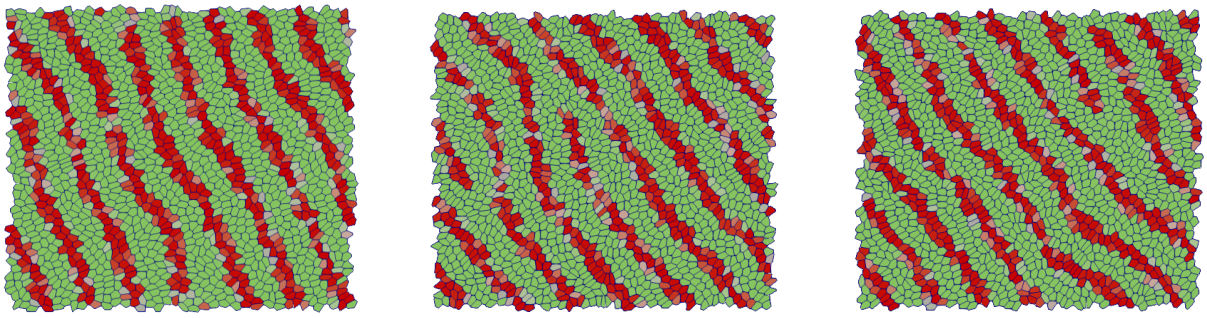

(a) time=0 (b) time=200 (c) time=500

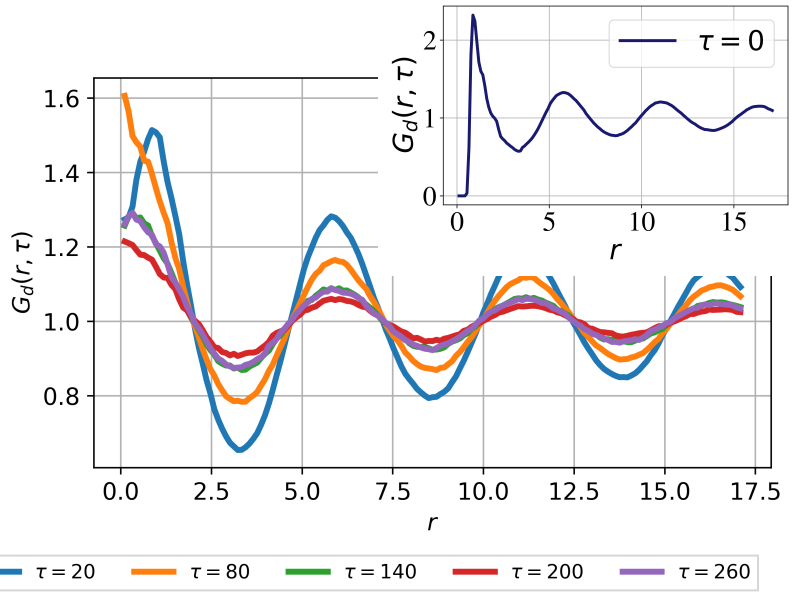

(d)

Figure 4.4: Screenshots and plots showing the effect of cell motility and tissue mechanics on Delta-Notch pattern formation. The parameters used for the simulations are $R_N = R_D = \rho = \mu = 10$, $\Lambda = -14.32$, $D_r = 0.1$, $\xi = 0.25$, $\Delta\theta = \pi/4$, $T = 0.5$ and $v_0 = 0.31$. The shape parameter for the cells $p_0 > 3.82$, the so called fluidization threshold. (a)-(c) The stripe-like Delta patterns keep re-arranging in space as a function of time. (d) Plot of the Delta-Delta correlation function $G_d(r, \tau)$ shows clear spatial pattern with a length scale of approximately 5 cell lengths. Although the shape of the function $G_d(r, \tau)$ does not change with τ, its amplitude decreases, thus indicating that the dynamic nature of the patterns.

Chapter 5

Role of Delta-Notch signaling molecules on cell-cell adhesion in determining heterogeneous chemical and cell morphological patterning

5.1 Introduction

Multicellular organisms are made of different tissues that are comprised of aggregates of various types of cells [5]. Across species, in these tissues, cells exhibit diverse morphologies at varying stages of their collective life-cycle [79, 148]. Nevertheless, many healthy tissues are comprised of cells of the same type and have similar protein expressions within them, resulting in overall homogeneity in their shape and size [199]. Hence, many epithelial tissues exhibit a striking regularity in the size and morphology of the constituent cells [87]. However, a number of diseased or tumor cells are pleomorphic and have a significant variation in shape and size within a tissue [60, 202]. It is known that morphology and mechanics of cells influence organ development and disease progression [38, 130, 211, 261]. Consequently, heterogeneity in cell size is generally an indication of an underlying pathology [87]. Indeed, such variations in shape and size of the cells are useful in the diagnosis of several cancers [64, 246].

Different types of normal sensory epithelia demonstrate heterogeneity in cell mor-

phology along with a characteristic spatial pattern [87]. For example, the olfactory epithelium (OE) that is involved in odor perception and resides inside the nasal cavity of mammals, contains larger supporting cells that surround the smaller olfactory cells and generate a mosaic pattern [51, 232]. In fact, the olfactory cells and supporting cells dynamically arrange themselves during development to create this arrangement [124]. Such mosaic patterns in cell morphologies are also observed in the auditory epithelium [243, 244] that is found in the ear canal. Studying the dynamic mechanisms that govern the distributions of cell shapes and sizes in any given tissue may therefore be important in understanding form and function of healthy tissues as well as the development of diseases such as cancer.

Cell shape, size, and position within a tissue are governed by physical forces, which could be generated either within individual cells or exerted from the surrounding tissue and transmitted via cell-cell junctions [61, 110, 192]. Specifically, the force transmission between the cells in a tissue and the associated deformation kinematics are largely governed by cadherin and acto-myosin complexes at the cell-cell junctions [183, 218, 253]. The dynamics of these molecules is in turn modulated by the underlying chemical signalling [165, 189]. Moreover, the signalling also simultaneously controls chemical patterning within the tissue by governing protein expressions within the cells and hence their biological fate [13, 132, 179]. Hence, an understanding of how the physical forces and the associated chemical signalling collectively modulate cell morphologies in tissues is crucial to get insights into the heterogeneous chemical and morphological patterns of cells in diseased and sensory epithelial tissues.

Size and shape of cells are strongly influenced by mechanical forces at its cell-cell boundary [24, 70, 135]. As observed in sensory epithelia, differential and cooperative adhesions and contractility among genetically heterogeneous cells impact cell shape, size, and cellular patterns [203, 242, 243]. For example, mosaic cellular patterning characterized by smaller supporting cells and larger olfactory cells in the tissue is reported to be due to heterophilic adhesion between multiple cell types such as hair cells and supporting cells [124, 203, 242, 243]. In a recent work, Cohen et al. [46] demonstrated that the mosaic pattern of the hair cells and supporting cells, and their combined spatial positioning in the auditory epithelium with respect to the pillar cells is also influenced by external mechanical forces.

There are many studies that investigate various aspects of heterogeneous cell morphology patterns in tissues. For example, though the exact origins of the mosaic patterns in olfactory epithelium are not well understood, it is known that the olfactory cells and supporting cells express different cadherins and nectins [124, 232]. It is also known that Delta-Notch signalling control the expression of these molecules either by repressing or upregulating [39, 72, 104, 139, 140, 262]. Similarly, in the auditory epithelium, members of the Notch pathway are involved in determining cell fates via lateral inhibition [125].

Differential cell adhesions, such as those mediated by integrins and cadherins/catenins, play an important role in morphogenesis [135, 236]. Their expression and modification are known to be linked to cell growth, intercellular signalling, cell differentiation, and apoptosis [112]. There is evidence that Notch signalling enhances cell-cell adhesion by inducing the expression and activation of cell adhesion molecules such as integrins [109, 176, 214]. Many studies further suggest that Notch is involved in controlling cell-cell adhesion in *Drosophila* eye cell [16]. Moreover, Notch signalling is linked to the adhesion force between cells expressing Notch receptors and Delta ligands [2]. Through modulation of cell adhesion, Notch also contributes to stem cell clustering [266]. For example, by enhancing integrin-mediated cell adhesion, Rap1b promotes Notch-signal-mediated development of hematopoietic stem cells [205]. Similarly, hepatic endothelial Notch activation regulates endothelial-tumor cell adhesion to protect against liver metastasis [214]. Additionally, periodic activation of Notch signalling is also shown to drive differential cell adhesion and coordinated adjustment of cell shape during feather branching in chicks [40]. Although, like Notch, Delta also plays a role in cell adhesion and motility [71], the extent of its direct contribution to these processes is not well known. However, there is some evidence, for example, that keratinocyte cohesiveness is promoted in cells that overexpress Delta1 [146].

It is known that Delta-Notch signalling typically relies on contact-based lateral inhibition to regulate the expression of Delta and Notch in tissues [30]. The dynamics of various spatio-temporal patterns that are formed during this signalling is addressed by a number of theoretical and computational models [15, 45, 47, 99, 226, 227]. It is known from these models that when the interactions between the cells are limited to the nearest neighbours, checkerboard pattern of Delta and Notch expressed cells are known to appear [15, 47]. On the other hand, some models demonstrate that when the contacts are created between non-adjacent neighbours due to cellular protrusions, then the dynamics

of components associated with these contacts can give rise to a wider range of Delta-Notch patterns in the tissue [15, 99]. Though these models delve into the intricacies of chemical pattern formation during Delta-Notch signalling, there are, to the best of our knowledge, very few models that also study the concomitant cell morphology patterns. However, as seen earlier, since the Delta-Notch molecules are also known to be involved in cell-cell adhesions, such chemical patterns also have the potential to be involved in controlling cell morphologies via the modulation of physical forces through adhesion molecules.

Thus far, there has no systematic theoretical or computational investigation of how these combined patterns concomitantly appear in the tissues, specifically in the context of contact based lateral inhibition signalling. Since, as discussed above, Delta-Notch signalling with lateral inhibition forms a wide variety of chemical patterns, we expect that a feedback between cell mechanics and signalling via modulation of cell-cell adhesivities could also give rise to a wide range of mechnochemical patterns in tissues. Hence, in this paper, we develop a simple mechanochemical vertex model of the tissue based on Delta-Notch signalling in which the expression levels of Notch and Delta in the cells is linked with the bond tension of the edges shared by them. The variations in bond tensions in turn can influence both cell morphologies and topological transitions in the tissue thus also influencing the signalling. In our model of lateral inhibition, we consider both the nearest neighbor interactions and long-range protrusional contacts. We systematically explore the broad range of chemical and morphological patterns in the tissue due to this mechanochemical process. We propose that, in general, a simple feedback between chemical signalling in cells and their mechanical properties can give rise to wide range of chemical and morphological patterning of cells in the tissues.

5.2 Methods and Model

Delta-Notch signalling, which relies on contact-based lateral inhibition, is used as the model chemical system in the present paper [15, 45, 47, 99]. A model for Delta-Notch kinetics is constructed by tracking the concentration of Notch and Delta in each cell N_α and D_α, respectively, in cell α. The growth rate of Notch in cell α is activated by the presence of Delta in its contact neighbours, whereas the rate of Delta a cell is inhibited

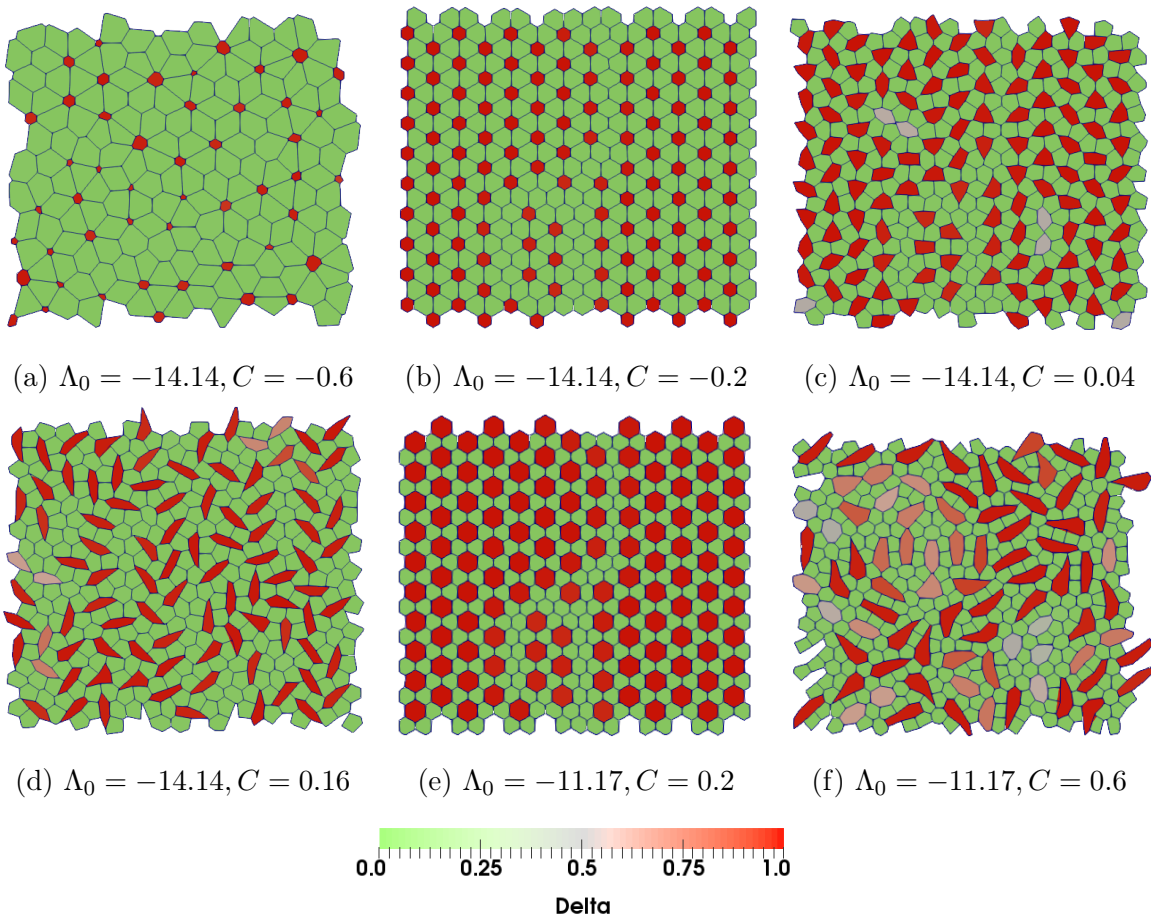

(a) $\Lambda_0 = -14.14, C = -0.6$ (b) $\Lambda_0 = -14.14, C = -0.2$ (c) $\Lambda_0 = -14.14, C = 0.04$

(d) $\Lambda_0 = -14.14, C = 0.16$ (e) $\Lambda_0 = -11.17, C = 0.2$ (f) $\Lambda_0 = -11.17, C = 0.6$

Figure 5.1: Delta-Notch patterns formed for Delta-dependent adhesivity $\Lambda_{\alpha\beta}$ (Eq. 5.4) with coupling coefficient $C =$ (a) -0.6, (b) -0.2, (c) 0.04, (d)0.16 (e) 0.2 and (f) $C = 0.6$. In (a)-(d), the basic edge adhesivity $\Lambda_0 = 14.14$, corresponding to the solid-like limit, and in (e)-(f), $\Lambda_0 = -11.17$, corresponding to the solid-like limit of tissue behaviour. In all these simulations $\beta_j/\beta_p \approx 100$, $B = 1$, $v_0 \approx 0$, $K = 1$, and $\Gamma = 1$.

by the presence of Notch within itself. These kinetics are represented as follows [15]:

$$\frac{dN_\alpha}{dt} = R_N \frac{\bar{D}_\alpha^2}{a + \bar{D}_\alpha^2} - \mu N_\alpha, \tag{5.1a}$$

$$\frac{dD_\alpha}{dt} = R_D \frac{1}{b + N_\alpha^2} - \rho D_\alpha, \tag{5.1b}$$

$$\bar{D}_\alpha = \frac{1}{2}[\beta_j \bar{D}_j^\alpha + \beta_p \bar{D}_p^\alpha], \tag{5.1c}$$

where $R_N|\mu$ and $R_D|\rho$ are, respectively, the rate of production | decay of Notch and Delta and $\bar{D}_\alpha$ is the mean Delta concentration in the cells that are in contact. β_j is the contact weight provided for the junctional contacts and β_p is the contact weight for protrusional contacts, such that $\beta_j + \beta_p = 1$. The junctional and protrusional averages are:

$$\bar{D}_j^\alpha = \frac{1}{n_j} \sum_{\gamma \in n_j} D_\gamma \text{ and} \tag{5.2a}$$

$$\bar{D}_p^\alpha = \frac{1}{n_p} \sum_{\gamma \in n_p} D_\gamma, \tag{5.2b}$$

where n_j denotes the number of cells that are in contact with cell α via junctional contact while the n_p is the number of cells that are in contact via protrusions. The details of the procedure to obtain $\bar{D}_p^\alpha$ due to protrusional contacts based on a threshold T are given in Section 2 of Ref. [15].

The tissue mechanics is implemented using a well established vertex model [22, 24, 70, 74], where the cells in the tissue monolayer are represented by the polygons having vertices and edges. For a tissue having N cells, the total work function U of the tissue

monolayer is given by

$$U = \sum_{\alpha=1}^{\mathcal{N}} [K_\alpha (A_\alpha - A_{\alpha,0})^2 + \Gamma_\alpha L_\alpha^2] + \sum_{\text{edges:}\gamma\beta} \Lambda_{\gamma\beta} l_{\gamma\beta}, \tag{5.3}$$

where, $\mathcal{N}$ is the total number of cells in the monolayer and K_α, A_α, $A_{\alpha,0}$, Γ_α, and L_α are the area stiffness, current area, preferred area, boundary contractility and perimeter, respectively, of cell α. $\Lambda_{\gamma\beta}$ is the differential line tension at junctions between two cells. $l_{\gamma\beta}$ is the length of the edges shared between cells γ and β and is summed over all the bonds in the tissue. The first and second terms result, respectively, from area elasticity and boundary contractility of the cells while the third term results from the forces at cell-cell junctions due to the acto-myosin contractility and nectin-cadherin adhesivity. $\Lambda_{\gamma\beta}$ is the differential adhesion parameter of cell-cell junction edge of length $l_{\gamma\beta}$ shared by cells γ and β.

In the model we couple the $\Lambda_{\gamma\beta}$ with Delta-Notch signalling using the following equations. We assume that the line tension parameter may depend on the Delta concentration of the two cells sharing the edge:

$$\Lambda_{\gamma\beta} = \Lambda_0[1 + C(|D_\gamma + BD_\beta|)] \tag{5.4}$$

where, D_γ and D_β are the Delta concentrations in the cells sharing the edge $\gamma\beta$. C and B are the coupling coefficient and sign constant respectively. Secondly, we asume that the line tension parameter depends on the Notch concentration of the two cells sharing the edge:

$$\Lambda_{\gamma\beta} = \Lambda_0[1 + C(|N_\gamma + BN_\beta|)] \tag{5.5}$$

where, N_γ and N_β is the Notch concentrations in the cells sharing the edge $\gamma\beta$. The values of $B = 1$ $B = -1$, model the cases where the Delta (Notch) levels in the neighboring cells α and β contribute cooperatively and antagonistically to the junctional adhesivity, respectively. Our goal in this paper is to explore the qualitative consequences of the dependence of adhesion on Delta or Notch. Since not much is known about this kind of

coupling, the linear expression we have chosen represents a necessary first step. Similar approach has been done in many active systems, for instance, in which the active stress due to actomyosin is equated with the experimentally measured myosin intensity [162, 204].

The elastic forces act on each cell vertex i arising from the work function U can be calculated as $\mathbf{F}_i^{\text{elastic}} = -\frac{\partial U}{\partial \mathbf{r}_i}$, where $\mathbf{r}_i$ is the position of vertex i. Along with the mechanical forces, the cells in the tissues have front-rear polarity and self-propelled motility. Therefore, the vertices of cells in the tissue move as a result of mechanical and active forces as [24, 234]

$$\mathbf{F}_i^{\text{active}} = \eta v_0 \frac{1}{n_i} \sum_{\beta} \hat{\mathbf{p}}_\beta, \tag{5.6}$$

where n_i is the number of cells β shared by vertex i, $\hat{\mathbf{p}}_\beta$ is the polarity of the cell β which acts in the direction of cell polarization, v_0 and η are the magnitude of velocity and viscous drag respectively acting on each cell vertex. The external viscous force balances the total force on vertex i, which is a combination of elastic and active forces. In our system, the cells also exchange neighbours (known as T1 transitions [73]) that promote tissue fluidity. As a result, the vertex position is described by the following dynamical equation of evolution

$$\eta \frac{d\mathbf{r}_i}{dt} = \mathbf{F}_i^{\text{elastic}} + \mathbf{F}_i^{\text{active}}. \tag{5.7}$$

The polarity of each cell is modeled by keeping in mind the observation that the cells tend to align themselves with the polarity director of the neigbouring cells ($\pm\mathbf{p}$). The cells also perform random rotational diffusion [17, 23, 36, 100, 170] along with the above alignment. Hence, the polarity of each cell is modeled as,

$$\frac{d\theta_\alpha}{dt} = \zeta_\alpha, \tag{5.8}$$

where θ_α is the polarity angle of cell. The cell polarity is represented by: $\hat{\mathbf{p}}_\alpha = \cos\theta_\alpha \hat{\mathbf{e}}_x + \sin\theta_\alpha \hat{\mathbf{e}}_y$. The polarity for any cells rotates with a random rotational diffusive noise that

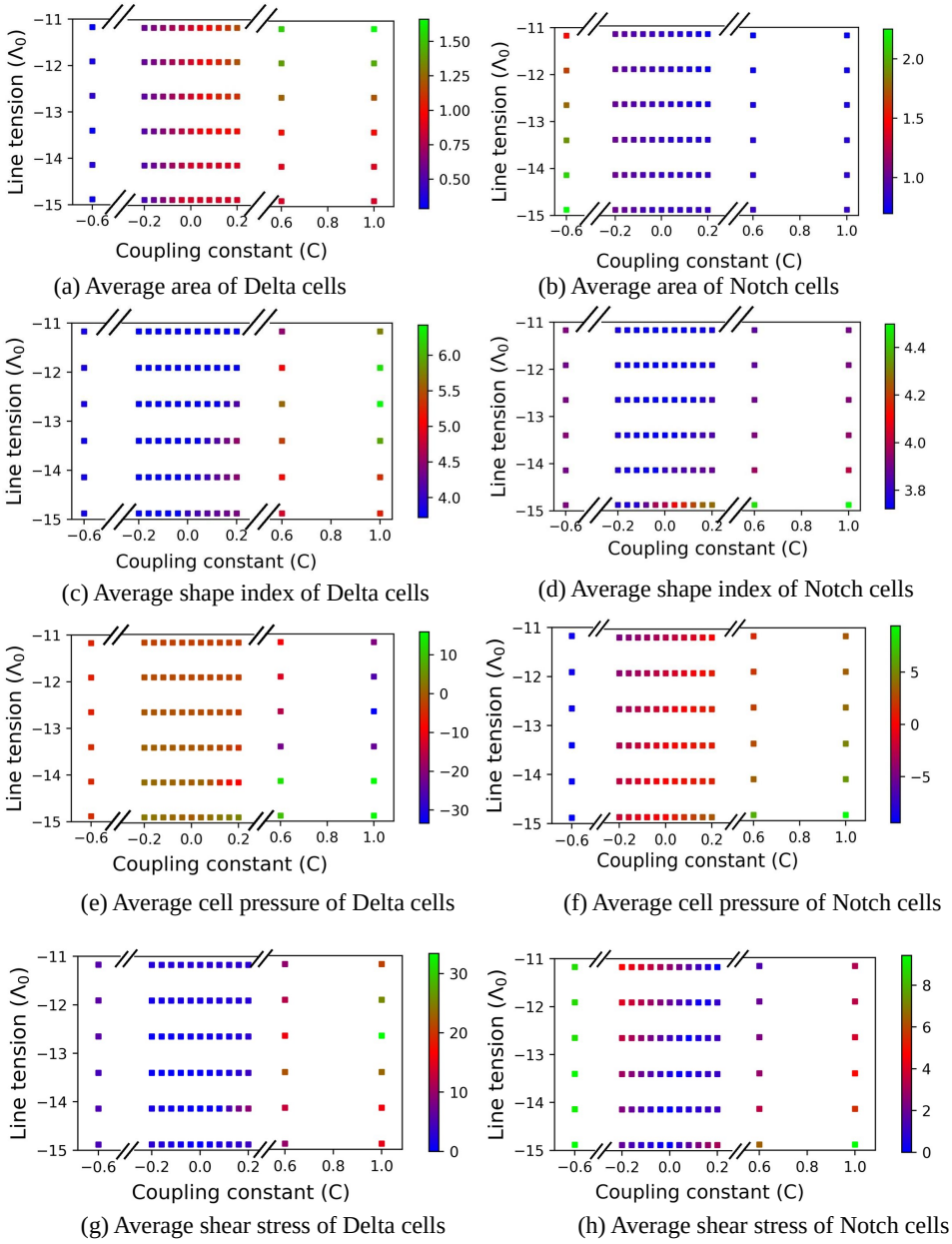

(a) Average area of Delta cells

(b) Average area of Notch cells

(c) Average shape index of Delta cells

(d) Average shape index of Notch cells

(e) Average cell pressure of Delta cells

(f) Average cell pressure of Notch cells

(g) Average shear stress of Delta cells

(h) Average shear stress of Notch cells

Figure 5.2: Effect of basic adhesivity (Λ_0) and coupling constant (C) on average features of patterns observed with Delta-dependent adhesion Eq. 5.4. (a,b) Average area of Delta and Notch cells respectively in a confluent tissue as a function Λ_0 and C (c,d) Average current shape index $\left\langle \frac{L_\alpha}{\sqrt{A_\alpha}} \right\rangle_\alpha$ of Delta and Notch cells, respectively, in a confluent tissue as a function of Λ_0 and C. (e, f) Average cell pressure of the Delta and Notch cells, respectively (see Appendix C for definition of stress for a vertex model). Positive and negative pressure values correspond, respectively, compression and tension. (g, h) Magnitude of shear stress of Delta and Notch cells, respectively (see Appendix C). The other parameters are: $\beta_j/\beta_p \approx 100$, $B = 1$, $v_0 \approx 0$, $K = 1$, $\Gamma = 1$

.

is represented as,

$$\begin{aligned} \langle \zeta_\alpha(t)\zeta_\alpha(t')\rangle &= 2D_r\delta(t-t'), \text{ and} \\ \langle \zeta_\alpha(t)\rangle &= 0. \end{aligned}$$

where $\zeta_\alpha(t)$ is a white-noise process with zero mean and standard deviation $\sqrt{2D_r}$.

Initially the cells were organised in a perfect hexagonal lattice with periodic boundary conditions and containing 400 cells. The model is implemented in CHASTE [73] and different parameters used in our model are non-dimensionalised as discussed in Appendix C and shown in Table C.1. The minimal diameter d of each hexagon was taken as the length scale in our simulations. The base value of line tension Λ_0 is chosen such that the shape index for any cell $p_0 = -\frac{\Lambda_0}{4\Gamma\sqrt{A_0}} \approx 3.81$, corresponding to the so called fluidisation limit for the vertex model. In our simulations, since we keep $A_0 = \sqrt{3}/2$ and $\Gamma = 1$, tissue fluidisation occurs for $\Lambda_0 \approx -14.13$, and any variations in Λ_0 in our simulations are made with respect to this value. T1 transitions or neighbour exchanges in the tissue are attempted at every time step such that when the length of any edge $l < \epsilon_c = 0.06$, the bond is closed and opened up in an orientation perpendicular to the original with a new length $l = \epsilon_o = 0.1$, i.e., $\epsilon_c < \epsilon_o$ [73]. In this framework, by default, more than three-way vertices are not permitted.

5.3 Results

Depending on the concentration of Delta and Notch, any cell α can exclusively be a Delta cell ($D_\alpha \approx 1$ and $N_\alpha \approx 0$) or a Notch cell ($D_\alpha \approx 0$ and $N_\alpha \approx 1$), or something in between with $D_\alpha \approx N_\alpha$. In a tissue with two cell types, namely Delta (D) and Notch (N), any pair of cells can potentially share three types of edges, DD, NN and DN. The Delta-Notch kinetics with only junctional contacts gives rise to checkerboard patterns of Delta and Notch cells [15, 47]. In such a scenario, the cell edges are shared only between Delta-Notch cells and Notch-Notch cells, giving rise to only two types of bonds DN and NN. However, the Delta-Notch kinetics with protrusional contacts gives rise to more complex patterns involving groups of both Delta and Notch cells. In such cases, the cell edges are

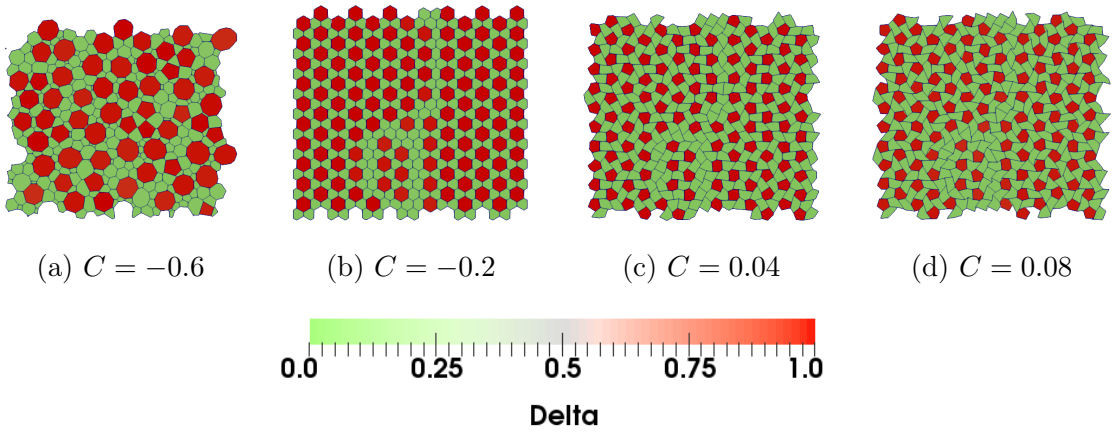

(a) $C = -0.6$ (b) $C = -0.2$ (c) $C = 0.04$ (d) $C = 0.08$

Figure 5.3: Steady-state patterns formed with Notch-dependent adhesion (Eq. 5.5) for (a-d) $C = -0.6, -0.2, 0.04, 0.08$ and $B = 1$ with only junctional contacts. Other parameters have fixed values, $\beta_j/\beta_p \approx 100$, $B = 1$, $v_0 \approx 0$, $K = 1$, $\Gamma = 1$. $\Lambda_0 = -14.14$ for all the cases, corresponding the fluid-like limit of the tissue. Modified checkerboard patterns of Delta-Notch with (a,b) bloated and (c, d) distorted Delta cells are seen.

shared between all three types of bonds.

In our model, if all the cells in the tissue are of the same type (N or D), cell-cell adhesion will be equal (Λ_{NN} or Λ_{DD}) for all pairs of contacting cells. In this case, the effective shape index of the cells can get homogeneously modified and, along with cell motility v_0, can influence the morphology of the cells [24]. On the other hand, when the cells in our model tissue exhibit a Delta-Notch pattern, then, depending on the N and D expression in the cells, adhesivity between any pair of cells can potentially achieve three different values $\Lambda_{DD}, \Lambda_{DN}$, or Λ_{NN}. Hence, in such a scenario, the chemical pattern dictates cell shape and size by modulating cell-cell adhesivity. In our previous work [15] (coupling parameter $C = 0$), we had seen that the existence or stability of the Delta-Notch checkerboard pattern that appears in junctional contact signalling depends on the relative time scales associated with signalling ($1/R_D, 1/R_N, 1/\rho, 1/\mu$ in Eq. 5.1) and cell neighbour exchanges that depend on cell motility (v_0). For $v_0 = 0$, we get a steady checkerboard pattern (Movie A). For intermediate values of v_0 ($v_0 = 0.1$, Movie B in Appendix C), the checkerboard pattern is initiated but is unable to be steadily maintained due to persistent exchange of cell neighbour. When the motility is much higher ($v_0 = 0.3$, Movie C in Appendix C), the checkerboard pattern fails to establish because the cells lose their nearest neighbour contacts before the checkerboard pattern could be established. Since

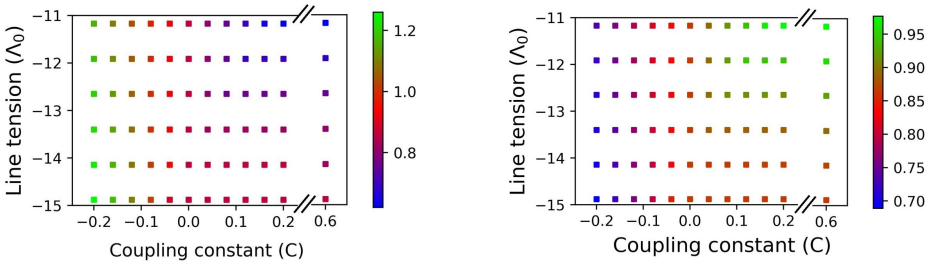

(a) Average area of Delta cells

(b) Average area of Notch cells

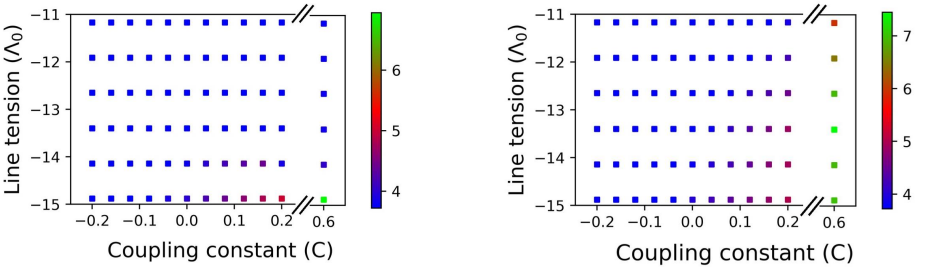

(c) Average shape index of Delta cells

(d) Average shape index of Notch cells

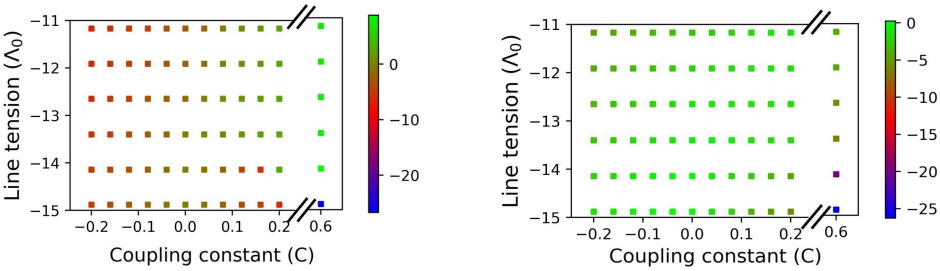

(e) Average cell pressure of Delta cells

(f) Average cell pressure of Notch cells

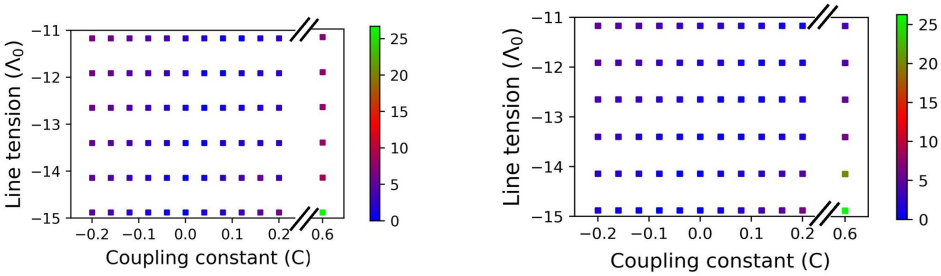

(g) Average shear stress of Delta cells

(h) Average shear stress of Notch cells

Figure 5.4: Effect of coupling constant (C) and basic adhesivity (Λ_0) on average features of patterns formed with Notch-dependent adhesion (Eq. 5.5): (a, b) Phase diagram for the average cell area of Delta and Notch cells in a confluent tissue as a function Λ_0 and C (c, d) Phase diagram for average current shape index $\left\langle \frac{L_\alpha}{\sqrt{A_0}} \right\rangle_\alpha$ of Delta and Notch cells in a confluent tissue as a function of Λ and C. (e-h) Phase diagram showing average cell pressure and shear stress in Delta and Notch cells (see Appendix C). The other parameters are: $\beta_j/\beta_p \approx 100$, $B = 1$, $v_0 \approx 0$, $K = 1$, $\Gamma = 1$.

the addition of v_0 did not add any interesting features in junctional contact signalling, we keep $v_0 = 0$ for this case (Secs. 5.3.1 and 5.3.2) while using $R_D = R_N = \rho = \mu = 1$ for the Delta-Notch kinetics [15]. On the other hand, in the case of protrusion dependent signalling (Section 5.3.3), although neighbour exchanges still take place due to non-zero v_0, protrusion-based contacts can still be formed with non-nearest neighbours. Consequently, we found that the Delta-Notch patterns are more complex and remain comparatively stable in time. Hence, in this case (Sec. 5.3.3), we use non-zero cell motility ($v_0 = 1$) while conservatively increasing the Delta-Notch kinetic parameters by a factor of 10 ($R_D = R_N = \mu = \rho = 10$) so that the signalling rate keeps up with cell neighbour exchanges [15].

5.3.1 Cell morphologies with Delta-dependent adhesion and junctional contact signalling

The model with Delta-dependent adhesion (Eq. 5.4) and junctional contact signalling ($\beta_j \gg \beta_p$ in Eq. 5.1c) shows two types of behaviour depending on the coupling coefficient C and parity of B. Since in signalling based on junctional contacts we get a checkboard pattern for Delta-Notch, we broadly get only two types of bonds NN and DN.

Effect of C and Λ_0 when $B = 1$

For Eq. 5.4, we first keep $B = 1$, i.e., cooperative adhesion between the neighboring cells, and vary C between negative and positive range for different values of Λ_0. This coupling results in the modification in the bond-tension parameter for DD and DN cells. The morphological configuration of the cells depends on the minimization of the work function in Eq. 5.1 and is subject to two constraints: (1) the total area of N and D cells is conserved and (2) due to lateral inhibition from Delta-Notch signalling between the nearest neighours, any steady state configuration with neighbouring D cells are not possible. As a result, the terms that ultimately decide the morphology of the cells in the tissue are, the (i) absolute and the relative values of bond energies Λ_{DN} and Λ_{NN}, (ii) the contractile part of the tissue work function, and (iii) the area deformation energy (Eq. 5.3). The overall configuration of D and N cells can thus appear from the competition between

area deformation and elongation of the cells subject to the constraints from signalling and total tissue area.

A few illustrations of the Delta-Notch and cell morphology patterns in the tissue from these parameters are shown in Fig. 5.1. When $C < 0$ and $\Lambda_0 = -14.14$, at steady state, $\Lambda_{DN} > \Lambda_{NN} \approx \Lambda_0$, resulting in smaller DD bonds and longer NN bonds. Such a combination gives rise to smaller sized Delta cells interspersed within bigger Notch cells (Fig. 5.1a,b; Movies 1 and 2 in Appendix C). For a much lower value of $C = -0.6$ (Fig. 5.1a; Movie 1 in Appendix C), we also observe Delta cell apoptosis, i.e., the cell number decreases with time and reaches a fixed number at steady state (Appendix C Fig. C.1). For a given Λ_0, increase in the value of C leads to a decrease in Λ_{DN} as a result of which the DN bonds become longer causing an increase in the size of Delta cells. When $C > 0$, Λ_{DN} decreases further and to lower the overall bond energy, the cells have a choice of either increasing their overall size by growing in area or increase their perimeter by elongating. Since the total area of the tissue is conserved, any increase in the area of D cells has to be accompanied with a corresponding decrease in the area of N cells. However, since $\Lambda_{NN} \approx \Lambda_0$ is mostly independent of C in the current case, the size of NN bonds are not expected to modify significantly with change in C. Consequently, we find that for $C > 0$, the D cells are mostly elongated to accommodate the overall increase in the bond size of D cells (Figs. 5.1b-d; Movies 2-4 in Appendix C).

The bond lengths DN and NN also directly depend on the value of Λ_0. Increase in Λ_0 would lead to the shortening of DN bonds and hence reduction in the overall size of N cells. In this case, when $C > 0$, $\Lambda_{DD} < \Lambda_{NN} \approx \Lambda_0$ due to which the length of DD bonds is expected to be larger than the NN bonds. Hence, D cells have the option to either elongate or increase in area, depending on the magnitude of C. For lower values of C, in order to make up for the tissue area left behind by the diminished N cells, the D cells increase in size (Fig. 5.1e; Movie 5; Appendix C). However, increase in C leads to a further decrease in Λ_{DN} due to which longer DN bonds are favorable. But since the total area of the tissue does not change, in this case, the D cells become elongated (Fig. 5.1e; Movie 6 in Appendix C). Thus we see that even such a simple coupling between cell-cell adhesivity and the concentration of signalling molecules, can give rise to a variety of cell morphological patterns in the tissue.

We now quantify the size/shape of Delta and Notch cells in the tissue for various combinations of Λ_0 and C_α. We define a Delta cell as a cell with $D_\alpha > 0.5$ and Notch cell as the cell $D \leq 0.5$. However, we find that the Delta and Notch cells typically have $D \approx 1$ and $D \approx 0$, respectively. The effective size of Delta and Notch cells is estimated by calculating their mean area (Fig. 5.2a,b; Appendix C). We can see from Fig. 5.2a that for a given value of Λ_0, the size of Delta (Notch) cells increase (decrease), respectively, with increasing strength of coupling constant C. This trend could be interpreted by realising that the corresponding line tensions Λ_{DN} and Λ_{NN} decrease and approximately remains the same (Λ_0), respectively, with increasing C thus making D cells bigger at the expense of N cells since the overall tissue area remains constant. To get insight into the shape of the cells, we calculated mean of the shape index $s_\alpha = P_\alpha/\sqrt{A_\alpha}$ of every Delta or Notch cell α, where P_α and A_α are the actual perimeter and area, respectively, of the cell. (Fig.5.2c,d). The average current shape index of the Delta cells ($P_\alpha/\sqrt{A_\alpha}$) increases as we increase the coupling constant from negative to positive. At negative value of $C = -0.6$ the the cells are regular hexagons and the shape index is lower ($s \approx 3.72$), whereas at the other extreme, when $C = 1$, their shape index is higher since the cells become elongated (Fig. 5.2c). On the other hand, Notch cells are comparatively less susceptible to elongation (Fig. 5.2) since Λ_{NN} is almost insensitive to C.

For completeness, we also study how Delta-Λ coupling influences the average stress in the cells. We quantify the average shear stress and average pressure, respectively, as the corresponding stress equivalents of cell shape and size of the Delta and Notch cells (see Appendix C and Figs. 5.2e-h). The average shear stress depends only on the effective tension that depends Λ_0, C, and the overall elongation of the cells (Eq. C.2; Appendix C). Similar to cell shape index, we find that the average shear stress in the Delta cells increases with C. Moreover, for larger values of $C > 0$, the shear stress shows a non-monotonous behaviour as also observed for average shape index (Fig. 5.2c). However, unlike shear stress, average cell pressure does not show the same qualitative correspondence with average cell area. For example, unlike average cell area, the average cell pressure is non-monotonic with respect to C for most values of Λ_0. This behavior could be understood by noting that in our case, cell pressure (Eq. C.2; Appendix C) is dominated by the value of bond tensions as compared to area deformation. Consequently, cell area mainly influences cell pressure in so much as it changes the bond lengths. Consistently,

we find that when Λ_0 is lower, the pressure is higher (> 0) and becomes more negative (tensile) with increasing Λ_0. In Notch cells, the average cell pressure goes from tensile to compressive with increasing C and shows the same trend as that for cell area. However, in this case, shear stress exhibits non-monotonicity with C, although the variation in the stress values are much lesser when compared with that of the Delta cells.

In this section, we used $B = 1$, i.e., positive coupling between the neighbours (Eq. 5.4). However, since as described above, we do not have DD cells in the system due to lateral inhibition, the use of $B = -1$, i.e., anti-coupling between the neighbouring cells does not change the overall nature of patterns of Delta-Notch and cell morphologies.

5.3.2 Cell morphologies with Notch-dependent adhesion and junctional contact signalling

We assume here that the adhesion $\Lambda_{\gamma\beta}$ for the cell bond shared between cells γ and β is differential and depends on Notch signals of cells γ and β (Eq. 5.5). The simulations show two different types of behaviour depending on the coupling coefficient C and Λ_0. As discussed earlier, in junction based signalling we get only two types of bonds NN and DN. We perform the simulations by fixing $B = 1$ and varying Λ_0 and C. The definitions of N and D cells remain the same as in the previous sub-section on Delta-dependent bond tensions.

Effect of C and Λ_0 when $B = 1$

First we vary C from $C = -0.6$ to $C \approx 0.1$, while keeping $\Lambda_0 = -14.14$, near the fluidisation threshold. When $C < 0$, on average, $\Lambda_0 < \Lambda_{DN} < \Lambda_{NN}$ at the steady state, as a result of which the length of the bonds $l_{NN} < l_{DN}$. Consequently, we get larger Delta cells and smaller Notch cells (Figs. 5.3a,b; Movies 7 and 8 in Appendix C). When $C > 0$, on average $\Lambda_{NN} < \Lambda_{DN} < \Lambda_0$ at the steady state, due to which the bond lengths $l_{NN} > l_{DN}$ on average. Moreover, with increasing C, as expected (Eq. 5.5), Λ_{NN} and Λ_{DN} falls more rapidly than for the Delta-dependent adhesion (Eq. 5.4). Consequently, in such cases, we see smaller Delta cells and deformed and irregularly shaped Notch cells

(Fig. 5.3c,d; Movies 9, 10a and 10b in Appendix C).

Similar to Fig. 5.3, we now quantify cell deformations and the associated internal stresses as a function of C and Λ_0 for Notch-dependent adhesions. In general, the average area (Fig. 5.4a) and isotropic pressure (Fig. 5.4e) of Delta cells decrease as, for a given Λ_0, we increase the value of coupling constant C from negative to positive, whereas the average area (Fig. 5.4b) and internal pressure (Fig. 5.4f) of Notch cells correspondingly increase. This trend is almost the reverse of that seen earlier in Fig. 5.2ab for Delta-dependent adhesivity. The average shape index, $s = \langle P_\alpha/\sqrt{A_\alpha}\rangle_\alpha$, of the Delta cells is relatively insensitive to changes in C (Fig. 5.4c). On the other hand, though s for the Notch cells is insensitive to C for lower values of C, when $C > 0$, the Notch cells become highly irregular leading to increase in s (Fig. 5.4d). As expected, the average shear stress in the Delta (Fig. 5.4g) and Notch (Fig. 5.4h) cells follow similar trends with C as the shape index.

Between the current and the previous subsection, we explored the role of Delta (Eq. 5.4) and Notch (Eq. 5.5) dependent adhesivity on cellular morphology patterning during Delta-Notch signalling via junctional contacts. As discussed before, the cell morphological patterns depend on the values of Λ_{DN} and Λ_{NN}, which in turn depend on the levels of N or D levels. DD junctions are not allowed due to lateral inhibition. As before, if we make an idealised assumption that in a Notch cell $N = 1, D = 0$, and for a Delta cell $N = 0, D = 1$, for Delta-dependent signalling (Eq. 5.4) and $B = 1$ (cooperative adhesion), we get

$$\Lambda_{NN} = \Lambda_0,$$
$$\Lambda_{DN} = \Lambda_0(1 + C).$$

If, we solve the equations for C and Λ_0, we get $\Lambda_0 = \Lambda_{NN}$ and $C = \Lambda_{DN}/\Lambda_{NN} - 1$. Similarly, for Notch-dependent adhesivity, we have

$$\Lambda_{NN} = \Lambda_0(1 + 2C),$$
$$\Lambda_{DN} = \Lambda_0(1 + C).$$

By solving the two equations above, we get, $\Lambda_0 = 2\Lambda_{DN} - \Lambda_{NN}$ and $C = \frac{1-r}{2r-1}$, where $r = \Lambda_{DN}/\Lambda_{NN}$. Thus, in principle, for any combination of Λ_{NN} and Λ_{DN}, we could obtain the equivalent parameters Λ_0 and C for both Delta and Lambda dependent adhesivity that should on average produce the same cell morphological patterns. In this work, we have considered the individual effect of D or N concentration on cell-cell adhesivity, Λ (Eqs. 5.4 and 5.5). However, even if their combined effect on Λ is included in the model, similar to individual D or N coupling, the overall concentration levels would still give rise to effective values of Λ_{DN} and Λ_{NN}. Hence, as per the discussion above, we do not expect any qualitative changes in our observations (Figs. 5.1-5.4) in such a scenario. Similarly, in our model, the relation between N or D and Λ is taken to be linear (Eqs. 5.4 and 5.5). Even if these couplings were nonlinear, by using the same logic as above, we would still expect qualitatively similar cell shape patterns as in this work. However, the effective coupling coefficient C is expected to be re-scaled depending upon the exact functional form of the combined/nonlinear coupling.

5.3.3 Cell morphologies with Delta-dependent adhesion and protrusional contact signalling

We now explore the role of long-range or protrusional contacts on the combined chemical and cell morphology patterns. The model for protrusional contacts is already mentioned in Section 5.2 (Eq. 5.1) and is discussed in detail in Ref. [15]. As seen there, the Delta-Notch patterns during protrusional contacts show a wide variety of patterns in which all three possible contacts DD, DN and NN are possible. In this model, cell polarity, which undergoes random rotational diffusion in time, acts as a surrogate for the protrusion orientation. In our earlier work, we had performed a systematic analysis of the protrusional and cell motility parameters on the resulting Delta-Notch patterns [15]. Based on this knowledge, we fix the simulation parameters for polarity dynamics and protrusional contacts as $\beta_j/\beta_p = 0.01$, $\Lambda_0 = -14.32$, $v_0 \approx 0.1$, $D_r = 0.001$, $\rho = 10$, $T = 0.9$, $\Delta\theta = \pi/4$, $K = 1$, $\Gamma = 1$, $\rho = \mu = R_N = R_D = 10$. These parameters ensure that the tissue is above the fluidisation limit, the cellular junctions are dynamic, and the Delta Notch patterns would mainly result from protrusional contacts and have stable spatiotemporal pattern.

As we get all three types bonds in protrusion based signalling, i.e., NN, DN, and DD, depending on the coupling coefficient C and the sign of constant B, the model with Delta or Notch-dependent adhesion is expected to show different behavior for the combinations (i) $C > 0, B = 1$, (ii) $C > 0, B = -1$, (iii) $C < 0, B = 1$, and (iv) $C > 0, B = -1$.

5.3.4 Protrusional signalling with Delta dependendent adhesivity

When $C = 0$, there is no coupling between the Delta or Notch levels in the cells and cell adhesivity. As a result all the bond tensions have the same value, i.e., $\Lambda_{DD} = \Lambda_{DN} = \Lambda_{NN} = \Lambda_0$. The corresponding chemical pattern (Fig. 5.5a; Movie 11 in Appendix C) is the same as that seen earlier in Ref. [15], Fig. 5.3e, where a percolating pattern of Delta cells is interspersed in a matrix of Notch cells.

When $B = 1$ and $C < 0$, at steady state, $\Lambda_{DD} > \Lambda_{DN} > \Lambda_{NN}$ giving the smallest length for DD bonds, intermediate for DN bonds and the largest for NN bonds, i.e., $l_{NN} > l_{DN} > l_{DD}$. Such bond tension structure gives rise to very small D cells that are nestled within D cells and with generally larger N cells that surround the D cell patches (Fig. 5.5b; Movie 12 in Appendix C). Despite the heterogeneities in cell size, the tissue retains the overall structure of the chemical pattern generated when $C = 0$.

When $B = 1$ and $C > 0$, $\Lambda_{NN} > \Lambda_{DN} > \Lambda_{DD}$. Hence, bonds between DD cells are preferred the most, followed by DN bonds, with NN bonds being the least preferred. Consequently, cells have relatively smaller NN bonds and elongated DD bonds, i.e, $l_{NN} < l_{DN} < l_{DD}$. However, as discussed earlier, the patterns have to respect the total area constraint and underlying signalling kinetics. Consequently, we get patches of elongated D cells that lie interspersed in a group of N cells (Fig. 5.5c; Movie 13 in Appendix C).

When $B = -1$ and $C < 0$, at steady state the $\Lambda_{NN} = \Lambda_{DD} < \Lambda_{DN}$. This situation is very similar to a collection of D and N cells with similar bond tensions but separated from each other by energetically unfavorable boundaries with higher junctional tension. Here, as expected, the separating boundary between the D and N cells is smooth to minimize the boundary energy (Fig. 5.5d; Movie 14 in Appendix C). Thus we obtain an *active* phase segregation between the Delta and Notch cells. The D and N patterns in Fig. 5.5d are obtained for intermediate $v_0 = 0.1$. However, the patterns are observed even

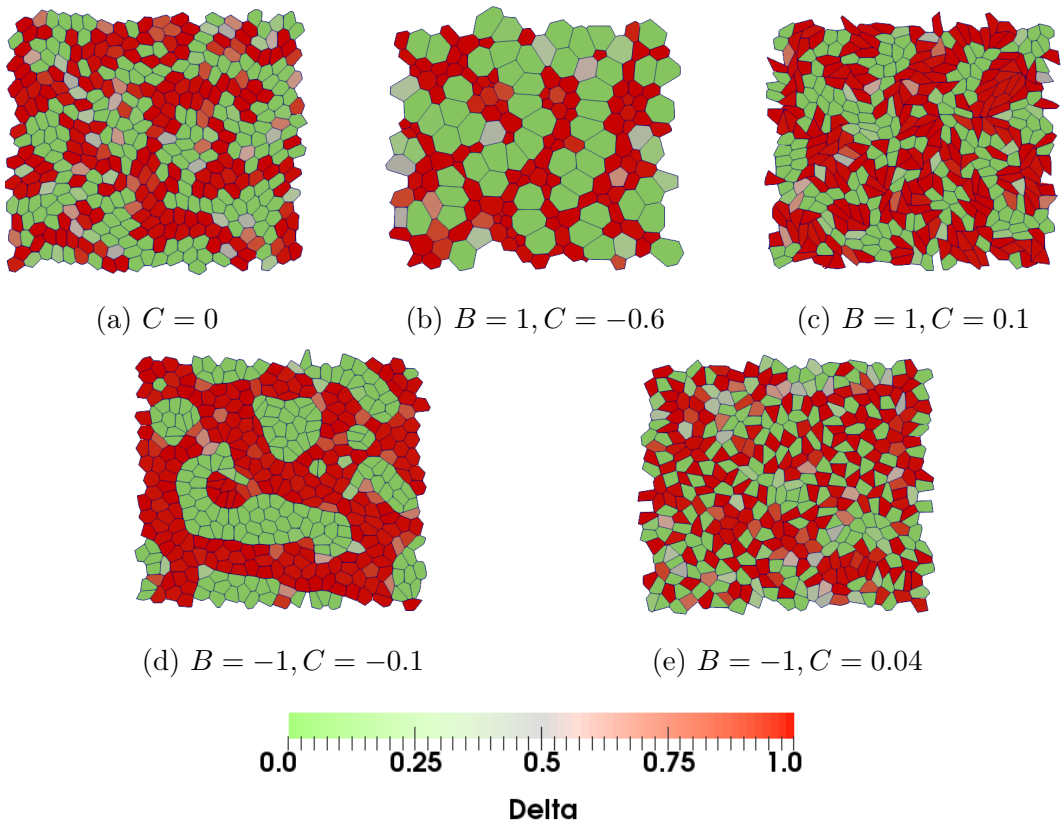

(a) $C = 0$ (b) $B = 1, C = -0.6$ (c) $B = 1, C = 0.1$

(d) $B = -1, C = -0.1$ (e) $B = -1, C = 0.04$

Figure 5.5: Patterns formed with protrusional contacts and Delta-dependent adhesion (Eq. 5.4). The coupling coefficient C and the sign constant B are (a) $C = 0$ (b) $B = 1$, $C = -0.6$ (c) $B = 1$, $C = 0.1$ (d) $B = -1$, $C = -0.1$ (e) $B = -1$, $C = 0.04$. Based on the adhesivity coupling details, there are variations in Delta expression and cell morphology arrangement around the basic pattern in (a) when there is no coupling, i.e., $C = 0$. The patterns seen are dynamic but upon visual inspection show overall steady-state behavior (Movies 11-15 corresponding to (a)-(e), respectively; Appendix C). The basic adhesivity Λ_0 is above the fluidisation limit for the tissue and the motility v_0 is sufficiently large for the cells to undergo neighbor exchanges. The other parameters are $\beta_j/\beta_p = 0.01$, $\Lambda_0 = -14.32$, $v_0 \approx 0.1$, $D_r = 0.001$, $\rho = 10$, $T = 0.9$, $\Delta\theta = \pi/4$, $K = 1$, $\Gamma = 1$, and $\rho = \mu = R_N = R_D = 10$.

for higher cell motility ($v_0 = 0.3$, Movie 20 in Appendix C).

When $B = -1$ and $C > 0$, at steady state $\Lambda_{DN} < \Lambda_{NN} = \Lambda_{DD}$. As a result, although both DD and NN bonds are equally likely, DN bonds are energetically the most favored, and hence we find that the D and N cells are well mixed with each other (Fig. 5.5e; Movie 15 in Appendix C).

5.3.5 Cell morphologies with Notch-dependent adhesion and protrusional contact signalling

Finally, we explore the mechanochemical patterns in the tissue due to Notch-dependent adhesion (Eq. 5.5) and long range signalling due to protrusional contact between cells. As for Delta-dependent adhesivity, here too, there are four possible combinations of B and C that could lead to varying strengths of Λ_{DD}, Λ_{DN}, and Λ_{NN}, that can influence the pattern formations in the tissue.

When $B = 1$ and $C < 0$, $\Lambda_{NN} > \Lambda_{DN} > \Lambda_{DD}$ due to which the DD interfaces are the most preferred whereas NN interfaces are preferred the least. Consequently, the Notch cells get extruded from the epithelial tissue and their space are encroached upon by the Delta cells. However, since the underlying signalling process does not allow the exclusive presence of D cells, D cells get converted to N cells, but the subsequent mechanics due to the differential adhesivity between the D and N cells will lead to the extrusion of the newly created N cells. Hence, in this case, the tissue is dominated with large D cells at any instant, but does not reach a steady state due to the persistent extrusion of N cells.

The case corresponding to $B = 1, C > 0$ (Fig. 5.6b) is similar to its counterpart in Fig. 5.5c. The only difference in this case is that $\Lambda_{DD} > \Lambda_{NN}$ due to which the N cells are more elongated as opposed to the D cells in Fig. 5.5c. Finally, when $B = -1$, the adhesivity of only DN bonds will be modified in this case, exactly as for Delta-dependent case discussed above. Hence, the corresponding patterns shown in Fig. 5.6c ($B = -1$ and $C > 0$) and Fig. 5.6d ($B = -1$ and $C > 0$) are, for all practical purposes, similar to their counterparts in Fig. 5.5d and Fig. 5.5e, respectively.

The structure of the basic Delta-Notch pattern in each of the cases above is governed

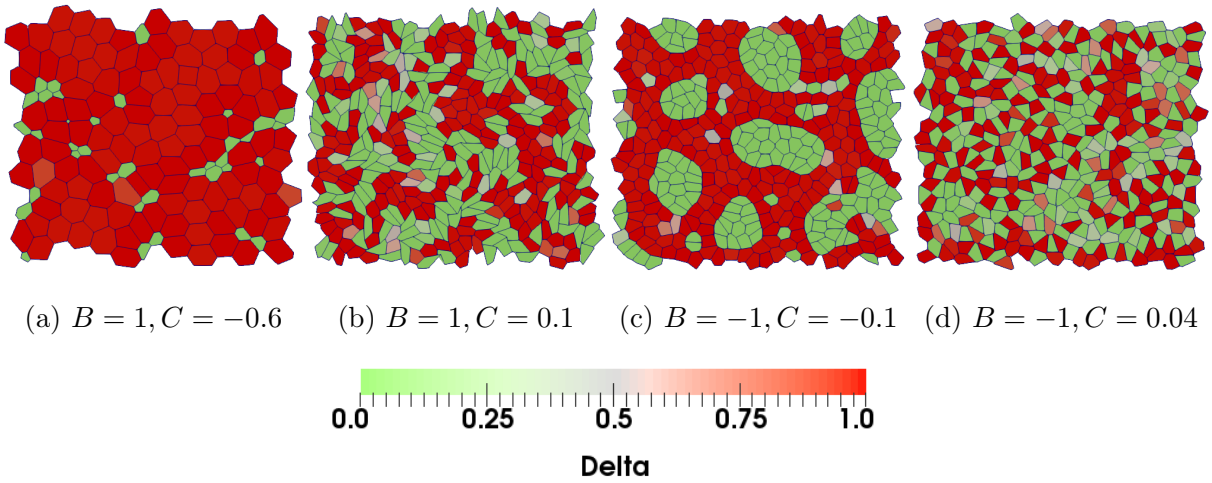

(a) $B = 1, C = -0.6$ (b) $B = 1, C = 0.1$ (c) $B = -1, C = -0.1$ (d) $B = -1, C = 0.04$

Figure 5.6: Snapshots showing the patterns formed with protrusional contacts and Notch-dependent line tension parameter (Eq. 5.5). The other fixed parameters are $\beta_j/\beta_p = 0.01$, $\Lambda_0 = -14.32$, $v_0 \approx 0.1$, $D_r = 0.001$, $\rho = 10$, $T = 0.9$, $\Delta\theta = \pi/4$, $K = 1$, $\Gamma = 1$, and $\rho = \mu = R_N = R_D = 10$. The basic adhesivity Λ_0 is above the fluidisation limit for the tissue and the motility v_0 is sufficiently large for the cells to undergo neighbor exchanges. The coupling coefficient C and the sign constant B are (a) $B = 1$, $C = -0.6$ (b) $B = 1$, $C = 0.1$ (c) $B = -1$, $C = -0.1$ (d) $B = -1$, $C = 0.04$. Based on the adhesivity coupling details, there are variations in Delta expression and cell morphology arrangement around the basic pattern in Fig. 5.5a when there is no coupling, i.e., $C = 0$. The patterns seen are dynamic but upon visual inspection show overall steady-state behavior (Movies 16-19 corresponding to (a)-(d), respectively).

by the activation threshold T, polarity rotation diffusion strength D_r, and cell motility v_0 [15]. However, due to cell motility and polarity diffusion, the patterns are dynamic and reach steady-state only in an average sense. Moreover, since the expressions of D and N in the cells are coupled to cell-cell adhesivity, the basic patterns get altered into a rich variety of chemical and cell morphological patterns in the tissue.

5.4 Discussion and Conclusions

A combination of junctional and protrusional Delta-Notch signalling due to contact based lateral inhibition can lead to a variety of chemical patterns in the tissue. When the

expression level of D and N in the cells is further coupled to cell-cell adhesivity, a wide range of chemical and cell morphological patterns could be generated in the epithelial monolayer. Notch/Delta-dependent adhesivity between cells results in the formation of differential bonds tensions in DD, DN and NN interfaces in the tissue. In junction dependent signalling, D and N forms a checkerboard chemical pattern with only NN and DN interfaces. However, the coupling to the D/N levels to bond tensions resulted in the modification of checkerboard pattern symmetry due to differential deformation of D and N cells. Based on the coupling strength, we find a wide range of cell morphologies even for the simplest underlying checkerboard pattern. For example, we see either tiny Delta cells surrounded by large Notch cells, or large Delta cells expanding out into the surrounding notch cells. When the DN interface energy much lower when compared to that of the NN interface, instead of expanding in size, the D cells elongated to maximize their contact with the N cells. When the signalling is long range due to protrusional contacts, all three types of bonds DD, DN and NN are feasible. In this case, we find that a broad variety of chemical and cell morphology patterns are formed that depended both on the details of the signalling kinetics and on the coupling between expression of Notch/Delta and cell-cell adhesivities. Overall, we find that the actual morphology of the cell patterns is governed by the competition between individual cell elastic energies and the interfacial adhesivity, and is constrained by the total area of the tissue and the lateral inhibition of the underlying signalling kinetics.

Differential adhesion is known to be important in the segregation of differentiated cell types during cell sorting. The heterogeneity in the mechanochemical properties of the tissue is also relevant in cell competition. Moreover, differential adhesion that is governed by underlying signalling kinetics can simultaneously give rise to chemical and mechanical patterns in the tissue such as in different types of cancers and in sensory epithelium. Our model based on a simple coupling between signalling molecules and cell adhesivity provides a simple common mechanism to generate a wide variety of biologically ubiquitious mechanochemical patterns in tissues. In our model, the signalling between neighboring cells is independent of the contact area (edge length) between the cells (Eqs. 5.4 and 5.5). However, it is observed for certain systems, such as the chick inner ear epithelium, that the cell fate is biased by cell size, an observation that could be explained by including size-dependent Notch signalling on a static heterogeneous cell network [220]. On the other

hand, depending on the sign of the coupling constant C (Eqs. 5.4 and 5.5), we too observe cell fates (chemical patterns) accompanied with size heterogeneities that are governed by bond adhesivities. It is plausible that both these affects, *i.e.*, size dependent signalling and signalling dependent adhesivities (governing size) work in tandem in a real system. In such a case, the relative time-scales associated with bond length changes and cell-cell signalling would be crucial in deciding the overall dynamics. A combination of these two effects is highly nonlinear and a detailed study in the future can provide a clearer understanding of their integrated effect on cell shape and fate patterns.

Our model suggests a unifying mechanistic basis for understanding several experimental observations of mosaic patterns in sensory epithelial tissues, and in some cancerous tissues. In reality, there could be a cascade of reactions leading up to the final mechanochemical coupling to cell-cell adhesivity that we have not included in our simple model. Moreover, unlike the simple linear relation that we use (Eqs. 5.4 and 5.5), the mechanochemical coupling could also be highly nonlinear. Consequently, we do not expect our model to make one-to-one connection between Notch-Delta expressions, cell adhesivity, and cell shapes observed experimentally. Our intention here is to take the first step in modeling many of these experimental systems. This framework, however, could be appropriately adapted to represent the mechanochemistry of a particular biological system of interest.

Chapter 6

Summary and Conclusions

As seen in the earlier chapters, cell-cell signaling, cell mechanics, and cell motility play a vital role during morphogenesis, development, and diseases such as cancer. Lateral inhibition is one of the most ubiquitous mode of signaling, and Delta-Notch signaling is the most prominent example of this mechanism. Experimentally, the Delta-Notch signaling mechanism has been studied in detail, and its involvement in cell migration, cell polarity dynamics, and mechanical aspects of morphogenesis is known and is discussed in detail in Chapter 2. Although, there are a few theoretical models that study the Delta-Notch pattern formation in tissues, there are no theoretical studies on how these patterns are themselves influenced by polarity and collective cell dynamics. On the other hand, there are a large number of theoretical studies on collective cell migration, especially on the role of cell motility, polarity and cell shape index on tissue unjamming. However, these studies generally do not consider the effect of tissue kinematics on the underlying signaling patterns. In Chapter 3 and 4, we combined both these aspects and showed how cell level interactions can lead to tissue level formation of a large variety of Delta-Notch patterns. In this first model, although the Delta-Notch pattern is influenced by cellular dynamics, the signaling itself does not influence the cell dynamics. Cellular polarity is expected to be crucial for determining the orientation, range and topology of cellular contacts in the tissue during the formation of signaling patterns. In Chapter 3, we investigate the role of cell polarity dynamics (random rotational diffusion and polarity alignment with the nearest neighbours) on the formation of signaling patterns by using the well-established vertex model with several significant additions. The lateral inhibition signaling kinetics are added on top of the modified vertex model. We also add a mechanism for long-

range signaling kinetics to the short-range signaling kinetics, that took into account the protrusional contacts. With the help of the new modified model we study the effect of the activation threshold on long-range signaling patterns. Then, we couple the orientation of the cell protrusions with the individual cell polarity and study the effect of polarity dynamics on the signaling patterns formed. We obtain a wide range of complex patterns that include spotted, striped as well as diffuse patterns. We demonstrate that the cell polarity dynamics significantly contribute to the diversity of signaling patterns resulting from contact-based signaling.

In Chapter 4, we investigate the role of cell motility and tissue mechanics on the formation of signaling patterns. In each cell, we include cell motility that is oriented along cell polarity. As a result, the cells rearrange themselves due to dynamic mechanical interactions between the cells. We show that the signaling patterns are maintained throughout, even though the cells keep dynamically rearranging in space and time. Using dynamic correlation function, we quantitatively characterize the spatiotemporal properties of the signaling patterns.

In Chapter 5 we investigate the governing mechanism by which cell signaling controls cell-cell adhesion. We propose a simple feedback mechanism between Delta-Notch signaling and cell-cell adhesion and observe that the shape and size of the cells varies within the tissue as observed in cancer tissues and the mosaic patterns in the in the olfactory epithelium. We systematically quantify the cellular morphologies as a function of the coupling parameters between Delta-Notch signaling and cell-cell adhesion. We also explore the role of long range connectivity on the adhesion between the cells and the resulting chemical patterns and cell morphologies.

We finally note that, although our modeling is developed in the context of Delta-Notch signaling, it is sufficiently general, and provides a broad framework to study the role of cell polarity, collective cell dynamics and tissue mechanics on pattern formation for any contact based signaling.

6.1 Future Directions

In the following section, we propose a few additional objectives, which, if achieved, would provide us a better understanding of how the cell-signaling, cell mechanics and motility affect each other and pattern formation during morphogenesis. These are some of the ideas I had contemplated during my PhD work in addition to those worked out and presented earlier.

6.1.1 Cell motility coupled to Delta-Notch signaling

It has been observed that Notch signaling regulates cell movement. Consideration of the interaction between Notch signaling and cell motility is crucial to understanding embryonic morphogenesis. As discussed earlier, numerous biological processes, including wound healing, metastasis, branching morphogenesis, and embryo development, show a coupling between cell migration and the Delta-Notch pathway [41, 85, 134]. Also, an increase in Delta is associated with an increase in motility, spreading of keratinocytes [41] and increased lamellipodia formation [145]. Theoretical modeling will prove to be a powerful tool, allowing us to understand how this interaction occurs during morphogenesis. Putting feedback between Notch signaling and cell motility can be achieved in a simplest manner by coupling the magnitude of cell motility v_0 and Delta/Notch concentration in cells.

6.1.2 Filopodia based signaling coupled with diffusing molecules

It is observed that skin patterns have often been represented in reaction-diffusion Turing type models [248]. Turing patterning is based on feedback interactions between morphogens (long-range diffusible ligands). It has been shown that such models can generate a variety of patterns [128, 167, 168]. It can also be argued that lateral inhibition with long-range filopodia is analogous to reaction-diffusion models [55]. The role of morphogens in Turing patterning can be replaced by long-range signaling through filopodia [101] that can be used in combination with diffusible ligands to transmit long-range signals. Filopodia-

based lateral inhibition models and reaction-diffusion models differ primarily in two ways. Mathematically, diffusion is a linear process and signaling is a non-linear process. The typical diffusion rates are typically too fast to match the time scale of pattern formation in a physical sense [93, 105, 239]. Striped patterns in zebrafish, for instance, develop over days and weeks. For morphogens to explain such patterns, diffusion rates would have to be orders of magnitude much smaller than diffusion rates observed in biological molecules. Thus, diffusion of molecules in combination with lateral inhibition based on the filopodia might better describe the process for skin patterning.

6.1.3 Notch signaling in cancer treatment

Activation of Notch contributes to the development and progression of different types of cancer in humans. Overexpression of Notch is reported in numerous cancer types such as leukemia [143, 147, 201, 268], solid cancers including breast cancer, glioblastoma (a form of brain tumor), pancreatic cancer [173, 274], lung cancer [83, 84], skin cancer [163, 184] and is associated with poor clinical outcomes. In leukemia, Notch1 has been identified as an oncogene, and have tumor suppressive function [143, 147, 201]. Notch signaling controls oncogenic processes within different cell types. In addition, Notch signaling activates various oncogenic factors that affect cellular functions such as metastasis, proliferation, drug-resistance, and angiogenesis [62, 150]. Notch is attracting increasing attention as a source of therapeutic targets for cancers [82, 263]. Recent proposed strategies for treating cancer with targeted drugs involves developing smart drugs based on known mechanisms. The link between Notch signaling and tumorigenesis indicates that Notch is a potential target candidate. Notch signaling has been proposed as a possible cancer therapeutic strategy. Cancer cells are characterized by unregulated cell proliferation that occurs as a result of a disrupted cell cycle. To understand the effect of Delta/Notch levels in the regulation of cell cycle network, Delta/Notch-dependent cell division can be included in the model and analyze the effect of increase/decrease levels of Delta/Notch on cell proliferation, and hence the role of the treatment on cancer progression.

6.1.4 Continuum approach by large-scale coarse-graining

Efforts are being made to obtain continuum theories of tissue mechanics, which are effective, coarse-grained descriptions of vertex models [8]. Vertex models can be used to estimate cellular shapes in tissues [22]. On the other hand, when describing tissue flow and deformation at larger scales, it is appropriate to use larger-scale fields, such as the velocity or the deformation of cells, which are averaged over lengths greater than the typical cell length [196]. The advantage of such an approach is that it is generic: the existing vertex model can produce identical continuum representations [152]. The development of continuum theories from existing vertex models has been attempted by researchers [196]. In recent years, coarse-grained vertex modelling approaches have been developed to study the morphogenesis and morphology of epithelia at a larger scale [177]. Despite the vertex models ability to describe the epithelial shape in detail, they are challenging to make an analytical prediction, especially if many parameters have to be specified. In contrast, continuum approaches can sometimes yield analytical solutions, allowing characterization of the generic behaviour of the tissue without relying on the specific details of stress generation at the cellular level. It is thus possible to represent the epithelia with moving cells in vertex models and understand the signaling dynamics and tissue mechanics more analytically using the continuum representation. It is possible to achieve this by representing a vertex model epithelia using a finite element mesh. The vertex model produces an inherent mesh for the finite element method, with moving vertices determined by forces. It can be combined with a Delta-Notch kinetic solver, and the Arbitrary-Lagrangian–Eulerian (ALE) approach, which is a part of CHASTE modeling framework, can be used for moving domains.

6.1.5 Effect of Noise and asymmetry in Delta-Notch signaling

We describe the Delta-Notch concentrations and their evolution by mass action type of deterministic differential equations. Here, we implicitly neglect any fluctuations that could result, for example, either from a small number of molecules or due to intrinsic/ extrinsic noise in the system [66, 81]. However, both these noise components could have important

role to play in the dynamics of small systems and it is important to explore their role on Delta-Notch signalling in tissues. As a part of future work, we can generalize our system and model the reactions using chemical master equation formalism that is practically implemented using the Gillespie algorithm [66]. Stochasticity can also be modeled by adding shot noise or white noise terms to the Delta-Notch evolution equation [122]. It was recently shown by Galbraith et al. [81] that intermediate noise levels can showed that intermediate noise levels in the Delta-Notch kinetics helps the system at a multi-cellular level to escape from frustrate disordered states to more ordered checkerboard patterns. On the other hand, higher noise levels takes the system away from the ordered patterns. In addition to these two sources, stochasticity can also arise from cell division and mechanical fluctuations, and is important the systematically explore the role of these noise contributions by appropriately modifying reaction kinetics.

Sensory organ precursor cells (SOPs) in *Drosophila* exhibit asymmetry, which is further enhanced to produce two different types of cells [258]. In the *Drosophila* pupal thorax, SOPs divide asymmetrically to produce two daughter cells, pIIa and pIIb, resulting in four types of cells that comprise a single mechanosensory hair [215]. During the division, Notch signalling between pIIa and pIIb cells determine their binary fate, and asymmetrical Notch segregation occurs in pIIb cells. Segregation bias is mediated by the polarized orientation of the microtubule at the central spindle, as more plus ends are oriented toward the pIIa side [58]. Such asymmetric segregation is also observed in other cell types, such as zebrafish neural precursor cells [131] and *Drosophila* intestinal stem cells [174]. In a future work, asymmetry in Notch concentration can be incorporated into the present model.

6.2 Contributions

During this course of research work, the following major contributions were made interms of new proposed mathematical model, extension of the existing model and detailed analysis of the system.

- A review of existing literature and the gaps in the current understanding in the

context of cell-cell signaling, cell mechanics and cell motility and their coupled behaviour is provided.

- A new mathematical model is developed for contact dependent signaling pathways. Role of polarity dynamics on the formation of signaling patterns is explored.
- The cell polarity model is coupled with cell motility and the effect of resulting cell movements on Delta-Notch signaling patterns is investigated.
- A feedback mechanism is provided that influences cell-cell adhesivity and incorporates differential cell-cell adhesion depending on Delta-Notch levels in the cells. The role of coupling parameters on chemical patterns and cell morphologies is investigated.

List of Publications

International Journal (published)

Bajpai, S., Prabhakar, R., Chelakkot, R., Inamdar, M. M., 2021. "Role of cell polarity dynamics and motility in pattern formation due to contact-dependent signalling", *Journal of the Royal Society Interface 18 (175), 20200825.*

International Journal (to be submitted)

Bajpai, S., Prabhakar, R., Chelakkot, R., Inamdar, M. M., 2021. "Role of Delta-Notch signalling molecules on cell-cell adhesion in determining heterogeneous chemical and cell morphological patterning. *To be submitted.*

Appendix A

A.1 Implementation Details of Vertex Model in CHASTE

The epithelial monolayer, in the vertex dynamics model can be implemented in **C**ancer, **H**eart And **S**oft **T**issue **E**nvironment (CHASTE) (https://www.cs.ox.ac.uk/chaste/) with Linux. Chaste is written in C++, which allows object-oriented classes. The codes are suitable for the extension and inheritance of existing functionalities. The epithelial monolayer is modeled as a polygon (in 2D) or polyhedron (in 3D), whose vertices move in response to forces. All cells in a monolayer are assumed to be of the same height, which makes it a two-dimensional model. A collection of polygonal cells are referred to as a 'mesh', which comprises a set of 'elements' and 'vertices'. Each vertex is a point in space, defined by its location and an index, and each element is defined by a polygon, with vertex indices, an ordered list, and an index. A pair of neighboring vertices in an element is referred to as an 'edge'. [Figure A.1] illustrates the structure of the vertex mesh. Each vertex that is not on the edge of the mesh is contained in exactly three elements, and vertices on the boundary of the mesh are in either one or two elements.

1. equations of motion which govern the motion of vertices are defined by [Equation A.4].

2. elements may move past each other as a result of the mesh undergoing local rearrangement.

3. elements may be removed from the mesh as a result of cell death.

Each element in this mesh is associated with a cell, which can influence the evolution of the monolayer through the above processes by changing parameters by inducing cell division or death.

A.1.1 Mesh restructuring operations in CHASTE

Vertex movement is implemented such that the elements are always non-intersecting and to allow cells to form and break bonds. In order to achieve this three types of elementary operations are considered [180, 181]. These operations are: edge rearrangement (a T1 swap); element removal (a T2swap); and element intersection (aT3swap). These operations are needed because the vertex dynamics models considered results in finite forces acting on a cell's vertices arbitrarily far from equilibrium; 'hard body' interactions are not considered.

T1 swap or edge rearrangement

When the distance between two vertices is less than a minimum threshold distance d_{min}, T1 swap or rearrangement of elements takes place (Nagai and Honda, 2001), as shown in Figure. ie, the vertices are moved and placed a distance d_{sep} apart where $d_{sep} = k_{sep}d_{min}$, where k_{sep} is the separation ratio.

T2 swap or element removal

If the area of a triangular element becomes smaller than A_{min} ie, a given threshold area, the element and the associated cell is removed from the mesh and simulation, as shown in Figure. For this to take place the target area for the element must be small.

A.1.2 Element division and removal

The cells divide into two equal areas when cell division takes place (Brodland and Veldhuis, 2002). The implementation of cell division is done by choosing an angle of cell division (drawn from a uniform distribution for isotropic cell division) or in the direc-

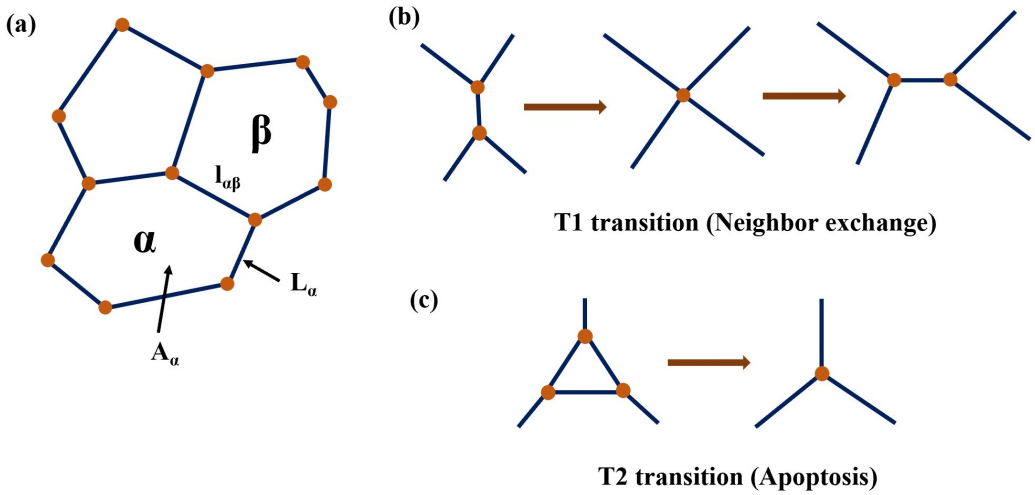

Figure A.1: schematic of tissue monolayer with polygonal cells and topological transitions. (a) 2-D representation of tissue monolayer or epithelial tissue with polygonal cells. Each cell has edges and vertices. A_α and L_α are the area and perimeter of a cell. $l_{\alpha\beta}$ is the edge shared between cells α and β. (b) T1 topological transition or neighbor exchange process takes place When two originally connected cells move away from each other and new neighbors are formed. (c) T2 transition or apoptosis takes place by removing the cells with area less than a critical area from the tissue monolayer.

tion of the shortest axis through the cell's centroid or biased in a certain direction if directed proliferation and cell polarity are considered. Two new vertices are placed at the intersection between the dividing line that passes through the cell's centroid and its cell perimeter, thereby creating two daughter cells from a single parent cell. The element is divided into two new elements using this division axis, as shown in Figure.

Cell death can also be modelled as apoptotic cell ie, the cell shrinks until it is destroyed. To achieve this the target area of the associated element is decreased until the element becomes small and triangular (see Figure. 6) and is removed by a T2 swap, leaving a continuous monolayer.

A.1.3 Force implementation

The forces act on the cell vertices and the movement of vertex i is due to the elastic and active forces. The gradient of free energy in terms of the cells surrounding the vertex i is

written as,

$$U = \sum_{\alpha=1}^{\mathcal{N}} [K_\alpha (A_\alpha - A_{\alpha,0})^2 + \Gamma_\alpha L_\alpha^2] + \sum_{\text{edges:}\gamma\beta} \Lambda_{\gamma\beta} l_{\gamma\beta}, \tag{A.1}$$

$$\mathbf{F}_i^{\text{elastic}} = -2 \sum_{\alpha=1}^{\aleph} [K_\alpha (A_\alpha - A_0) \nabla_i A_\alpha + \Gamma_\alpha L_\alpha \nabla_i L_\alpha] - \sum_{\text{edges:}\gamma\beta} \Lambda_{\gamma\beta} \nabla_i l_{\gamma\beta} \tag{A.2}$$

$$\mathbf{F}_i^{\text{elastic}} = -2 \sum_{\alpha=1}^{\aleph} [K_\alpha (A_\alpha - A_0) \nabla_i A_\alpha + \Gamma_\alpha L_\alpha (\nabla_i l_{\alpha,I_\alpha - 1} + \nabla_i l_{\alpha,I_\alpha})] - \sum_{\text{edges:}\gamma\beta} \Lambda_{\gamma\beta} \nabla_i l_{\gamma\beta} \tag{A.3}$$

where α is the cell containing the vertex i, ordered counterclockwise, and I_α is the local index of vertex i of cell α. The gradient of area is computed as,

$$\nabla_i A_\alpha = \frac{1}{2} \begin{bmatrix} y_{I+1}^\alpha - y_{I-1}^\alpha \\ x_{I-1}^\alpha - x_{I+1}^\alpha \end{bmatrix}$$

where $(x_{I-1}^\alpha, y_{I-1}^\alpha)$ are the coordinates of the vertex one position further clockwise than the I_αth vertex of cell α and $(x_{I+1}^\alpha, y_{I+1}^\alpha)$ are the coordinates of the vertex one position further counter-clockwise than the I_αth vertex of cell α.

A.1.4 Numerical implementation and details of timestepping algorithm

The mesh and the corresponding cells are updated at each time step as follows:

1. update all the cell properties of the model.
2. implement the mesh restructuring operations, if required.
3. update the positions of all vertices and calculate and apply the forces F_i, applied at

each vertex.

The equations of motion is solved numerically using a simple forward Euler discretization for all vertices. The displacement of each vertex i in a small time interval Δt is given by

$$\mathbf{r_i}(t + \Delta t) = \mathbf{r_i}(t) + \frac{\Delta t}{\eta}\mathbf{F_i}(t) \tag{A.4}$$

The above numerical method is explicit, therefore, the chosen time step must be sufficiently small for the system to remain stable.

For accurate solution of the equations of motion the time step must be chosen such that the vertices move not more than a distance of $d_{min}/2$ in Δt time interval to avoid elements intersection.

Appendix B

B.1 Model parameters and non-dimensionalization

The mechanical energy function and the signalling kinetics equations are non-dimensionalized with characteristic time scale $\frac{\eta}{\Gamma} = 1$ and characteristic length scale $L_c = 1$ (Figure.1a) (Table C.1).

We simulate a monolayer of tissue with periodic boundary and $\mathcal{N}$ number of cells (no cell divisions or apoptosis). The model is implemented in CHASTE [172] using the C++ libraries. The equation of motion is solved numerically using a simple forward Euler discretization. The signalling equations are solved using Runge-Kutta-Merson method. We choose the time step size $\Delta t = 0.01$ (sufficiently small) to maintain the numerical stability. The initial levels of Notch and Delta concentration are chosen randomly from uniform random number in (0,1) for each cell α.

B.2 Tissue phase change: solid-like to fluid-like

In equation 3.1, the value of $\Lambda_{\gamma\beta}$ and Γ_α is equal for all bonds and cell is equal to Λ and Γ respectively. It is possible to incorporate strong feedback between contractility of the junction Λ and boundary contractility Γ in the equation 3.1, which can be written as: $\sum_\alpha \Gamma(L_\alpha - p_0)^2$, where p_0 is the shape index. Here, $\Lambda = -4\Gamma p_0\sqrt{A_0}$ and the term $4\Gamma p_0\sqrt{A_0}$ is a constant that is responsible for shift in the overall energy. It does not contribute to

Table B.1: The model parameters relative to characteristic length scale $L_c = 1$ (Figure.1a) and characteristic time scale $T_c = 1$

Dimensionless parameters	**Parameter values**
L_c	1.0
η	1.0
Γ	1.0
$K \equiv \frac{KT_cL_c^2}{\eta}$	1.15
$\Lambda \equiv \frac{\Lambda T_c}{4L_c\eta}$	$[-13.77, -14.32]$
$v_0 \equiv {}^{v_0T_c}/_{L_c\eta}$	$3.1 \times 10^{-4}, 0.31$
$A_0 \equiv A_0/L_c^2$	0.866
$\xi \equiv \xi T_c$	$0 - 2$
$D_r \equiv D_rT_c$	$[0.001, 0.1]$
$D_\alpha \equiv {}^{D_\alpha}/_{D_0}$	$0 - 1$
$N_\alpha \equiv {}^{N_\alpha}/_{N_0}$	$0 - 1$
$R_D \equiv R_DT_c$	$1, 10$
$R_N \equiv R_NT_c$	$1, 10$
$\rho \equiv \rho T_c$	$1, 10$
$\mu \equiv \mu T_c$	$1, 10$
$l \equiv l/L_c$	1.7
$\Delta l \equiv \Delta l/L_c$	1.2
$\Delta\theta \equiv \Delta\theta$	$\pi/24 - \pi/2$
$\Delta t \equiv \Delta t/T_c$	0.01
a	[0.01]
b	[100]
$D_{\text{critical}} \equiv {}^{D_{\text{critical}}}/_{D_0}$	0.5
$\mathcal{N}$	$[400, 1600]$
Δr	0.1

the cell force. As the relevant effective forces are only obtained from the derivatives of the energy with respect to the degrees of freedom, equation 3.1 can be rewritten as [22]

$$U = \sum_{\alpha=1}^{N} [K(A_\alpha - A_0)^2 + \Gamma(L_\alpha - p_0)^2] \tag{B.1}$$

where $p_0 = \frac{-\Lambda}{4\Gamma\sqrt{A_0}}$ is the target shape index. The shape index value p_0 of different shapes of cell is given below;

Cell shape	Hexagon	Pentagon	Square	Triangle
p_0 Values	3.722	3.812	4.0	4.559

Fluid-like behaviour of the tissues (where cells exchange neighbours), have been observed at $p_0 >= 3.812$ (for pentagon, square, and triangular cell shapes) and solid-like behaviour (where cells do not exchange neighbours) have been observed for $p_0 < 3.812$, corresponding to a regular hexagon [23].

B.3 Number of clusters and cluster size

The median number of clusters and the median cluster size is calculated for 400 cells using the density-based spatial clustering (DBSCAN) algorithm [68]. The cell α is considered a Delta cell if the concentration of Delta molecule in the cell is greater than D_{critical}. A group of Delta cells is considered to be in dense region if minimum number of Delta cells in the cluster is 3. Two cells are considered to be touching each other if the Euclidean distance between both the cells are less than or equal to 1.5.

Each data point shown in Figs.3g-i is obtained using five sets of simulations. In each set, for a given combination of parameters, initial polarity $\hat{\mathbf{p}}$ for individual cells was generated from uniform random orientation in the range $[-\pi, \pi]$. Similarly, the initial concentration of Delta and Notch for individual cells was generated from uniform random distribution in the range $(0, 1)$. Then, after removing the transient part of the corresponding simulation, the quantity X_t^β (cluster number, cluster size, shape ratio) for each simulation β and at every sampling time t was pooled together and its median $\bar{X}$ over t and β was used as one data point. The sampling interval for every simulation

was $\Delta T = 1$. A similar procedure was followed to obtain Figs.4g-i, except that the total number of simulation runs in this case was six instead of five.

The quantification and visualization is done using python2.7, python3.5, using numpy (scientific computing library), pandas (data analysis library), scikit-learn (machine learning library) and matplotlib (data visualization library), ParaView (an open-source, data analysis and visualization application).

B.3.1 DBSCAN algorithm

DBSCAN (Density-based spatial clustering of applications with noise) is a data clustering algorithm (density based algorithm). The algorithm is capable of finding non-linearly separable clusters. With a given set of points in space, ϵ specifies the radius of a neighborhood for a particular point, and k is the minimum point. All the points can be classified as core points, reachable points, and outliers:

1. A point p is considered a core point if at least k number of points lies within a distance of ϵ including the point p itself.

2. Directly reachable points t are those points that are within a distance of ϵ of the core point p.

3. A reachable point t from p is that point if a path reaches from p to t via $p_1, p_2....p_n$, where the successive point on the path is directly reachable from the previous point.

4. Outliers or noise points are all points that can't be reached by any other point.

The core point p forms a cluster along with all points that can be reached (cores and non-cores). A cluster consists of at least one core point and non-core points.

B.4 Shape ratio

The shape ratio is calculated for 400 cells. The cell α is considered a Delta cell if the concentration of Delta molecule in the cell is greater than D_{critical}. The inertia matrix of

a single cluster is computed as follows:

$$\mathbf{A} = \begin{bmatrix} \mathbf{I}_{xx} & \mathbf{I}_{xy} \\ \mathbf{I}_{xy} & \mathbf{I}_{yy} \end{bmatrix}$$

$$\mathbf{I}_{xx} = \sum_{i=1}^{N_c} (A_i(\mathbf{x}_i - \mathbf{x}_{\text{mean}})^2), \tag{B.2}$$

$$\mathbf{I}_{yy} = \sum_{i=1}^{N_c} (A_i(\mathbf{y}_i - \mathbf{y}_{\text{mean}})^2), \tag{B.3}$$

$$\mathbf{I}_{xy} = \sum_{i=1}^{N_c} (A_i(\mathbf{x}_i - \mathbf{x}_{\text{mean}})(\mathbf{y}_i - \mathbf{y}_{\text{mean}})) \tag{B.4}$$

where, N_c is the number of cells in a cluster. Eigen values of $\mathbf{A}$ is calculated and shape ratio is estimated as the ratio of the maximum and minimum eigen values. The median shape ratio is calculated using the same procedure as described in Section B.3 above.

The median of the shape ratios of all the clusters of a time frame is calculated, and the median of all the shape ratios obtained from all time frames is the final shape ratio.

B.5 Movie Captions

Movie link is as follows:
https://drive.google.com/drive/folders/1Km-EfchGNWROoF7wDVreOAmfjRbiDDZO?usp=sharing

Movie-1 corresponding to Figure.2a. signalling pattern formed by contact mediated

signalling via junctional contacts $\frac{\beta_j}{\beta_p} = 99$.

Movie-2 corresponding to Figure.3a. Pattern obtained using the model for $R_N = R_D = \rho = \mu = 1$, $D_r = 10^{-3}$, $\frac{\beta_j}{\beta_p} = 10^{-2}$, $\Delta\theta = \pi/4$, $v_0 = 3.1 \times 10^{-4}$, and $\Lambda = -13.77$ and $T = 0.1$.

Movie-3 corresponding to Figure.3b. Pattern obtained using the model for $R_N = R_D = \rho = \mu = 1$, $D_r = 10^{-3}$, $\frac{\beta_j}{\beta_p} = 10^{-2}$, $\Delta\theta = \pi/4$, $v_0 = 3.1 \times 10^{-4}$, and $\Lambda = -13.77$ and $T = 0.5$.

Movie-4 corresponding to Figure.3c. Pattern obtained using the model for $R_N = R_D = \rho = \mu = 1$, $D_r = 10^{-3}$, $\frac{\beta_j}{\beta_p} = 10^{-2}$, $\Delta\theta = \pi/4$, $v_0 = 3.1 \times 10^{-4}$, and $\Lambda = -13.77$ and $T = 0.6$.

Movie-5 corresponding to Figure.3d. Pattern obtained using the model for $R_N = R_D = \rho = \mu = 1$, $D_r = 10^{-3}$, $\frac{\beta_j}{\beta_p} = 10^{-2}$, $\Delta\theta = \pi/4$, $v_0 = 3.1 \times 10^{-4}$, and $\Lambda = -13.77$ and $T = 0.8$.

Movie-6 corresponding to Figure.3e. Pattern obtained using the model for $R_N = R_D = \rho = \mu = 1$, $D_r = 10^{-3}$, $\frac{\beta_j}{\beta_p} = 10^{-2}$, $\Delta\theta = \pi/4$, $v_0 = 3.1 \times 10^{-4}$, and $\Lambda = -13.77$ and $T = 0.9$.

Movie-7 corresponding to Figure.3f. Pattern obtained using the model for $R_N = R_D = \rho = \mu = 1$, $D_r = 10^{-3}$, $\frac{\beta_j}{\beta_p} = 10^{-2}$, $\Delta\theta = \pi/4$, $v_0 = 3.1 \times 10^{-4}$, and $\Lambda = -13.77$ and $T = 0.94$.

Movie-8 corresponding to Figure.4a. Pattern obtained using the model with parameter $R_N = R_D = \rho = \mu = 1$, $\Lambda = -13.77$, $D_r = 0.1$, $v_0 = 3.1 \times 10^{-4}$, $\frac{\beta_j}{\beta_p} = 0.01$, $T = 0.5$ and $\Delta\theta = \pi/4$ and $\xi/D_r = 0$.

Movie-9 corresponding to Figure.4b. Pattern obtained using the model with parameter $R_N = R_D = \rho = \mu = 1$, $\Lambda = -13.77$, $D_r = 0.1$, $v_0 = 3.1 \times 10^{-4}$, $\frac{\beta_j}{\beta_p} = 0.01$, $T = 0.5$ and $\Delta\theta = \pi/4$ and $\xi/D_r = 0.5$.

Movie-10 corresponding to Figure.4c. Pattern obtained using the model with parameter $R_N = R_D = \rho = \mu = 1$, $\Lambda = -13.77$, $D_r = 0.1$, $v_0 = 3.1 \times 10^{-4}$, $\frac{\beta_j}{\beta_p} = 0.01$, $T = 0.5$ and $\Delta\theta = \pi/4$ and $\xi/D_r = 1.0$.

Movie-11 corresponding to Figure.4d. Pattern obtained using the model with parameter $R_N = R_D = \rho = \mu = 1$, $\Lambda = -13.77$, $D_r = 0.1$, $v_0 = 3.1 \times 10^{-4}$, $\frac{\beta_j}{\beta_p} = 0.01$,

$T = 0.5$ and $\Delta\theta = \pi/4$ and $\xi/D_r = 1.5$.

Movie-12 corresponding to Figure.4e. Pattern obtained using the model with parameter $R_N = R_D = \rho = \mu = 1$, $\Lambda = -13.77$, $D_r = 0.1$, $v_0 = 3.1 \times 10^{-4}$, $\frac{\beta_j}{\beta_p} = 0.01$, $T = 0.5$ and $\Delta\theta = \pi/4$ and $\xi/D_r = 2.0$.

Movie-13 corresponding to Figure.4f. Pattern obtained using the model with parameter $R_N = R_D = \rho = \mu = 1$, $\Lambda = -13.77$, $D_r = 0.1$, $v_0 = 3.1 \times 10^{-4}$, $\frac{\beta_j}{\beta_p} = 0.01$, $T = 0.5$ and $\Delta\theta = \pi/4$ and $\xi/D_r = 2.5$.

Movie-14 corresponding to Figure.5a-c. The parameter values used for the simulations are $R_N = R_D = \rho = \mu = 10$, $\frac{\beta_j}{\beta_p} = 0.01$, $\Lambda = -14.32$, $D_r = 0.001$, $\xi = 0$, $\Delta\theta = \pi/2$, $T = 0.1$ and $v_0 = 0.31$. The shape parameter for the cells $p_0 > 3.82$.

Movie-15 for the tissue in fluid region with stripe-like pattern. The parameter values used for the simulations are $R_N = R_D = \rho = \mu = 10$, $\frac{\beta_j}{\beta_p} = 0.01$, $\Lambda = -14.32$, $D_r = 0.1$, $\xi = 0.25$, $\Delta\theta = \pi/4$, $T = 0.5$ and $v_0 = 0.31$. The shape parameter for the cells $p_0 > 3.82$.

Movie-16 Pattern obtained using the model with parameter $R_N = R_D = \rho = \mu = 1$, $\Lambda = -13.77$, $D_r = 0.1$, $v_0 = 3.1 \times 10^{-4}$, $\frac{\beta_j}{\beta_p} = 0.01$, $T = 0.94$ and $\Delta\theta = \pi/4$ and $\xi/D_r = 0$.

Movie-17 Pattern obtained using the model with parameter $R_N = R_D = \rho = \mu = 1$, $\Lambda = -13.77$, $D_r = 0.1$, $v_0 = 3.1 \times 10^{-4}$, $\frac{\beta_j}{\beta_p} = 0.01$, $T = 0.94$ and $\Delta\theta = \pi/4$ and $\xi/D_r = 0.5$.

Movie-18 Pattern obtained using the model with parameter $R_N = R_D = \rho = \mu = 1$, $\Lambda = -13.77$, $D_r = 0.1$, $v_0 = 3.1 \times 10^{-4}$, $\frac{\beta_j}{\beta_p} = 0.01$, $T = 0.94$ and $\Delta\theta = \pi/4$ and $\xi/D_r = 1.0$.

Movie-19 Pattern obtained using the model with parameter $R_N = R_D = \rho = \mu = 1$, $\Lambda = -13.77$, $D_r = 0.1$, $v_0 = 3.1 \times 10^{-4}$, $\frac{\beta_j}{\beta_p} = 0.01$, $T = 0.94$ and $\Delta\theta = \pi/4$ and $\xi/D_r = 1.5$.

Movie-20 Pattern obtained using the model with parameter $R_N = R_D = \rho = \mu = 1$, $\Lambda = -13.77$, $D_r = 0.1$, $v_0 = 3.1 \times 10^{-4}$, $\frac{\beta_j}{\beta_p} = 0.01$, $T = 0.94$ and $\Delta\theta = \pi/4$ and $\xi/D_r = 2.0$.

Movie-21 Pattern obtained using the model with parameter $R_N = R_D = \rho = \mu = 1$, $\Lambda = -13.77$, $D_r = 0.1$, $v_0 = 3.1 \times 10^{-4}$, $\frac{\beta_j}{\beta_p} = 0.01$, $T = 0.94$ and $\Delta\theta = \pi/4$ and

$\xi/D_r = 2.5$.

Movie-22 Pattern obtained using the model with parameter $R_N = R_D = \rho = \mu = 1$, $\Lambda = -13.77$, $D_r = 0.1$, $v_0 = 3.1 \times 10^{-4}$, $\frac{\beta_j}{\beta_p} = 0.01$, $T = 0.94$ and $\Delta\theta = \pi/4$ and $\xi/D_r = 10.0$.

Movie-23 Pattern obtained using the model for $R_N = R_D = \rho = \mu = 1$, $D_r = 0$, $\frac{\beta_j}{\beta_p} = 10^{-2}$, $\Delta\theta = \pi/4$, $v_0 = 3.1 \times 10^{-4}$, and $\Lambda = -13.77$ and $T = 0.6$.

Movie-24 Pattern obtained using the model for $R_N = R_D = \rho = \mu = 1$, $D_r = 1$, $\frac{\beta_j}{\beta_p} = 10^{-2}$, $\Delta\theta = \pi/4$, $v_0 = 3.1 \times 10^{-4}$, and $\Lambda = -13.77$ and $T = 0.6$.

B.6 CHASTE and Python Codes

In addition to the codes provided in the CHASTE library, the following additional codes are written for implementing the proposed model in Chapter 3 and Chapter 4, in CHASTE (C++) and Python. Ubuntu 16.04 LTS (operating system) and High Performance Computing (HPC) Systems (Noether cluster, Physics Department, IIT Bombay, India and MonARCH cluster, Monash University, Australia) are used to run the simulations.

```
                                        /* Polarity - random rotational diffusion
                                        */

        #include "ThetaAlignmentRule.hpp"
        #include "SmartPointers.hpp"
        #include "RandomNumberGenerator.hpp"
        #include <stdio.h>      /* printf, NULL */
        #include <stdlib.h>     /* srand, rand */
        #include <time.h>       /* time */
        #include <cmath>
        #include <math.h>
        #include <iostream>
        #include <fstream>
        #include <vector>
        #define PI 3.14159265
        using namespace std;

        template<unsigned DIM>
        ThetaAlignmentRule<DIM>::ThetaAlignmentRule()
            : AbstractForce<DIM>()

        {
        }

        template<unsigned DIM>
        ThetaAlignmentRule<DIM>::~ThetaAlignmentRule()
        {
        }



        template<unsigned DIM>
        void ThetaAlignmentRule<DIM>::SetMotility(double motility)
        {
            mMotility=motility;
        }


        template<unsigned DIM>
        double ThetaAlignmentRule<DIM>::GetMotility()
        {
            double motility = mMotility;
            return motility;
        }

        template<unsigned DIM>
        void ThetaAlignmentRule<DIM>::SetDiffusionCoefficient(double
diffusioncoefficient)
        {
            mDiffusioncoefficient=diffusioncoefficient;
        }

        template<unsigned DIM>
        double ThetaAlignmentRule<DIM>::GetDiffusionCoefficient()
        {
            double diffusioncoefficient=mDiffusioncoefficient;
            return diffusioncoefficient;
        }

        template<unsigned DIM>
        void ThetaAlignmentRule<DIM>::SetThetaValue(std::vector<double> theta)
        {
```

```
            mTheta=theta;

        }

        template<unsigned DIM>
        std::vector<double> ThetaAlignmentRule<DIM>::GetThetaValue()
        {

                //define element index here
                std::vector<double> theta=mTheta;
                return theta;
        }

        template<unsigned DIM>
        double ThetaAlignmentRule<DIM>::GetThetaValueForSingleCell(unsigned cell_id)
        {

                //define element index here
                double theta=mTheta[cell_id];
                return theta;
        }


        template<unsigned DIM>
        void ThetaAlignmentRule<DIM>::UpdateThetaValueForSingleCell (unsigned
cell_id, double theta)
        {


            RandomNumberGenerator* p_gen = RandomNumberGenerator::Instance();
            double mean = 0;
            double standard_deviation = 1.0;

            double delta_t= SimulationTime::Instance()->GetTimeStep();
            double D_r=GetDiffusionCoefficient();
                double noise=p_gen->NormalRandomDeviate(mean, standard_deviation);
                double theta_noise=noise*sqrt(2*D_r*delta_t);
                theta=theta+theta_noise;


            mTheta[cell_id]=theta;

        }

        template<unsigned DIM>
        void ThetaAlignmentRule<DIM>::UpdateThetaValue(std::vector<double>theta)
        {


                time_t t;
                srand(time(&t));
                unsigned num_of_cells=theta.size();
                std::vector<double> theta_noise(num_of_cells);
                std::vector<double> noise(num_of_cells);
            RandomNumberGenerator* p_gen = RandomNumberGenerator::Instance();
            double mean = 0;
            double standard_deviation = 1.0;
            double delta_t= SimulationTime::Instance()->GetTimeStep();
            double D_r=GetDiffusionCoefficient();

                for (int i=0;i<num_of_cells;i++)
                {
```

```
                        noise[i]=p_gen->NormalRandomDeviate(mean, standard_deviation);
                        theta_noise[i]=noise[i]*sqrt(2*D_r*delta_t);
                        theta[i]=theta[i]+theta_noise[i];
                }

            mTheta=theta;



        }

        template<unsigned DIM>
        void ThetaAlignmentRule<DIM>::AddForceContribution(AbstractCellPopulation<DIM>
(& rCellPopulation))

        {
            // Throw an exception message if not using a VertexBasedCellPopulation
            if (dynamic_cast<VertexBasedCellPopulation<DIM>*>(&rCellPopulation) ==
NULL)
            {
                EXCEPTION("polarisation_random_value is to be used with a
VertexBasedCellPopulation only");
            }

            // Helper variable that is a static cast of the cell population
            VertexBasedCellPopulation<DIM>* p_cell_population =
static_cast<VertexBasedCellPopulation<DIM>*>(&rCellPopulation);


                for (typename AbstractCellPopulation<DIM,DIM>::Iterator cell_iter =
p_cell_population->Begin();
                          cell_iter != p_cell_population->End();
                          ++cell_iter)
                {
                        VertexElement<DIM, DIM>* p_element = p_cell_population-
>GetElementCorrespondingToCell(*cell_iter);
                        unsigned cell_id = cell_iter->GetCellId();

                        double theta=GetThetaValueForSingleCell(cell_id);

                        c_vector<double,DIM> polarisation_direction;

                        polarisation_direction(0) = cos(theta);
                        polarisation_direction(1) = sin(theta);

                        double magnitude_of_force = GetMotility();


                        c_vector<double,DIM> force =
magnitude_of_force*polarisation_direction;
                        //for all nodes of a single element

                    for (unsigned node_local_index=0;node_local_index<p_element-
>GetNumNodes();node_local_index++)

                        {
                                unsigned node_global_index = p_element->GetNode
(node_local_index)->GetIndex();
                            unsigned num_containing_elements = p_element->GetNode
(node_local_index)->GetNumContainingElements();
                            //double
n_sq=num_containing_elements*num_containing_elements;
```

```
                            c_vector<double,DIM> force_new =
magnitude_of_force*polarisation_direction/num_containing_elements;

                            rCellPopulation.GetNode(node_global_index)-
>AddAppliedForceContribution(force_new);
                        }


                        UpdateThetaValueForSingleCell(cell_id, theta);

            }

        }

        template<unsigned DIM>
        void ThetaAlignmentRule<DIM>::OutputForceParameters(out_stream& rParamsFile)
        {
            // Call method on direct parent class
            AbstractForce<DIM>::OutputForceParameters(rParamsFile);
        }

        /////////////////////////////////////////////////////////////////////////////
        // Explicit instantiation
        /////////////////////////////////////////////////////////////////////////////

        template class ThetaAlignmentRule<1>;
        template class ThetaAlignmentRule<2>;
        template class ThetaAlignmentRule<3>;

        // Serialization for Boost >= 1.36
        #include "SerializationExportWrapperForCpp.hpp"
        EXPORT_TEMPLATE_CLASS_SAME_DIMS(ThetaAlignmentRule)
```

```
                                        /* Polarity - polarity alignment with the
nearest neighbors
                                        */

        #include "SamePolarityAlignmentRule.hpp"
        #include "SmartPointers.hpp"
        #include "RandomNumberGenerator.hpp"
        #include <stdio.h>      /* printf, NULL */
        #include <stdlib.h>     /* srand, rand */
        #include <time.h>       /* time */
        #include <cmath>
        #include <math.h>
        #include <iostream>
        #include <fstream>
        #include <vector>
        #include <tgmath.h>
        #define PI 3.14159265
        using namespace std;

        template<unsigned DIM>
        SamePolarityAlignmentRule<DIM>::SamePolarityAlignmentRule()
            : AbstractForce<DIM>()

        {
        }

        template<unsigned DIM>
        SamePolarityAlignmentRule<DIM>::~SamePolarityAlignmentRule()
        {
        }



        template<unsigned DIM>
        void SamePolarityAlignmentRule<DIM>::SetMotility(double motility)
        {
            mMotility=motility;
        }


        template<unsigned DIM>
        double SamePolarityAlignmentRule<DIM>::GetMotility()
        {
            double motility = mMotility;
            return motility;
        }

        template<unsigned DIM>
        void SamePolarityAlignmentRule<DIM>::SetDiffusionCoefficient(double
diffusioncoefficient)
        {
            mDiffusioncoefficient=diffusioncoefficient;
        }

        template<unsigned DIM>
        double SamePolarityAlignmentRule<DIM>::GetDiffusionCoefficient()
        {
            double diffusioncoefficient=mDiffusioncoefficient;
            return diffusioncoefficient;
        }

        template<unsigned DIM>
```

```
        void SamePolarityAlignmentRule<DIM>::SetThetaValue(std::vector<double> theta)
        {
            mTheta=theta;

        }

        template<unsigned DIM>
        std::vector<double> SamePolarityAlignmentRule<DIM>::GetThetaValue()
        {

                //define element index here
                std::vector<double> theta=mTheta;
                return theta;
        }

        template<unsigned DIM>
        double SamePolarityAlignmentRule<DIM>::GetThetaValueForSingleCell(unsigned
cell_id)
        {

                //define element index here
                double theta=mTheta[cell_id];
                return theta;
        }


        template<unsigned DIM>
        void SamePolarityAlignmentRule<DIM>::UpdateThetaValueForSingleCell (unsigned
cell_id, double theta)
        {
            mTheta[cell_id]=theta;

        }

        template<unsigned DIM>
        void SamePolarityAlignmentRule<DIM>::SetStrength(double strength)
        {
            mStrength=strength;
        }


        template<unsigned DIM>
        double SamePolarityAlignmentRule<DIM>::GetStrength()
        {
            double strength = mStrength;
            return strength;
        }

        template<unsigned DIM>
        void SamePolarityAlignmentRule<DIM>::UpdateThetaValue
(std::vector<double>theta)
        {


                time_t t;
                srand(time(&t));
                unsigned num_of_cells=theta.size();
                std::vector<double> theta_noise(num_of_cells);
                std::vector<double> noise(num_of_cells);
            RandomNumberGenerator* p_gen = RandomNumberGenerator::Instance();
            double mean = 0;
            double standard_deviation = 1.0;
```

```
            double delta_t= SimulationTime::Instance()->GetTimeStep();
            double D_r=GetDiffusionCoefficient();

                for (int i=0;i<num_of_cells;i++)
                {
                        noise[i]=p_gen->NormalRandomDeviate(mean, standard_deviation);
                        theta_noise[i]=noise[i]*sqrt(2*D_r*delta_t);
                        theta[i]=theta[i]+theta_noise[i];
                }

            mTheta=theta;



        }

        template<unsigned DIM>
        void SamePolarityAlignmentRule<DIM>::AddForceContribution
(AbstractCellPopulation<DIM>(& rCellPopulation))

        {
            // Throw an exception message if not using a VertexBasedCellPopulation
            if (dynamic_cast<VertexBasedCellPopulation<DIM>*>(&rCellPopulation) ==
NULL)
            {
                EXCEPTION("polarisation_random_value is to be used with a
VertexBasedCellPopulation only");
            }

            // Helper variable that is a static cast of the cell population
            VertexBasedCellPopulation<DIM>* p_cell_population =
static_cast<VertexBasedCellPopulation<DIM>*>(&rCellPopulation);
                double strength=GetStrength();


                for (typename AbstractCellPopulation<DIM,DIM>::Iterator cell_iter =
p_cell_population->Begin();
                          cell_iter != p_cell_population->End();
                          ++cell_iter)
                {
                        VertexElement<DIM, DIM>* p_element = p_cell_population-
>GetElementCorrespondingToCell(*cell_iter);
                    unsigned cell_id = cell_iter->GetCellId();

                        double theta=GetThetaValueForSingleCell(cell_id);

                        c_vector<double,DIM> polarisation_direction;

                        polarisation_direction(0) = cos(theta);
                        polarisation_direction(1) = sin(theta);

                        double magnitude_of_force = GetMotility();



                        c_vector<double,DIM> force =
magnitude_of_force*polarisation_direction;
                //for all nodes of a single element

                    for (unsigned node_local_index=0;node_local_index<p_element-
>GetNumNodes();node_local_index++)
```

```
                        {
                                unsigned node_global_index = p_element->GetNode
(node_local_index)->GetIndex();
                            unsigned num_containing_elements = p_element->GetNode
(node_local_index)->GetNumContainingElements();
                            double
n_sq=num_containing_elements*num_containing_elements;
                            c_vector<double,DIM> force_new =
magnitude_of_force*polarisation_direction/n_sq;

                            rCellPopulation.GetNode(node_global_index)-
>AddAppliedForceContribution(force_new);

                        }

                        std::set<unsigned> neighbour_indices =
rCellPopulation.GetNeighbouringLocationIndices(*cell_iter);
                double theta_desired=0.0;
                double sin_sum=0.0;
                double num_cells=0.0;
                c_vector<double,DIM> unit_vector= zero_vector<double>(DIM);;
                for (std::set<unsigned>::iterator iter = neighbour_indices.begin();
                     iter != neighbour_indices.end();
                     ++iter)
                 {
                                CellPtr p_cell2 =
rCellPopulation.GetCellUsingLocationIndex(*iter);
                                unsigned cell_id_neighbour =
rCellPopulation.GetLocationIndexUsingCell(p_cell2);

                                double theta_neighbour=GetThetaValueForSingleCell
(cell_id_neighbour);

                                sin_sum+=sin(2.0*(theta_neighbour-theta));
                                num_cells+=1.0;

                    }

                double delta_t=SimulationTime::Instance()->GetTimeStep();

                        double first_term=strength*sin_sum*delta_t;
                        RandomNumberGenerator* p_gen = RandomNumberGenerator::Instance
();
                        double mean = 0;
                        double standard_deviation =1.0;


                        double D_r=GetDiffusionCoefficient();
                        double noise=p_gen->NormalRandomDeviate(mean,
standard_deviation);
                        double second_term=noise*sqrt(2*D_r*delta_t);
                        theta=theta+first_term+second_term;
                        UpdateThetaValueForSingleCell(cell_id, theta);

            }

        }

        template<unsigned DIM>
        void SamePolarityAlignmentRule<DIM>::OutputForceParameters(out_stream&
rParamsFile)
        {
```

```
        // Call method on direct parent class
        AbstractForce<DIM>::OutputForceParameters(rParamsFile);
    }

    /////////////////////////////////////////////////////////////////////////////
    // Explicit instantiation
    /////////////////////////////////////////////////////////////////////////////

    template class SamePolarityAlignmentRule<1>;
    template class SamePolarityAlignmentRule<2>;
    template class SamePolarityAlignmentRule<3>;

    // Serialization for Boost >= 1.36
    #include "SerializationExportWrapperForCpp.hpp"
    EXPORT_TEMPLATE_CLASS_SAME_DIMS(SamePolarityAlignmentRule)
```

```
                                /* Delta-Notch patterns with random rotational
diffusion
                                           Used in Chapter 3 (Sections - 3.3.3)
                                        */


        #include "DeltaNotchTrackingModifierWithThetaAlignRuleNew.hpp"
        #include "DeltaNotchSrnModel.hpp"

        using namespace std;
        #define PI 3.141592654

        template<unsigned DIM>
        DeltaNotchTrackingModifierWithThetaAlignRuleNew<DIM>::
             DeltaNotchTrackingModifierWithThetaAlignRuleNew
(boost::shared_ptr<ThetaAlignmentRule<DIM>> ptar)
            : AbstractCellBasedSimulationModifier<DIM>()
        {
                mptar=ptar;
        }

        template<unsigned DIM>
        DeltaNotchTrackingModifierWithThetaAlignRuleNew<DIM>::
                DeltaNotchTrackingModifierWithThetaAlignRuleNew()
            : AbstractCellBasedSimulationModifier<DIM>()
        {
        }

        template<unsigned DIM>
        DeltaNotchTrackingModifierWithThetaAlignRuleNew<DIM>::
                ~DeltaNotchTrackingModifierWithThetaAlignRuleNew()
        {
        }

        template<unsigned DIM>
        void DeltaNotchTrackingModifierWithThetaAlignRuleNew<DIM>::
                SetActivationThreshold(double activation_threshold)
        {
            mActivationThreshold=activation_threshold;
        }


        template<unsigned DIM>
        double
DeltaNotchTrackingModifierWithThetaAlignRuleNew<DIM>::GetActivationThreshold()
        {
            double activation_threshold = mActivationThreshold;
            return activation_threshold;
        }

        template<unsigned DIM>
        void DeltaNotchTrackingModifierWithThetaAlignRuleNew<DIM>::SetdTheta(double
dtheta)
        {
            mdTheta=dtheta;
        }


        template<unsigned DIM>
        double DeltaNotchTrackingModifierWithThetaAlignRuleNew<DIM>::GetdTheta()
        {
            double dtheta = mdTheta;
```

```
            return dtheta;
        }

        template<unsigned DIM>
        void DeltaNotchTrackingModifierWithThetaAlignRuleNew<DIM>::SetBoxLength(double
box_length)
        {
            mBoxLength=box_length;
        }


        template<unsigned DIM>
        double DeltaNotchTrackingModifierWithThetaAlignRuleNew<DIM>::GetBoxLength()
        {
            double box_length = mBoxLength;
            return box_length;
        }

        template<unsigned DIM>
        void DeltaNotchTrackingModifierWithThetaAlignRuleNew<DIM>::
                SetFilopodiaLength(double filopodia_length)
        {
            mFilopodiaLength=filopodia_length;
        }


        template<unsigned DIM>
        double
DeltaNotchTrackingModifierWithThetaAlignRuleNew<DIM>::GetFilopodiaLength()
        {
            double filopodia_length = mFilopodiaLength;
            return filopodia_length;
        }

        template<unsigned DIM>
        void DeltaNotchTrackingModifierWithThetaAlignRuleNew<DIM>::
                UpdateAtEndOfTimeStep(AbstractCellPopulation<DIM,DIM>&
rCellPopulation)
        {
            UpdateCellData(rCellPopulation);
        }

        template<unsigned DIM>
        void DeltaNotchTrackingModifierWithThetaAlignRuleNew<DIM>::
                SetupSolve(AbstractCellPopulation<DIM,DIM>& rCellPopulation,
std::string outputDirectory)
        {

            UpdateCellData(rCellPopulation);
        }

        template<unsigned DIM>
        void DeltaNotchTrackingModifierWithThetaAlignRuleNew<DIM>::
                UpdateCellData(AbstractCellPopulation<DIM,DIM>& rCellPopulation)
        {

            rCellPopulation.Update();
                std::vector<unsigned> location_index_all;
                double L=0.0;

            // First recover each cell's Notch and Delta concentrations from the ODEs
and store in CellData
```

```
            for (typename AbstractCellPopulation<DIM>::Iterator cell_iter =
rCellPopulation.Begin();
                 cell_iter != rCellPopulation.End();
                 ++cell_iter)
            {
                DeltaNotchSrnModel* p_model = static_cast<DeltaNotchSrnModel*>
(cell_iter->GetSrnModel());
                double this_delta = p_model->GetDelta();
                double this_notch = p_model->GetNotch();


                // Note that the state variables must be in the same order as listed
in DeltaNotchOdeSystem
                cell_iter->GetCellData()->SetItem("notch", this_notch);
                cell_iter->GetCellData()->SetItem("delta", this_delta);


               // CellPtr p_cell1 = rCellPopulation.GetCellUsingLocationIndex
(*cell_iter);
                unsigned location_index_cell =
rCellPopulation.GetLocationIndexUsingCell(*cell_iter);
                location_index_all.push_back(location_index_cell);
                //cell_centre_location_all = rCellPopulation.GetLocationOfCellCentre
(*cell_iter);
                unsigned index = rCellPopulation.GetLocationIndexUsingCell
(*cell_iter);
                        CellPtr p_cell3 = rCellPopulation.GetCellUsingLocationIndex
(index);

                c_vector<double, DIM>locat=rCellPopulation.GetLocationOfCellCentre
(p_cell3);

                if(locat(0)>L)
                {L=locat(0);}
                if(locat(1)>H)
                {H=locat(1);}
            }

            // Next iterate over the population to compute and store each cell's
neighbouring Delta concentration in CellData
            for (typename AbstractCellPopulation<DIM>::Iterator cell_iter =
rCellPopulation.Begin();
                 cell_iter != rCellPopulation.End();
                 ++cell_iter)
            {
                        unsigned location_index_cell =
rCellPopulation.GetLocationIndexUsingCell(*cell_iter);
                        CellPtr p_cell1 = rCellPopulation.GetCellUsingLocationIndex
(location_index_cell);
                // Get the set of neighbouring location indices
                std::set<unsigned> neighbour_indices =
rCellPopulation.GetNeighbouringLocationIndices(*cell_iter);
                std::set<unsigned> all_other_cells;


                // Compute this cell's average neighbouring Delta concentration and
store in CellData

                double mean_delta1 = 0.0;

                for (std::set<unsigned>::iterator iter = neighbour_indices.begin();
                     iter != neighbour_indices.end();
```

```
                    ++iter)
                {
                    CellPtr p_cell = rCellPopulation.GetCellUsingLocationIndex
(*iter);
                    double this_delta = p_cell->GetCellData()->GetItem("delta");
                    mean_delta1 += this_delta/neighbour_indices.size();

                }
                    unsigned location_index_current_cell =
rCellPopulation.GetLocationIndexUsingCell(*cell_iter);
                c_vector<double,DIM>
current_cell_location_n=rCellPopulation.GetLocationOfCellCentre(p_cell1);
                std::vector<unsigned> neighbour_indices_vector;
                std::copy(neighbour_indices.begin(), neighbour_indices.end(),
std::back_inserter(neighbour_indices_vector));
                neighbour_indices_vector.push_back(location_index_current_cell) ;
                std::set_difference(location_index_all.begin(), location_index_all.end
(), neighbour_indices_vector.begin(),
                     neighbour_indices_vector.end(), std::inserter
(all_other_cells, all_other_cells.begin()));

                    double theta1=mptar->GetThetaValueForSingleCell
(location_index_current_cell);
                    c_vector<double,DIM> p1;
                    p1(0)=cos(theta1);
                    p1(1)=sin(theta1);

                     double sum_delta2=0.0;
                    double count=0.0;
                    double mean_delta2=0.0;
                    double mean_delta=0.0;
                    double W_sum=0.0;

                    for (std::set<unsigned>::iterator iter2 =
all_other_cells.begin();
                     iter2 != all_other_cells.end();
                     ++iter2)
                {
                                        CellPtr p_cell2 =
rCellPopulation.GetCellUsingLocationIndex(*iter2);
                                        unsigned location_index_of_contact_cell =
rCellPopulation.GetLocationIndexUsingCell(p_cell2);
                                        c_vector<double,DIM>
cell_location_p=rCellPopulation.GetLocationOfCellCentre(p_cell2);

                                        c_vector<double,DIM>
R_np=current_cell_location_n-cell_location_p;

                                        if(R_np(0)<-L/2.0)
                                        {
                                                R_np(0)+=L;
                                        }
                                        if(R_np(0)>L/2.0)
                                        {
                                                R_np(0)-=L;
                                        }
                                        if(R_np(1)<-H/2.0)
                                        {
                                                R_np(1)+=H;
                                        }
                                        if(R_np(1)>H/2.0)
                                        {
```

```
                                                R_np(1)-=H;
                                        }

                                        double D=norm_2(R_np);
                                        R_np=R_np/D;
                                        double theta2=mptar-
>GetThetaValueForSingleCell(location_index_of_contact_cell);
                                        double l1=(GetFilopodiaLength()-0.3)*2.0;
                                        double l2=(GetFilopodiaLength()+0.3)*2.0;
                                        if(l2>=D && D>=l1)

                                        {
                                                c_vector<double,DIM> p2;
                                                p2(0)=cos(theta2);
                                                p2(1)=sin(theta2);


                                                double del_theta=GetdTheta();
                                                double thresh1=GetActivationThreshold
();

                                                double C11=((p1(0)*R_np(0))+(p1
(1)*R_np(1)))*((p1(0)*R_np(0))+(p1(1)*R_np(1)));
                                                double C12=((p2(0)*R_np(0))+(p2
(1)*R_np(1)))*((p2(0)*R_np(0))+(p2(1)*R_np(1)));
                                                double C1=pow(((1.0/2.0)*(C11
+C12)),1.0);
                                                double C2=pow((sin(del_theta)),2.0);

                                                double W=std::max(C1,C2);

                                                double this_delta = p_cell2-
>GetCellData()->GetItem("delta");

                                                if(W>=thresh1){sum_delta2 +=
this_delta;
                                                        count+=1.0;}
                                                else{count+=0;}


                                        }

                    }
                double beta1=0.01; //0.01
                double beta2=0.99; //0.99

                if(count==0.0)

                {

                                mean_delta=beta1*mean_delta1;
                        }
                        else
                        {
                                mean_delta2=sum_delta2/count;
                                mean_delta=(beta1*mean_delta1+beta2*mean_delta2)/2.0;

                        }

                cell_iter->GetCellData()->SetItem("mean delta", mean_delta);
```

```
                        /* Delta-Notch patterns with polarity alignment with the
nearest neighbors
                                            Used in Chapter 3 (Sections - 3.3.1 and
3.3.2)
                                        */


        #include "DeltaNotchTrackingModifierWithSamePolarityAlign.hpp"
        #include "DeltaNotchSrnModel.hpp"

        using namespace std;
        #define PI 3.141592654

        template<unsigned DIM>
        DeltaNotchTrackingModifierWithSamePolarityAlign<DIM>::
        DeltaNotchTrackingModifierWithSamePolarityAlign(boost::
                shared_ptr<SamePolarityAlignmentRule<DIM>> ptar2)
            : AbstractCellBasedSimulationModifier<DIM>()
        {
                mptar2=ptar2;
        }

        template<unsigned DIM>
        DeltaNotchTrackingModifierWithSamePolarityAlign<DIM>::
                DeltaNotchTrackingModifierWithSamePolarityAlign()
            : AbstractCellBasedSimulationModifier<DIM>()
        {
        }

        template<unsigned DIM>
        DeltaNotchTrackingModifierWithSamePolarityAlign<DIM>::
                ~DeltaNotchTrackingModifierWithSamePolarityAlign()
        {
        }

        template<unsigned DIM>
        void DeltaNotchTrackingModifierWithSamePolarityAlign<DIM>::
        SetActivationThreshold(double activation_threshold)
        {
            mActivationThreshold=activation_threshold;
        }


        template<unsigned DIM>
        double DeltaNotchTrackingModifierWithSamePolarityAlign<DIM>::
                GetActivationThreshold()
        {
            double activation_threshold = mActivationThreshold;
            return activation_threshold;
        }

        template<unsigned DIM>
        void DeltaNotchTrackingModifierWithSamePolarityAlign<DIM>::SetdTheta(double
dtheta)
        {
            mdTheta=dtheta;
        }


        template<unsigned DIM>
        double DeltaNotchTrackingModifierWithSamePolarityAlign<DIM>::GetdTheta()
        {
```

```
            double dtheta = mdTheta;
            return dtheta;
        }

        template<unsigned DIM>
        void DeltaNotchTrackingModifierWithSamePolarityAlign<DIM>::SetBoxLength(double
box_length)
        {
            mBoxLength=box_length;
        }


        template<unsigned DIM>
        double DeltaNotchTrackingModifierWithSamePolarityAlign<DIM>::GetBoxLength()
        {
            double box_length = mBoxLength;
            return box_length;
        }

        template<unsigned DIM>
        void DeltaNotchTrackingModifierWithSamePolarityAlign<DIM>::
                SetFilopodiaLength(double filopodia_length)
        {
            mFilopodiaLength=filopodia_length;
        }


        template<unsigned DIM>
        double
DeltaNotchTrackingModifierWithSamePolarityAlign<DIM>::GetFilopodiaLength()
        {
            double filopodia_length = mFilopodiaLength;
            return filopodia_length;
        }

        template<unsigned DIM>
        void DeltaNotchTrackingModifierWithSamePolarityAlign<DIM>::
                UpdateAtEndOfTimeStep(AbstractCellPopulation<DIM,DIM>&
rCellPopulation)
        {
            UpdateCellData(rCellPopulation);
        }

        template<unsigned DIM>
        void DeltaNotchTrackingModifierWithSamePolarityAlign<DIM>::
                SetupSolve(AbstractCellPopulation<DIM,DIM>& rCellPopulation,
std::string outputDirectory)
        {

            UpdateCellData(rCellPopulation);
        }

        template<unsigned DIM>
        void DeltaNotchTrackingModifierWithSamePolarityAlign<DIM>::
                UpdateCellData(AbstractCellPopulation<DIM,DIM>& rCellPopulation)
        {
                std::ofstream OFileObject;
                OFileObject.open("PolarityDrpt1Spt15.csv", ios::app);

            rCellPopulation.Update();
                std::vector<unsigned> location_index_all;
                double L=0.0;
```

```
                double H=0.0;

            for (typename AbstractCellPopulation<DIM>::Iterator cell_iter =
rCellPopulation.Begin();
                 cell_iter != rCellPopulation.End();
                 ++cell_iter)
            {
                DeltaNotchSrnModel* p_model = static_cast<DeltaNotchSrnModel*>
(cell_iter->GetSrnModel());
                double this_delta = p_model->GetDelta();
                double this_notch = p_model->GetNotch();


                // Note that the state variables must be in the same order as listed
in DeltaNotchOdeSystem
                cell_iter->GetCellData()->SetItem("notch", this_notch);
                cell_iter->GetCellData()->SetItem("delta", this_delta);



                unsigned location_index_cell =
rCellPopulation.GetLocationIndexUsingCell(*cell_iter);
                location_index_all.push_back(location_index_cell);

                unsigned index = rCellPopulation.GetLocationIndexUsingCell
(*cell_iter);
                        CellPtr p_cell3 = rCellPopulation.GetCellUsingLocationIndex
(index);

                c_vector<double, DIM>locat=rCellPopulation.GetLocationOfCellCentre
(p_cell3);

                if(locat(0)>L)
                {L=locat(0);}
                if(locat(1)>H)
                {H=locat(1);}

            }

            // Next iterate over the population to compute and store each cell's
neighbouring Delta concentration in CellData
            for (typename AbstractCellPopulation<DIM>::Iterator cell_iter =
rCellPopulation.Begin();
                 cell_iter != rCellPopulation.End();
                 ++cell_iter)
            {


                        unsigned location_index_cell =
rCellPopulation.GetLocationIndexUsingCell(*cell_iter);
                        CellPtr p_cell1 = rCellPopulation.GetCellUsingLocationIndex
(location_index_cell);
                // Get the set of neighbouring location indices
                std::set<unsigned> neighbour_indices =
rCellPopulation.GetNeighbouringLocationIndices(*cell_iter);
                std::set<unsigned> all_other_cells;



                double mean_delta1 = 0.0;

                for (std::set<unsigned>::iterator iter = neighbour_indices.begin();
```

```
                    iter != neighbour_indices.end();
                    ++iter)
                {
                    CellPtr p_cell = rCellPopulation.GetCellUsingLocationIndex
(*iter);
                    double this_delta = p_cell->GetCellData()->GetItem("delta");

                    mean_delta1 += this_delta/neighbour_indices.size();

                 }


                unsigned location_index_current_cell =
rCellPopulation.GetLocationIndexUsingCell(*cell_iter);
                c_vector<double,DIM>
current_cell_location_n=rCellPopulation.GetLocationOfCellCentre(p_cell1);
                std::vector<unsigned> neighbour_indices_vector;
                std::copy(neighbour_indices.begin(), neighbour_indices.end(),
std::back_inserter(neighbour_indices_vector));
                neighbour_indices_vector.push_back(location_index_current_cell) ;
                std::set_difference(location_index_all.begin(), location_index_all.end
(),neighbour_indices_vector.begin(),
                         neighbour_indices_vector.end(), std::inserter
(all_other_cells, all_other_cells.begin()));

                        double theta1=mptar2->GetThetaValueForSingleCell
(location_index_current_cell);
                        c_vector<double,DIM> p1;
                        p1(0)=cos(theta1);
                        p1(1)=sin(theta1);
                        unsigned simulation_time= SimulationTime::Instance()-
>GetTimeStepsElapsed();
                        if(simulation_time%100==0)
                        {
                                OFileObject <<simulation_time<< " ";
                                OFileObject <<theta1<< " "<<"\n";
                        }
                        double sum_delta2=0.0;
                        double count=0.0;
                        double mean_delta2=0.0;
                        double mean_delta=0.0;

                        for (std::set<unsigned>::iterator iter2 =
all_other_cells.begin();
                         iter2 != all_other_cells.end();
                         ++iter2)
                    {
                                        CellPtr p_cell2 =
rCellPopulation.GetCellUsingLocationIndex(*iter2);
                                        unsigned location_index_of_contact_cell =
rCellPopulation.GetLocationIndexUsingCell(p_cell2);
                                        c_vector<double,DIM>
cell_location_p=rCellPopulation.GetLocationOfCellCentre(p_cell2);
                                        c_vector<double,DIM>
R_np=current_cell_location_n-cell_location_p;
                                        if(R_np(0)<-L/2.0)
                                        {
                                                R_np(0)+=L;
                                        }
                                        if(R_np(0)>L/2.0)
                                        {
                                                R_np(0)-=L;
```

```
                                        }
                                        if(R_np(1)<-H/2.0)
                                        {
                                                R_np(1)+=H;
                                        }
                                        if(R_np(1)>H/2.0)
                                        {
                                                R_np(1)-=H;
                                        }

                                        double D=norm_2(R_np);
                                        R_np=R_np/D;
                                        double theta2=mptar2-
>GetThetaValueForSingleCell(location_index_of_contact_cell);
                                        double l1=(GetFilopodiaLength()-0.3)*2.0;
                                        double l2=(GetFilopodiaLength()+0.3)*2.0;
                                        if(l2>=D && D>=l1)

                                        {
                                                c_vector<double,DIM> p2;
                                                p2(0)=cos(theta2);
                                                p2(1)=sin(theta2);


                                                double del_theta=GetdTheta();
                                                double thresh=GetActivationThreshold
();
                                                double C11=((p1(0)*R_np(0))+(p1
(1)*R_np(1)))*((p1(0)*R_np(0))+(p1(1)*R_np(1)));
                                                double C12=((p2(0)*R_np(0))+(p2
(1)*R_np(1)))*((p2(0)*R_np(0))+(p2(1)*R_np(1)));
                                                double C1=pow(((1.0/2.0)*(C11
+C12)),1.0);
                                                double C2=pow((sin(del_theta)),2.0);

                                                double W=std::max(C1,C2);

                                                double this_delta = p_cell2-
>GetCellData()->GetItem("delta");

                                                if(W>=thresh){sum_delta2 +=
this_delta;
                                                        count+=1.0;}
                                                else{count+=0;}



                                        }

                    }
                double beta1=0.01;
                double beta2=0.99;

                if(count==0.0)

                {

                                mean_delta=beta1*mean_delta1;
                        }
                        else
                        {
                                mean_delta2=sum_delta2/count;
```

```
                                mean_delta=(beta1*mean_delta1+beta2*mean_delta2)/2.0;

                        }

                cell_iter->GetCellData()->SetItem("mean delta", mean_delta);

            }
            OFileObject.close();

        }


        template<unsigned DIM>
        void
DeltaNotchTrackingModifierWithSamePolarityAlign<DIM>::OutputSimulationModifierParameters
(out_stream& rParamsFile)
        {
            // No parameters to output, so just call method on direct parent class

AbstractCellBasedSimulationModifier<DIM>::OutputSimulationModifierParameters
(rParamsFile);
        }

        // Explicit instantiation
        template class DeltaNotchTrackingModifierWithSamePolarityAlign<1>;
        template class DeltaNotchTrackingModifierWithSamePolarityAlign<2>;
        template class DeltaNotchTrackingModifierWithSamePolarityAlign<3>;

        // Serialization for Boost >= 1.36
        #include "SerializationExportWrapperForCpp.hpp"
        EXPORT_TEMPLATE_CLASS_SAME_DIMS
(DeltaNotchTrackingModifierWithSamePolarityAlign)
```

```
import numpy as np
import csv
from sklearn.cluster import DBSCAN
from sklearn import metrics
from sklearn.datasets.samples_generator import make_blobs
from sklearn.preprocessing import StandardScaler
import pandas as pd
from numpy import math
from scipy.spatial.distance import pdist,squareform
import matplotlib.pyplot as plt

median_cluster=[]


# In[4]:


import numpy as np

from sklearn.cluster import DBSCAN
from sklearn import metrics
from sklearn.datasets.samples_generator import make_blobs
from sklearn.preprocessing import StandardScaler
import pandas as pd
from numpy import math
from scipy.spatial.distance import pdist,squareform
import matplotlib.pyplot as plt
N=400
tmax=301
min_sample=3
dis=1.5
df=pd.read_csv('celldeltanotchdthetaPIby3Tpt1.csv', sep=' ', names=["id", "X", "Y",
"Delta", "Notch", "Mean_Notch","Area", "Nothing"])
df = df.iloc[80000:]

X11=df['X'].values.reshape(tmax,N)

Y11=df['Y'].values.reshape(tmax,N)
#print(np.max(X11))
delta_matrix=df['Delta'].values.reshape(tmax,N)
indicesList_list=[]
uniqueValues_list=[]
total_num_of_clusters=[]


#print(X1.shape)
median_cluster_size_list=[]
for t in range(0,tmax):
    indices,=np.where(delta_matrix[t,:]>0.5)
    N=len(indices)
    X1=X11[t,indices]

    Y1=Y11[t,indices]
    L=np.max(X11[t,:])
    H=np.max(Y11[t,:])
    rnew=np.zeros([N,N])
    for i in range(0,N):
        for j in range(0,N):

            xx=X1[i]-X1[j]
            #print('xx shape',xx.shape)
            yy=Y1[i]-Y1[j]
```

```
            if(xx>0.5*L): xx=xx-L
            if(xx<-0.5*L): xx=xx+L
            if(yy>0.5*L): yy=yy-L
            if(yy<-0.5*L): yy=yy+L

            r=np.sqrt(xx**2+yy**2)

            rnew[i,j]=r
    db = DBSCAN(eps=dis, min_samples=min_sample, metric="precomputed").fit(rnew)
    labels = db.labels_
    core_samples_mask = np.zeros_like(labels, dtype = bool)
    core_samples_mask[db.core_sample_indices_] = True
    n_clusters_ = len(set(labels)) - (1 if -1 in labels else 0)
    n_noise_ = list(labels).count(-1)
    #print('Estimated number of clusters: %d' % n_clusters_)
    total_num_of_clusters.append(n_clusters_)

    #print('Estimated number of noise points: %d' % n_noise_)
    ch1_counts = np.bincount((labels[labels>=0]).astype(int))
    Num_of_particles_per_cluster=ch1_counts
    median_cluster_siz=np.median(Num_of_particles_per_cluster)
    median_cluster_size_list.append(median_cluster_siz)

    #print('Number of particles per cluster:', ch1_counts)
    #uniqueValues, indicesList = np.unique(ch1_counts, return_counts=True)
    #uniqueValues_list.append(uniqueValues)
    #indicesList_list.append(indicesList)
median_cluster_size=np.median(median_cluster_size_list)
median_cluster.append(median_cluster_size)

#print('total_num_of_clusters',total_num_of_clusters)
```

```
import numpy as np
import csv
from sklearn.cluster import DBSCAN
from sklearn import metrics
from sklearn.datasets.samples_generator import make_blobs
from sklearn.preprocessing import StandardScaler
import pandas as pd
from numpy import math
from scipy.spatial.distance import pdist,squareform
import matplotlib.pyplot as plt
from numpy import linalg as LA

inertia_median_list=[]


# In[3]:


N=400
tmax=301
min_sample=3
dis=1.5
df=pd.read_csv('celldeltanotchS0dthetaPIby2.csv', sep=' ', names=["id", "X", "Y",
"Delta", "Notch", "Mean_Notch","Area", "Nothing"])
df = df.iloc[80000:]

X11=df['X'].values.reshape(tmax,N)

Y11=df['Y'].values.reshape(tmax,N)
#print(np.max(X11))
delta_matrix=df['Delta'].values.reshape(tmax,N)
indicesList_list=[]
uniqueValues_list=[]
total_num_of_clusters=[]
A0=0.866

#print(X1.shape)
inertia_mean=[]
for t in range(0,tmax):
    indices,=np.where(delta_matrix[t,:]>0.5)
    N=len(indices)
    X1=X11[t,indices]
    #print(X1.shape)

    Y1=Y11[t,indices]
    L=np.max(X11[t,:])
    H=np.max(Y11[t,:])
    rnew=np.zeros([N,N])
    for i in range(0,N):
        for j in range(0,N):

            xx=X1[i]-X1[j]
            #print('xx shape',xx.shape)
            yy=Y1[i]-Y1[j]
            if(xx>0.5*L): xx=xx-L
            if(xx<-0.5*L): xx=xx+L
            if(yy>0.5*L): yy=yy-L
            if(yy<-0.5*L): yy=yy+L

            r=np.sqrt(xx**2+yy**2)

            rnew[i,j]=r
```

```
db = DBSCAN(eps=dis, min_samples=min_sample, metric="precomputed").fit(rnew)
labels = db.labels_   #-1,2...13 ie no. of clusters and noise
#print("labels",labels)
core_samples_mask = np.zeros_like(labels, dtype = bool)
core_samples_mask[db.core_sample_indices_] = True
n_clusters_ = len(set(labels)) - (1 if -1 in labels else 0)
n_noise_ = list(labels).count(-1)
#print('Estimated number of clusters: %d' % n_clusters_)
total_num_of_clusters.append(n_clusters_)

#print('Estimated number of noise points: %d' % n_noise_)
ch1_counts = np.bincount(labels[labels>=0])
L=20.0
H=18.0
xyold=np.zeros([1,2])
X1=X1.reshape(len(X1),1)
Y1=Y1.reshape(len(Y1),1)
#print(X1.shape, Y1.shape)
Xnew=np.concatenate((X1,Y1),axis=1)
unique_labels = set(labels)
colors = [plt.cm.Spectral(each)
          for each in np.linspace(0, 1, len(unique_labels))]
inertia_list=[]
for k, col in zip(unique_labels, colors):
    if k == -1:
        # Black used for noise.
        col = [0, 0, 0, 1]

    class_member_mask = (labels == k)

    xy = Xnew[class_member_mask & core_samples_mask]
    #plt.plot(xy[:, 0], xy[:, 1], 'o', markerfacecolor=tuple(col),
     #        markeredgecolor='k', markersize=14)
    #print(xy.shape)
    #print(xy)

    #with open('cluster_xy', 'w') as f:
    #    writer = csv.writer(f, delimiter=' ')
    #    writer.writerows(xyold)
    #f.close()

    x_mean=np.mean(xy[:,0])
    y_mean=np.mean(xy[:,1])
    xx=xy[:, 0]-x_mean
    yy=xy[:, 1]-y_mean
    #print(xx)
    xy[:, 0]=np.where(xx>-L/2.0, xy[:, 0], xy[:, 0]+L)
    xy[:, 0]=np.where(xx<L/2.0, xy[:, 0], xy[:, 0]-L)
    xy[:, 1]=np.where(yy>-H/2.0, xy[:, 1], xy[:, 1]+H)
    xy[:, 1]=np.where(yy<H/2.0, xy[:, 1], xy[:, 1]-H)
    x_mean=np.mean(xy[:,0])
    y_mean=np.mean(xy[:,1])
    xx=xy[:, 0]-x_mean
    yy=xy[:, 1]-y_mean
    #print(xx)
    Ixx=np.sum(A0*(xx**2.0))
    Iyy=np.sum(A0*(yy**2.0))
    Ixy=np.sum(A0*(xx*yy))
    A=[[Ixx,Ixy],[Ixy,Iyy]]
    igen_val, igen_vec = LA.eig(A)
    #print(igen_val)
    Imax=np.max(igen_val)
```

```
        Imin=np.min(igen_val)
        inertial_ratio=Imax/float(Imin)

        if xy.shape[0]>2:
            #print(xy)
            #print(inertial_ratio)
            inertia_list.append(inertial_ratio)
        #print(xy)
        #print(x_mean)
        #print(y_mean)

        #print(x_mean)
        #print(Ixx,Iyy)

        #print(Ixx/float(Iyy))
        xy = Xnew[class_member_mask & ~core_samples_mask]

        #plt.plot(xy[:, 0], xy[:, 1], 'o', markerfacecolor=tuple(col),
        #         markeredgecolor='k', markersize=6)
    inertia_mean.append(np.median(inertia_list))
    #plt.title('Estimated number of clusters: %d' % n_clusters_)
    #plt.show()
inertia_median=np.median(inertia_mean)
inertia_median_list.append(inertia_median)
```

```
import numpy as np
import csv
import pandas as pd
#from sklearn import preprocessing
import matplotlib.pyplot as plt
from numpy import math
df=pd.read_csv('celldeltanotchDeltaDeltaCorr-1.csv', sep=' ', names=["id", "X", "Y",
"Delta", "Notch", "Mean_Notch","Area", "Nothing"])
PI=3.141592654
N=1600
total_time=2701
L=40.0
H=34.64
ti=0
tf=2701
A0=0.866
lc=np.sqrt(A0)
delta_t=tf-ti

R=np.arange(0.0,16.0,0.1)/lc
dt_i=0
dt_f=300
dtt=20
tp=(dt_f-dt_i-1)/dtt
dd_avg_value=np.zeros([tf-ti,len(R)-1])
dd_corr=np.zeros([tf-ti,len(R)-1])
df = df.iloc[480000:]
#df = df.iloc[4320000:]
X_matrix=df['X'].values.reshape(total_time,N)
Y_matrix=df['Y'].values.reshape(total_time,N)
delta_matrix=df['Delta'].values.reshape(total_time,N)

#r=np.zeros([(tf-ti),N])
#delta_delta=np.zeros([(tf-ti),N])
for dt in range(dt_i,dt_f,dtt):# 0-tf
    dd_sum=0.0

    for t in range(0,tf-dt):  # 0-1
        for i in range(0,N): # 0-N
            j=list(xrange(N))  # 0-N
            j.remove(i)
            xx=X_matrix[t,i]-X_matrix[t+dt,j]
            yy=Y_matrix[t,i]-Y_matrix[t+dt,j]
            dd=delta_matrix[t,i]*delta_matrix[t+dt,j]
            dd_sum+=np.sum(dd)
            #print(dd.shape)
            xx=np.where(xx>-L/2.0, xx, xx+L)

            xx=np.where(xx<L/2.0, xx, xx-L)
            yy=np.where(yy>-H/2.0, yy, yy+H)
            yy=np.where(yy<H/2.0, yy, yy-H)

            r=np.sqrt(np.square(xx)+np.square(yy))

            #print(r)
            for k in range(0,len(R)-1):
                bools1 = r > R[k]
                bools2 = r <= R[k+1]
                index,=np.where(bools1*bools2)
                dd_value=dd[index]
                annular_area=PI*(np.square(R[k+1])-np.square(R[k]))
                dd_avg_value[dt,k]+=np.sum(dd_value)/annular_area
```

```
        #dd_avg_value=dd_avg_value#/(tf-dt)#(tf+ti-dt)
    dd_corr[dt,:]=dd_avg_value[dt,:]/(N*(tf-dt))  #(N*(tf-ti)
    dd_avg=dd_sum/(N*(N-1)*(tf-dt))
    dd_corr[dt,:]=dd_corr[dt,:]/dd_avg
#R=np.arange(0.1,16.0,0.1)/lc
#print(dd_corr.shape)
#print(R.shape)

df = pd.DataFrame(data=dd_corr)
df.to_csv('VanHoveDeltaDeltaCorr-1.csv', sep=' ', header=False, index=False)
```

Appendix C

C.1 Mean Area and mean current shape index

The mean area of Delta and Notch cells is calculated for $\mathcal{N} = 400$ cells for $M = 500$ time-frames after removing the transient part of the corresponding simulation. Any cell α is considered a Delta or a Notch cell if the concentration of Delta and Notch molecules in the cell $D_\alpha \geq D_{\text{critical}} = 0.5$ and $N_\alpha \geq N_{\text{critical}} = 0.5$, respectively. Each data point for average cell area is calculated by taking the average of areas of $\mathcal{N}_D$ Delta cells (Figs 5.2a and 5.4a) and $\mathcal{N}_N$ Notch cells (Fig 5.2b and 5.4b) separately as: $\frac{1}{\mathcal{N}_X T}\sum_{t=0}^{T}\sum_{\alpha=1}^{\mathcal{N}_X} A_\alpha^t$, where $X \equiv D, N$. In a similar manner, each data point of the average shape index is calculated by taking the average of current shape index $L_\alpha/\sqrt{A_\alpha}$ of individual Delta cells (Fig 5.2c and 5.4c) and Notch cells (Fig 5.2d and 5.4d) separately.

C.2 Stress tensor in the vertex model

In a vertex model, for a given cell α, the average stress tensor is given by [7]

$$\sigma_{xx}^{(\alpha)} = -P_\alpha + \frac{1}{A_\alpha}\sum_{\beta} T_{\alpha\beta} l_{\alpha\beta} \sin^2\phi_{\alpha\beta} \tag{C.1a}$$

Table C.1: Dimensionless parameters of the model with respect to the characteristic length scale $L_c = d$ (minimal cell diameter of initial hexagonal cell), characteristic time scale $T_c = \frac{\eta}{Kd^2}$ and characteristic force scale $F_c = Kd^3$ in terms of dimensional parameters that appear in equations 5.3 and 5.7.

Dimensionless parameters	**Parameter values**
$d \equiv \frac{d}{L_c}$	1.0
$\eta \equiv \frac{\eta L_c}{F_c T_c}$	1.0
$K \equiv \frac{K L_c^3}{F_c}$	1.0
$\Gamma \equiv \frac{\Gamma L_c}{F_c}$	1.0
$\Lambda \equiv \frac{\Lambda}{F_c}$	$[-11.17, -14.88]$
C	$-0.6 - 0.6$
B	$[-1.0, 1.0]$
$v_0 \equiv {}^{v_0 T_c}/_{L_c}$	$[0, 0.1, 0.3]$
$A_0 \equiv A_0/L_c^2$	0.866
$\xi \equiv \xi T_c$	$0 - 2$
$D_r \equiv D_r T_c$	1.0
$D_\alpha \equiv {}^{D_\alpha}/_{D_0}$	$0 - 1$
$N_\alpha \equiv {}^{N_\alpha}/_{N_0}$	$0 - 1$
$R_D \equiv R_D T_c$	$[1, 10]$
$R_N \equiv R_N T_c$	$[1, 10]$
$\rho \equiv \rho T_c$	$[1, 10]$
$\mu \equiv \mu T_c$	$[1, 10]$
$l \equiv l/L_c$	1.7
$\Delta l \equiv \Delta l/L_c$	1.2
$\Delta\theta \equiv \Delta\theta$	$\pi/4$
$\Delta t \equiv \Delta t/T_c$	0.01
a	[0.01]
b	[100]
$D_{\text{critical}} \equiv {}^{D_{\text{critical}}}/_{D_0}$	0.5
$N_{\text{critical}} \equiv {}^{N_{\text{critical}}}/_{N_0}$	0.5
$\mathcal{N}$	400
T	0.9
Δr	0.1

$$\sigma_{yy}^{(\alpha)} = -P_\alpha + \frac{1}{A_\alpha}\sum_\beta T_{\alpha\beta} l_{\alpha\beta} \cos^2\phi_{\alpha\beta} \tag{C.1b}$$

$$\sigma_{xy}^{(\alpha)} = \sigma_{yx}(\alpha) = \frac{1}{A_\alpha}\sum_\beta T_{\alpha\beta} l_{\alpha\beta} \sin\phi_{\alpha\beta}\cos\phi_{\alpha\beta}, \tag{C.1c}$$

where P_α is the area pressure of cell α is given by $P_\alpha = -2K(A_\alpha - A_{\alpha,0})$ (see Eq. 5.3). $T_{\alpha\beta}$ is the effective tension of the bond $\alpha\beta$ and is equal to $T_{\alpha\beta} = \frac{1}{2}\Lambda_{\alpha\beta} + 2\Gamma L_\alpha$, where L_α is the perimeter of cell α. The isotropic stress is the trace of the stress tensor and represents effective cell pressure

$$P_\alpha^{\text{total}} = P_\alpha - \frac{1}{2A_\alpha}\sum_\beta T_{\alpha\beta} l_{\alpha\beta} \tag{C.2}$$

The anisotropic part of the overall stress tensor, i.e, the pure shear stress tensor, is symmetric and traceless, and is given by

$$\tilde{\sigma}_\alpha = \frac{1}{2A_\alpha}\begin{bmatrix} -\sum_\beta T_{\alpha\beta} l_{\alpha\beta}\cos 2\phi_{\alpha\beta} & \sum_\beta T_{\alpha\beta} l_{\alpha\beta}\sin 2\phi_{\alpha\beta} \\ \sum_\beta T_{\alpha\beta} l_{\alpha\beta}\sin 2\phi_{\alpha\beta} & \sum_\beta T_{\alpha\beta} l_{\alpha\beta}\cos 2\phi_{\alpha\beta} \end{bmatrix}$$

where, ϕ is the orientation of the shear axis. Dropping the index α, the shear stress for the cell can be written in a compact notation,

$$\tilde{\boldsymbol{\sigma}} = \gamma \begin{bmatrix} \cos 2\phi & \sin 2\phi \\ \sin 2\phi & -\cos 2\phi \end{bmatrix}$$

where, $\gamma = \sqrt{\tilde{\sigma}_{xx}^2 + \tilde{\sigma}_{xy}^2}$ represents the magnitude of shear stress.

Each data point of the average isotropic stress or total cell pressure in Fig 5.2 and 5.4, is calculated by taking simple average of total cell pressure of all Delta cells and Notch cells separately, and is calculated calculated with the initial number of cells equal to $\mathcal{N} = 400$ cells and for $M = 500$ time frames after removing the transient part of the corresponding

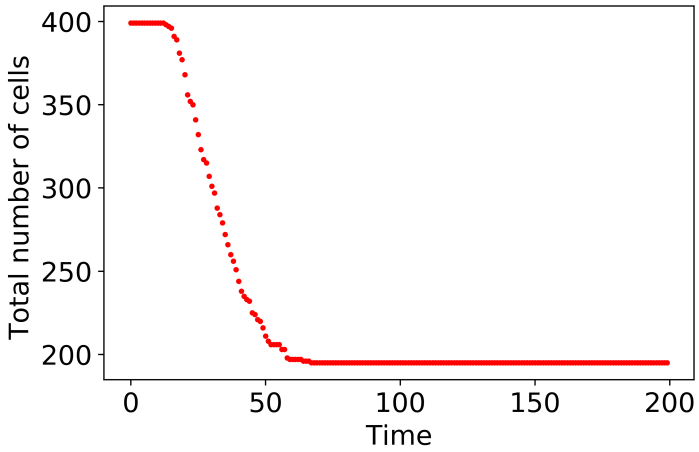

Figure C.1: Plot showing the number of cells as a function of time with Delta-dependent line tension parameter and negative coupling constant C, corresponding Fig. 5.1a. The parameters are $\beta_j/\beta_p \approx 100$, $\Lambda_0 = -14.14$, $v_0 \approx 0$, $K = 1$, $\Gamma = 1$, $\rho = \mu = R_N = R_D = 1$ and $C = -0.6$. The number of cells decreases with time indicating cell extrusion, and reaches steady state after some time by maintaining a fixed number of cells.

simulation as discussed above.

C.3 Cell extrusions in the tissue

For much lower values of C, the tissue exhibit steady apoptosis or cell extrusion. The cell number decreases with time and ultimately reaches a steady state value (Fig. C.1).

C.4 Movie Captions

Movie link is as follows:
https://drive.google.com/drive/folders/1dOcZo8etkHlcOwtDvwFNg1ufjOrOPOOQ?usp=sharing

Movie-1 corresponding to Fig. 1a. Pattern obtained using the model for $R_N = R_D = \rho = \mu = 1$, $\frac{\beta_j}{\beta_p} = 0.99$, $v_0 = 0$ and $\Lambda = -14.14$, $B = 1$ and $C = -0.6$.

Movie-2 corresponding to Fig. 1b. Pattern obtained using the model for $R_N = R_D = \rho = \mu = 1$, $\frac{\beta_j}{\beta_p} = 0.99$, $v_0 = 0$ and $\Lambda = -14.14$, $B = 1$ and $C = -0.2$.

Movie-3 corresponding to Fig. 1c. Pattern obtained using the model for $R_N = R_D = \rho = \mu = 1$, $\frac{\beta_j}{\beta_p} = 0.99$, $v_0 = 0$ and $\Lambda = -14.14$, $B = 1$ and $C = 0.04$.

Movie-4 corresponding to Fig. 1d. Pattern obtained using the model for $R_N = R_D = \rho = \mu = 1$, $\frac{\beta_j}{\beta_p} = 0.99$, $v_0 = 0$ and $\Lambda = -14.14$, $B = 1$ and $C = 0.16$.

Movie-5 corresponding to Fig. 1e. Pattern obtained using the model for $R_N = R_D = \rho = \mu = 1$, $\frac{\beta_j}{\beta_p} = 0.99$, $v_0 = 0$ and $\Lambda = -11.17$, $B = 1$ and $C = 0.2$.

Movie-6 corresponding to Fig. 1f. Pattern obtained using the model for $R_N = R_D = \rho = \mu = 1$, $\frac{\beta_j}{\beta_p} = 0.99$, $v_0 = 0$ and $\Lambda = -11.17$, $B = 1$ and $C = 0.6$.

Movie-7 corresponding to Fig. 3a. Pattern obtained using the model for $R_N = R_D = \rho = \mu = 1$, $\frac{\beta_j}{\beta_p} = 0.99$, $v_0 = 0$ and $\Lambda = -14.14$, $B = 1$ and $C = -0.6$.

Movie-8 corresponding to Fig. 3b. Pattern obtained using the model for $R_N = R_D = \rho = \mu = 1$, $\frac{\beta_j}{\beta_p} = 0.99$, $v_0 = 0$ and $\Lambda = -14.14$, $B = 1$ and $C = -0.2$.

Movie-9 corresponding to Fig. 3c. Pattern obtained using the model for $R_N = R_D = \rho = \mu = 1$, $\frac{\beta_j}{\beta_p} = 0.99$, $v_0 = 0$ and $\Lambda = -14.14$, $B = 1$ and $C = 0.04$.

Movie-10a corresponding to Fig. 3d. Pattern obtained using the model for $R_N = R_D = \rho = \mu = 1$, $\frac{\beta_j}{\beta_p} = 0.99$, $v_0 = 0$ and $\Lambda = -14.14$, $B = 1$ and $C = 0.08$.

Movie-10b Pattern obtained using the model for $R_N = R_D = \rho = \mu = 1$, $\frac{\beta_j}{\beta_p} = 0.99$, $v_0 = 0$ and $\Lambda = -14.14$, $B = 1$ and $C = 0.2$.

Movie-11 corresponding to Fig. 5a. Pattern obtained using the model for $R_N = R_D = \rho = \mu = 10$, $D_r = 10^{-3}$, $\frac{\beta_j}{\beta_p} = 10^{-2}$, $\Delta\theta = \pi/4$, $v_0 = 0.1 \times 10^{-4}$, $\Lambda = -14.32$, $T = 0.9$ and $C = 0$.

Movie-12 corresponding to Fig. 5b. Pattern obtained using the model for $R_N = R_D = \rho = \mu = 10$, $D_r = 10^{-3}$, $\frac{\beta_j}{\beta_p} = 10^{-2}$, $\Delta\theta = \pi/4$, $v_0 = 0.1$, $\Lambda = -14.32$, $T = 0.9$, $B = 1$ and $C = -0.6$.

Movie-13 corresponding to Fig. 5c. Pattern obtained using the model for $R_N = R_D = \rho = \mu = 10$, $D_r = 10^{-3}$, $\frac{\beta_j}{\beta_p} = 10^{-2}$, $\Delta\theta = \pi/4$, $v_0 = 0.1$, $\Lambda = -14.32$, $T = 0.9$, $B = 1$ and $C = 0.1$.

Movie-14 corresponding to Fig. 5d. Pattern obtained using the model for $R_N = R_D = \rho = \mu = 10$, $D_r = 10^{-3}$, $\frac{\beta_j}{\beta_p} = 10^{-2}$, $\Delta\theta = \pi/4$, $v_0 = 0.1$, $\Lambda = -14.32$, $T = 0.9$, $B = -1$ and $C = -0.1$.

Movie-15 corresponding to Fig. 5e. Pattern obtained using the model for $R_N = R_D = \rho = \mu = 10$, $D_r = 10^{-3}$, $\frac{\beta_j}{\beta_p} = 10^{-2}$, $\Delta\theta = \pi/4$, $v_0 = 0.1$, $\Lambda = -14.32$, $T = 0.9$, $B = -1$ and $C = 0.04$.

Movie-16 corresponding to Fig. 6a. Pattern obtained using the model for $R_N = R_D = \rho = \mu = 10$, $D_r = 10^{-3}$, $\frac{\beta_j}{\beta_p} = 10^{-2}$, $\Delta\theta = \pi/4$, $v_0 = 0.1$, $\Lambda = -14.32$, $T = 0.9$, $B = 1$ and $C = -0.6$.

Movie-17 corresponding to Fig. 6b. Pattern obtained using the model for $R_N = R_D = \rho = \mu = 10$, $D_r = 10^{-3}$, $\frac{\beta_j}{\beta_p} = 10^{-2}$, $\Delta\theta = \pi/4$, $v_0 = 0.1$, $\Lambda = -14.32$, $T = 0.9$, $B = 1$ and $C = 0.1$.

Movie-18 corresponding to Fig. 6c. Pattern obtained using the model for $R_N = R_D = \rho = \mu = 10$, $D_r = 10^{-3}$, $\frac{\beta_j}{\beta_p} = 10^{-2}$, $\Delta\theta = \pi/4$, $v_0 = 0.1$, $\Lambda = -14.32$, $T = 0.9$, $B = -1$ and $C = -0.1$.

Movie-19 corresponding to Fig. 6d. Pattern obtained using the model for $R_N = R_D = \rho = \mu = 10$, $D_r = 10^{-3}$, $\frac{\beta_j}{\beta_p} = 10^{-2}$, $\Delta\theta = \pi/4$, $v_0 = 0.1$, $\Lambda = -14.32$, $T = 0.9$, $B = -1$ and $C = 0.04$.

Movie-20 Pattern obtained using Delta-dependent line tension model for $R_N = R_D = \rho = \mu = 10$, $D_r = 10^{-3}$, $\frac{\beta_j}{\beta_p} = 10^{-2}$, $\Delta\theta = \pi/4$, $v_0 = 0.3$, $\Lambda = -14.32$, $T = 0.9$, $B = -1$ and $C = -0.1$.

Movie-A Pattern obtained using the model for $R_N = R_D = \rho = \mu = 1$, $\frac{\beta_j}{\beta_p} = 0.99$, $v_0 = 0$ and $\Lambda = -14.14$, $B = 1$ and $C = 0$.

Movie-B Pattern obtained using the model for $R_N = R_D = \rho = \mu = 1$, $\frac{\beta_j}{\beta_p} = 0.99$, $v_0 = 0.1$ and $\Lambda = -14.14$, $B = 1$ and $C = 0$.

Movie-C Pattern obtained using the model for $R_N = R_D = \rho = \mu = 1$, $\frac{\beta_j}{\beta_p} = 0.99$, $v_0 = 0.3$ and $\Lambda = -14.14$, $B = 1$ and $C = 0$.

C.5 Codes

In addition to the codes provided in the CHASTE library, the following additional codes are written for implementing the proposed model in Chapter 5, in CHASTE (C++). Ubuntu 16.04 LTS (operating system) and High Performance Computing (HPC) Systems (Noether cluster, Physics Department, IIT Bombay, India and MonARCH cluster, Monash University, Australia) are used to run the simulations. The quantification and visualization is done in python2.7, python3.5, using numpy (scientific computing library), pandas (data analysis library), and matplotlib (data visualization library), ParaView (an open-source, data analysis and visualization application).

```
#include "FarhadifarDifferentialAdhesionForceDiffDelta.hpp"
#include <vector>
#include <iostream>
#include <fstream>

#include <math.h>
#define PI 3.14159265

template<unsigned DIM>
FarhadifarDifferentialAdhesionForceDiffDelta<DIM>::FarhadifarDifferentialAdhesionForceDiffDelta
()
    : FarhadifarForceWithStress<DIM>(),
      //mFarhadifarLabeledCellLabeledCellAdhesionEnergyParameter(1.0),
      mFarhadifarDifferentialCellCellAdhesionEnergyParameter(1.0),
      mCouplingConstant(0.0),
      mLambda0(1.0),
      mBCoeff(1.0)
      //mFarhadifarLabeldCellBoundaryAdhesionEnergyParameter(1.0)
{
}

template<unsigned DIM>
FarhadifarDifferentialAdhesionForceDiffDelta<DIM>::~FarhadifarDifferentialAdhesionForceDiffDelta
()
{
}

template<unsigned DIM>
double FarhadifarDifferentialAdhesionForceDiffDelta<DIM>::GetLineTensionParameter
(Node<DIM>* pNodeA,
                                                                    Node<DIM>*
pNodeB,

VertexBasedCellPopulation<DIM>& rVertexCellPopulation)
{
        //std::ofstream OFileObject;
        //OFileObject.open("Deff.dat", ios::app);


    // Find the indices of the elements owned by each node
    std::set<unsigned> elements_containing_nodeA = pNodeA-
>rGetContainingElementIndices();
    std::set<unsigned> elements_containing_nodeB = pNodeB-
>rGetContainingElementIndices();

    // Find common elements
    std::set<unsigned> shared_elements;
    std::set_intersection(elements_containing_nodeA.begin(),
                          elements_containing_nodeA.end(),
                          elements_containing_nodeB.begin(),
                          elements_containing_nodeB.end(),
                          std::inserter(shared_elements, shared_elements.begin()));

    // Check that the nodes have a common edge
    assert(!shared_elements.empty());

    // If the edge corresponds to a single element, then the cell is on the boundary
    if (shared_elements.size() == 1)
    {
        unsigned element_index = *(shared_elements.begin());
```

```
        // Get cell associated with this element
        CellPtr p_cell = rVertexCellPopulation.GetCellUsingLocationIndex
(element_index);

         double boundary_tension=this->GetBoundaryLineTensionParameter();
         //OFileObject <<boundary_tension<<"\n";
         return boundary_tension;

    }

    else
    {
                 std::vector<double>delta_vector(0);
                 //std::vector<double>notch_vector(0);
        // Work out the number of labelled cells: 0,1 or 2
        //unsigned num_labelled_cells = 0;
        for (std::set<unsigned>::iterator iter = shared_elements.begin();
             iter != shared_elements.end();
             ++iter)
        {
            unsigned element_index = *(iter);

            // Get cell associated with this element
            CellPtr p_cell = rVertexCellPopulation.GetCellUsingLocationIndex
(element_index);

                        double delta= p_cell->GetCellData()->GetItem("delta");
                        //double notch= p_cell->GetCellData()->GetItem("notch");
                        delta_vector.push_back(delta);
                        //notch_vector.push_back(notch);
                        //OFileObject <<delta_vector[1]<<" ";
                }
                //double delta_diff_abs;
                //for(unsigned i=0; i<delta_vector.size(); i++)
                //{
                double B=this->GetB();
                double delta_diff=delta_vector[0]+(B*delta_vector[1]);
                double delta_diff_abs=fabs(delta_diff);
                //double notch_diff=notch_vector[0]-notch_vector[1];
                //double notch_diff_abs=abs(notch_diff);
                //}
                //unsigned simulation_time= SimulationTime::Instance()-
>GetTimeStepsElapsed();
                //if(simulation_time%100==0)
                //{
                //      OFileObject <<delta_vector[0]<<" "<<delta_vector[1]<<" ";
                //      OFileObject <<delta_diff_abs<<"\n";
                //}
                //OFileObject <<notch_diff_abs<<" ";
                double A=this->GetCouplingConstant();
                double lambda_ij = this->GetLambda0()*(1+A*delta_diff_abs);
                //OFileObject <<lambda_ij<< "\n";
                return lambda_ij;







    }
    //OFileObject <<"\n";
```

```
    //OFileObject.close();
}

template<unsigned DIM>
double
FarhadifarDifferentialAdhesionForceDiffDelta<DIM>::GetFarhadifarDifferentialCellCellAdhesionEnergy
()
{
    return mFarhadifarDifferentialCellCellAdhesionEnergyParameter;
}



template<unsigned DIM>
void
FarhadifarDifferentialAdhesionForceDiffDelta<DIM>::SetFarhadifarDifferentialCellCellAdhesionEnergy
(double differentialCellCellAdhesionEnergyParameter)
{
    mFarhadifarDifferentialCellCellAdhesionEnergyParameter =
differentialCellCellAdhesionEnergyParameter;
}

template<unsigned DIM>
void FarhadifarDifferentialAdhesionForceDiffDelta<DIM>::SetCouplingConstant(double
couplingConstant)
{
    mCouplingConstant = couplingConstant;
}

template<unsigned DIM>
double FarhadifarDifferentialAdhesionForceDiffDelta<DIM>::GetCouplingConstant()
{
    return mCouplingConstant;
}

template<unsigned DIM>
void FarhadifarDifferentialAdhesionForceDiffDelta<DIM>::SetLambda0(double lambda0)
{
    mLambda0 = lambda0;
}

template<unsigned DIM>
double FarhadifarDifferentialAdhesionForceDiffDelta<DIM>::GetLambda0()
{
    return mLambda0;
}

template<unsigned DIM>
void FarhadifarDifferentialAdhesionForceDiffDelta<DIM>::SetB(double b_coeff)
{
    mBCoeff = b_coeff;
}

template<unsigned DIM>
double FarhadifarDifferentialAdhesionForceDiffDelta<DIM>::GetB()
{
    return mBCoeff;
}



template<unsigned DIM>
```

```
void FarhadifarDifferentialAdhesionForceDiffDelta<DIM>::OutputForceParameters
(out_stream& rParamsFile)
{
    // Output member variables
        //*rParamsFile << "\t\t
\t<FarhadifarLabeledCellLabeledCellAdhesionEnergyParameter>" <<
mFarhadifarLabeledCellLabeledCellAdhesionEnergyParameter << "</
FarhadifarLabeledCellLabeledCellAdhesionEnergyParameter> \n";
        *rParamsFile << "\t\t
\t<FarhadifarDifferentialCellCellAdhesionEnergyParameter>" <<
mFarhadifarDifferentialCellCellAdhesionEnergyParameter << "</
FarhadifarLabeledCellCellAdhesionEnergyParameter> \n";
        *rParamsFile << "\t\t\t<CouplingConstant>" << mCouplingConstant << "</
CouplingConstant> \n";
        //*rParamsFile << "\t\t
\t<FarhadifarLabeledCellBoundaryAdhesionEnergyParameter>" <<
mFarhadifarLabeledCellBoundaryAdhesionEnergyParameter << "</
FarhadifarLabeledCellBoundaryAdhesionEnergyParameter> \n";

        // Call method on direct parent class
        FarhadifarForceWithStress<DIM>::OutputForceParameters(rParamsFile);
}

// Explicit instantiation
template class FarhadifarDifferentialAdhesionForceDiffDelta<1>;
template class FarhadifarDifferentialAdhesionForceDiffDelta<2>;
template class FarhadifarDifferentialAdhesionForceDiffDelta<3>;

// Serialization for Boost >= 1.36
#include "SerializationExportWrapperForCpp.hpp"
EXPORT_TEMPLATE_CLASS_SAME_DIMS(FarhadifarDifferentialAdhesionForceDiffDelta)
```

```
#include "FarhadifarForceWithStress.hpp"
#include <iostream>  //added
#include <fstream>   //added

#include <math.h>    //added
#define PI 3.14159265 //added
#include <string>  //added
using namespace std; //added

template<unsigned DIM>
FarhadifarForceWithStress<DIM>::FarhadifarForceWithStress()
   : AbstractForce<DIM>(),
     mAreaElasticityParameter(1.0), // These parameters are Case I in Farhadifar's
paper
     mPerimeterContractilityParameter(0.04),
     mLineTensionParameter(0.12),
     mBoundaryLineTensionParameter(0.12), // this parameter as such does not exist in
Farhadifar's model.
     mFileName()
{
}

template<unsigned DIM>
FarhadifarForceWithStress<DIM>::~FarhadifarForceWithStress()
{
}

template<unsigned DIM>
void FarhadifarForceWithStress<DIM>::AddForceContribution
(AbstractCellPopulation<DIM>& rCellPopulation)
{
    // Throw an exception message if not using a VertexBasedCellPopulation
    ///\todo: check whether this line influences profiling tests - if so, we should
remove it.
    if (dynamic_cast<VertexBasedCellPopulation<DIM>*>(&rCellPopulation) == NULL)
    {
        EXCEPTION("FarhadifarForce is to be used with a VertexBasedCellPopulation
only");
    }

        string file_name=this->GetFileName();//"Stress_check.dat"

        std::ofstream OFileObject;
        OFileObject.open(file_name, ios::app);
    // Define some helper variables
    VertexBasedCellPopulation<DIM>* p_cell_population =
static_cast<VertexBasedCellPopulation<DIM>*>(&rCellPopulation);
    unsigned num_nodes = p_cell_population->GetNumNodes();
    unsigned num_elements = p_cell_population->GetNumElements();
   // TetrahedralMesh<DIM,DIM>* p_tetrahedral_mesh=p_cell_population-
>GetTetrahedralMeshUsingVertexMesh();
        //c_vector<double,DIM> centre_location = pCellPopulation-
>GetLocationOfCellCentre(pCell);

    // Begin by computing the area and perimeter of each element in the mesh, to
avoid having to do this multiple times
    std::vector<double> element_areas(num_elements);
    std::vector<double> element_perimeters(num_elements);
    std::vector<double> target_areas(num_elements);
    std::vector<double> shape_index(num_elements);
```

```
    // Iterate over vertices in the cell population
    for (unsigned node_index=0; node_index<num_nodes; node_index++)
    {
        Node<DIM>* p_this_node = p_cell_population->GetNode(node_index);


        c_vector<double, DIM> area_elasticity_contribution = zero_vector<double>(DIM);
        c_vector<double, DIM> perimeter_contractility_contribution =
zero_vector<double>(DIM);
        c_vector<double, DIM> line_tension_contribution = zero_vector<double>(DIM);

        // Find the indices of the elements owned by this node
        std::set<unsigned> containing_elem_indices = p_cell_population->GetNode
(node_index)->rGetContainingElementIndices();

        // Iterate over these elements
        for (std::set<unsigned>::iterator iter = containing_elem_indices.begin();
             iter != containing_elem_indices.end();
             ++iter)
        {
            // Get this element, its index and its number of nodes
            VertexElement<DIM, DIM>* p_element = p_cell_population->GetElement(*iter);
            unsigned elem_index = p_element->GetIndex();
            unsigned num_nodes_elem = p_element->GetNumNodes();

            // Find the local index of this node in this element
            unsigned local_index = p_element->GetNodeLocalIndex(node_index);

            // Add the force contribution from this cell's area elasticity (note the
minus sign)
            c_vector<double, DIM> element_area_gradient =
                    p_cell_population->rGetMesh().GetAreaGradientOfElementAtNode
(p_element, local_index);
            area_elasticity_contribution -= 2.0*GetAreaElasticityParameter()*
(element_areas[elem_index] -
                    target_areas[elem_index])*element_area_gradient;

            // Get the previous and next nodes in this element
            unsigned previous_node_local_index = (num_nodes_elem+local_index-1)%
num_nodes_elem;
            Node<DIM>* p_previous_node = p_element->GetNode
(previous_node_local_index);

            unsigned next_node_local_index = (local_index+1)%num_nodes_elem;
            Node<DIM>* p_next_node = p_element->GetNode(next_node_local_index);

            // Compute the line tension parameter for each of these edges - be aware
that this is half of the actual
            // value for internal edges since we are looping over each of the
internal edges twice
            double previous_edge_line_tension_parameter = GetLineTensionParameter
(p_previous_node, p_this_node, *p_cell_population);
            double next_edge_line_tension_parameter = GetLineTensionParameter
(p_this_node, p_next_node, *p_cell_population);

            // Compute the gradient of each these edges, computed at the present node
            c_vector<double, DIM> previous_edge_gradient =
                    -p_cell_population->rGetMesh().GetNextEdgeGradientOfElementAtNode
(p_element, previous_node_local_index);
            c_vector<double, DIM> next_edge_gradient = p_cell_population->rGetMesh
```

```
().GetNextEdgeGradientOfElementAtNode(p_element, local_index);

            // Add the force contribution from cell-cell and cell-boundary line
tension (note the minus sign)
            line_tension_contribution -=
previous_edge_line_tension_parameter*previous_edge_gradient +
                    next_edge_line_tension_parameter*next_edge_gradient;

            // Add the force contribution from this cell's perimeter contractility
(note the minus sign)
            c_vector<double, DIM> element_perimeter_gradient = previous_edge_gradient
+ next_edge_gradient;
            perimeter_contractility_contribution -
=2.0*GetPerimeterContractilityParameter()* element_perimeters[elem_index]*

element_perimeter_gradient;
        }

        c_vector<double, DIM> force_on_node = area_elasticity_contribution +
perimeter_contractility_contribution + line_tension_contribution;
        p_cell_population->GetNode(node_index)->AddAppliedForceContribution
(force_on_node);
    }
   //double stress = GetStress(*p_cell_population);   //added




    for (typename VertexMesh<DIM,DIM>::VertexElementIterator elem_iter =
p_cell_population->rGetMesh().GetElementIteratorBegin();
         elem_iter != p_cell_population->rGetMesh().GetElementIteratorEnd();
         ++elem_iter)
    {
        unsigned elem_index = elem_iter->GetIndex();

        element_areas[elem_index] = p_cell_population->rGetMesh().GetVolumeOfElement
(elem_index);
        element_perimeters[elem_index] = p_cell_population->rGetMesh
().GetSurfaceAreaOfElement(elem_index);
        shape_index[elem_index]=element_perimeters[elem_index]/sqrt(element_areas
[elem_index]);
        try
        {
            // If we haven't specified a growth modifier, there won't be any target
areas in the CellData array and CellData
            // will throw an exception that it doesn't have "target area" entries.
We add this piece of code to give a more
            // understandable message. There is a slight chance that the exception is
thrown although the error is not about the
            // target areas.
            target_areas[elem_index] = p_cell_population->GetCellUsingLocationIndex
(elem_index)->GetCellData()->GetItem("target area");

        }
        catch (Exception&)
        {
            EXCEPTION("You need to add an AbstractTargetAreaModifier to the
simulation in order to use a FarhadifarForce");
        }
        //unsigned elem_index=elem_iter->GetIndex();
        c_vector<double,DIM>location=p_cell_population->rGetMesh
```

```
().GetCentroidOfElement(elem_index);
                VertexElement<DIM,DIM>*p_element=p_cell_population->GetElement
(elem_index);

                unsigned num_nodes_in_elem=p_element->GetNumNodes();
                double element_perimeter = p_cell_population->rGetMesh
().GetSurfaceAreaOfElement(elem_index);
                //OFileObject <<num_nodes_in_elem<< " ";
                double element_area = p_cell_population->rGetMesh().GetVolumeOfElement
(elem_index);
                double shape_index_elem=element_perimeter/sqrt(element_area);
                //OFileObject <<element_area<< " ";
                double target_area = p_cell_population->GetCellUsingLocationIndex
(elem_index)->GetCellData()->GetItem("target area");
                //OFileObject <<target_area<< " ";
                double bond_gamma = GetPerimeterContractilityParameter();
                //OFileObject <<bond_gamma<< " ";
                double gamma_perimeter = bond_gamma*element_perimeter;
                //OFileObject <<gamma_perimeter<< " ";
                double sum_xx=0.0;
                //double sum_yy=0.0;
                double sum_xy=0.0;
                //OFileObject <<"\n";
                double sum_total=0.0;
                double sum_bond_adhesion=0.0;

                for(unsigned node_index=0; node_index<num_nodes_in_elem; node_index++)
                {
                        //unsigned curr_node_local_index=p_element->GetNodeGlobalIndex
(node_index);
                        unsigned curr_node_local_index=node_index;
                        //OFileObject <<curr_node_local_index<< " ";
                        Node<DIM>*p_curr_node=p_element->GetNode
(curr_node_local_index);
                        //unsigned next_node_local_index=p_element->GetNodeLocalIndex
((curr_node_local_index+1)%num_nodes);
                        unsigned next_node_local_index=(curr_node_local_index+1)%
num_nodes_in_elem;
                        //OFileObject <<next_node_local_index<< " ";
                        Node<DIM>*p_next_node=p_element->GetNode
(next_node_local_index);
                        double bond_adhesion=GetLineTensionParameter(p_curr_node,
p_next_node, *p_cell_population);
                        //OFileObject <<bond_adhesion<<" ";   //correct

                        double T_b_alpha = (bond_adhesion/2.0) + 2.0*gamma_perimeter;
                        //OFileObject <<T_b_alpha<< " ";    //correct
                        c_vector<double, DIM> location_curr_node=p_curr_node-
>rGetLocation();
                        c_vector<double, DIM> location_next_node=p_next_node-
>rGetLocation();

                        c_vector<double, DIM> dist_betw_nodes=location_next_node-
location_curr_node;
                        double L=GetBoxLength();
                        double H=GetBoxHeight();

                        if(dist_betw_nodes(0)>L/2.0)
                        {
                                location_next_node(0)=location_next_node(0)-L;
                        }
                        if(dist_betw_nodes(1)>H/2.0)
```

```
                        {
                                location_next_node(1)=location_next_node(1)-H;
                        }
                        if(dist_betw_nodes(0)<-L/2.0)
                        {
                                location_next_node(0)=location_next_node(0)+L;
                        }
                        if(dist_betw_nodes(1)<-H/2.0)
                        {
                                location_next_node(1)=location_next_node(1)+H;
                        }

                        //for(unsigned j=0; j<2; j++)
                        //{
                        //      OFileObject <<location_curr_node(j)<< " ";
                        //      OFileObject <<location_next_node(j)<< " ";
                        //}
                        double phi_b = atan2((location_next_node(1)-location_curr_node
(1)),(location_next_node(0)-location_curr_node(0)));
                        //double phi_b = atan(dist_betw_nodes(0)/dist_betw_nodes(1))*
(180/PI);
                        //OFileObject <<theta<< "\n";
                        double cos_2phi_b = cos(2.0*phi_b);
                        double sin_2phi_b = sin(2.0*phi_b);
                        c_vector<double, DIM>
dist_betw_nodes_modified=location_next_node-location_curr_node;
                        double bond_length=norm_2(dist_betw_nodes_modified);
                        //OFileObject <<bond_length<< " ";   //wrong
                        double T_length_xx=bond_length*T_b_alpha*cos_2phi_b;
                        sum_xx=T_length_xx+sum_xx;
                        double T_length_xy=bond_length*T_b_alpha*sin_2phi_b;
                        sum_xy=T_length_xy+sum_xy;
                        //double
T_length_xy=bond_length*T_b_alpha*cos_theta*sin_theta;
                        //double sum_xy=T_length_xy+sum_xy;
                        double T_length=bond_length*T_b_alpha;
                        //OFileObject <<T_length<<" ";
                        sum_total=sum_total+T_length;
                        //OFileObject <<sum_total;
                        sum_bond_adhesion=sum_bond_adhesion+(bond_adhesion/
num_nodes_in_elem);

                }
                double shape_index_correct=sum_bond_adhesion/(2.0*bond_gamma*sqrt
(target_area));
                //OFileObject <<sum_total<<"\n";

                //double second_part_xx = (1.0/element_area)*sum_xx;
                //double second_part_yy = (1.0/element_area)*sum_yy;
                //double second_part_xy = (1.0/element_area)*sum_xy;
                double second_part_total=(0.5/element_area)*sum_total;
                double P_alpha = -2.0*GetAreaElasticityParameter()*(element_area-
target_area);
                //OFileObject <<GetAreaElasticityParameter()<<" "<<element_area<<"
"<<target_area<<" "<<P_alpha<<" "<< sum_total<<" "<<second_part_total<<" ";

                //double sigma_xx = -P_alpha + second_part_xx;
                //double sigma_yy = -P_alpha + second_part_yy;
                //double sigma_xy = -P_alpha + second_part_xy;

                double P_alpha_total= P_alpha-second_part_total;
                double sigma_xx=0.5*sum_xx;
```

```
                double sigma_xy=0.5*sum_xy;

                double gamma=sqrt(sigma_xx*sigma_xx+sigma_xy*sigma_xy);
                //OFileObject <<P_alpha_total<<" "<<gamma<<"\n";
                double si_p_by_a=element_perimeter/sqrt(element_area);
                unsigned simulation_time= SimulationTime::Instance()-
>GetTimeStepsElapsed();
                if(simulation_time%100==0)
                {
                        OFileObject <<simulation_time<< " ";
                        OFileObject <<elem_index<< " ";
                        for (unsigned i=0; i<DIM; i++)
                        {
                                OFileObject << location[i] << " ";
                        }
                        OFileObject <<shape_index_correct<< " ";
                        OFileObject <<element_area<< " ";
                //      OFileObject <<target_area<< " ";
                        OFileObject <<element_perimeter<< " ";
                //      //OFileObject <<sigma_xx<< " ";
                //      //OFileObject <<sigma_yy<< " ";
                //      //OFileObject <<sigma_xy<< " ";
                        OFileObject <<P_alpha_total<< " ";
                        OFileObject <<gamma<< " ";
                        OFileObject <<si_p_by_a<< " ";
                        OFileObject <<sigma_xx<< " ";
                        OFileObject <<sigma_xy<< "\n";



                }

    }

    OFileObject.close();

}

template<unsigned DIM>
double FarhadifarForceWithStress<DIM>::GetLineTensionParameter(Node<DIM>* pNodeA,
Node<DIM>* pNodeB, VertexBasedCellPopulation<DIM>& rVertexCellPopulation)
{
        //ofstream OFileObject;
        //OFileObject.open("Stress2.dat", ios::app);
    // Find the indices of the elements owned by each node
    std::set<unsigned> elements_containing_nodeA = pNodeA-
>rGetContainingElementIndices();
    std::set<unsigned> elements_containing_nodeB = pNodeB-
>rGetContainingElementIndices();

    // Find common elements
    std::set<unsigned> shared_elements;
    std::set_intersection(elements_containing_nodeA.begin(),
                          elements_containing_nodeA.end(),
                          elements_containing_nodeB.begin(),
                          elements_containing_nodeB.end(),
                          std::inserter(shared_elements, shared_elements.begin()));

    // Check that the nodes have a common edge
    assert(!shared_elements.empty());

    // Since each internal edge is visited twice in the loop above, we have to use
```

```
half the line tension parameter
    // for each visit.
   // double line_tension_parameter_in_calculation = GetLineTensionParameter()/2.0;
    double line_tension_parameter_in_calculation = GetLineTensionParameter();
        //unsigned c=0;
    // If the edge corresponds to a single element, then the cell is on the boundary
    if (shared_elements.size() == 1)
    {
                //line_tension_parameter_in_calculation =
GetBoundaryLineTensionParameter();  //original
        line_tension_parameter_in_calculation = GetLineTensionParameter()/2.0;   //
edited
    }

        //OFileObject.close();
    return line_tension_parameter_in_calculation;
}

template<unsigned DIM>
double FarhadifarForceWithStress<DIM>::GetAreaElasticityParameter()
{
    return mAreaElasticityParameter;
}

template<unsigned DIM>
double FarhadifarForceWithStress<DIM>::GetPerimeterContractilityParameter()
{
    return mPerimeterContractilityParameter;
}

template<unsigned DIM>
double FarhadifarForceWithStress<DIM>::GetLineTensionParameter()
{
    return mLineTensionParameter;
}

template<unsigned DIM>
double FarhadifarForceWithStress<DIM>::GetBoundaryLineTensionParameter()
{
    return mBoundaryLineTensionParameter;
}

template<unsigned DIM>
void FarhadifarForceWithStress<DIM>::SetAreaElasticityParameter(double
areaElasticityParameter)
{
    mAreaElasticityParameter = areaElasticityParameter;
}

template<unsigned DIM>
void FarhadifarForceWithStress<DIM>::SetPerimeterContractilityParameter(double
perimeterContractilityParameter)
{
    mPerimeterContractilityParameter = perimeterContractilityParameter;
}

template<unsigned DIM>
void FarhadifarForceWithStress<DIM>::SetLineTensionParameter(double
lineTensionParameter)
{
    mLineTensionParameter = lineTensionParameter;
}
```

```
template<unsigned DIM>
void FarhadifarForceWithStress<DIM>::SetBoundaryLineTensionParameter(double
boundaryLineTensionParameter)
{
    mBoundaryLineTensionParameter = boundaryLineTensionParameter;
}
template<unsigned DIM>
void FarhadifarForceWithStress<DIM>::SetBoxLength(double box_length)
{
    mBoxLength = box_length;
}

template<unsigned DIM>
void FarhadifarForceWithStress<DIM>::SetBoxHeight(double box_height)
{
    mBoxHeight = box_height;
}

template<unsigned DIM>
void FarhadifarForceWithStress<DIM>::SetFileName(string file_name)
{
    mFileName = file_name;
}


template<unsigned DIM>
double FarhadifarForceWithStress<DIM>::GetBoxLength()
{
    return mBoxLength;
}

template<unsigned DIM>
double FarhadifarForceWithStress<DIM>::GetBoxHeight()
{
    return mBoxHeight;
}

template<unsigned DIM>
string FarhadifarForceWithStress<DIM>::GetFileName()
{
    return mFileName;
}



template<unsigned DIM>
void FarhadifarForceWithStress<DIM>::OutputForceParameters(out_stream& rParamsFile)
{
    *rParamsFile << "\t\t\t<AreaElasticityParameter>" << mAreaElasticityParameter <<
"</AreaElasticityParameter>\n";
    *rParamsFile << "\t\t\t<PerimeterContractilityParameter>" <<
mPerimeterContractilityParameter << "</PerimeterContractilityParameter>\n";
    *rParamsFile << "\t\t\t<LineTensionParameter>" << mLineTensionParameter << "</
LineTensionParameter>\n";
    *rParamsFile << "\t\t\t<BoundaryLineTensionParameter>" <<
mBoundaryLineTensionParameter << "</BoundaryLineTensionParameter>\n";

    // Call method on direct parent class
    AbstractForce<DIM>::OutputForceParameters(rParamsFile);
}
```

```cpp
// Explicit instantiation
template class FarhadifarForceWithStress<1>;
template class FarhadifarForceWithStress<2>;
template class FarhadifarForceWithStress<3>;

// Serialization for Boost >= 1.36
#include "SerializationExportWrapperForCpp.hpp"
EXPORT_TEMPLATE_CLASS_SAME_DIMS(FarhadifarForceWithStress)
```

```
import numpy as np
import pandas as pd
import matplotlib
import matplotlib.pyplot as plt

import  matplotlib.font_manager
flist = matplotlib.font_manager.get_fontconfig_fonts()
names = [matplotlib.font_manager.FontProperties(fname=fname).get_name() for fname in
flist]
#print(names)
if "Times New Roman" in names:
    print("Yes")
else:
    print("font not available")
plt.rcParams["font.family"] = "Times New Roman"



x_C = ["$-0.6$","$-0.2$","$-0.16$","$-0.12$","$-0.08$","$-0.04$", "$0$", "$0.04$",
"$0.08$", "$0.12$",
             "$0.16$", "$0.2$","$0.6$","$1.0$"]#, "$-0.2$", "$-0.6$", "$-1.0$", "$-1.4
$",'N']
x=[-0.6,-0.2,-0.16,-0.12,-0.08,-0.04, 0, 0.04, 0.08, 0.12, 0.16, 0.2, 0.6,1.0]

y_p0 = ["-14.88", "-14.14", "-13.4",
           "-12.65", "-11.91", "-11.17"]
y = [-14.88, -14.14, -13.4,
           -12.65, -11.91, -11.17]

df1=pd.read_csv('BDColier-Delta_area1.csv', sep=' ', names=
["1","2","3","4","5","6","7","8"])#,'Nothing'])
df2=pd.read_csv('SDColier-Delta_area1.csv', sep=' ', names=
["11","12","13","14","15","16","17","18"])#,"6","7","8","9",'Nothing'])

df1=df1.drop(["1","8"],axis=1)#,inplace=True) #df1=df1.drop
(["1","8"],axis=1,inplace=True)

df1=df1[df1.columns[::-1]]

df0=pd.concat([df1,df2],axis=1)
print(df0)
df0=df0.values
df0 = np.flip(df0, axis=0)

df_area=np.round(df0,3)

fig, ax = plt.subplots()
X, Y = np.meshgrid(x, y)

marker_size=30
plot1=ax.scatter(X,Y, marker='s',s=10, c=df_area, cmap='brg')


cbar= plt.colorbar(plot1,shrink=0.5)
#cbar.ax.tick_params(labelsize=14)
ax.set_aspect(0.2)

#ax.set_xlim([-0.65,1.05])
#ax2.set_xlim(0.4,1) # outliers only

xl=[-0.6, -0.4, -0.2, 0, 0.2, 0.4, 0.6]
# Make the spacing between the two axes a bit smaller
```

```
#plt.subplots_adjust(wspace=0.15)

#ax.set_xlim([-0.8,1.2])
ax.set_ylim([-15,-11])
#ax2.set_ylim([-15,-11])

ax.tick_params(axis="x", labelsize=10)
ax.tick_params(axis="y", labelsize=10)

ax.set_xlabel('Coupling constant (C)', fontsize=14)
ax.set_ylabel(r'Line tension $(\Lambda_{0})$ ', fontsize=14)

#plt.show()
fig.tight_layout()
#plt.savefig('DeltaDepenJunct_Delta_Area2.png', dpi=500)
```

References

[1] Adachi, K., Suemori, H., Yasuda, S.-y., Nakatsuji, N., Kawase, E., 2010. Role of sox2 in maintaining pluripotency of human embryonic stem cells. Genes to Cells 15 (5), 455–470.

[2] Ahimou, F., Mok, L.-P., Bardot, B., Wesley, C., 2004. The adhesion force of notch with delta and the rate of notch signaling. The Journal of cell biology 167 (6), 1217–1229.

[3] Ahn, S.-H., Susztak, K., 2010. Getting a notch closer to understanding diabetic kidney disease. Diabetes 59 (8), 1865–1867.

[4] Albelda, S. M., Buck, C. A., 1990. Integrins and other cell adhesion molecules. The FASEB Journal 4 (11), 2868–2880.

[5] Alberts, B., Johnson, A., Lewis, J., Raff, M., Roberts, K., Walter, P., et al., 2003. Molecular biology of the cell. Scandinavian Journal of Rheumatology 32 (2), 125–125.

[6] Alert, R., Trepat, X., 2020. Physical models of collective cell migration. Annual Review of Condensed Matter Physics 11, 77–101.

[7] Aliee, M., 2013. Dynamics and mechanics of compartment boundaries in developing tissues.

[8] Alt, S., Ganguly, P., Salbreux, G., 2017. Vertex models: from cell mechanics to tissue morphogenesis. Philosophical Transactions of the Royal Society B: Biological Sciences 372 (1720), 20150520.

[9] Amack, J. D., Manning, M. L., 2012. Knowing the boundaries: extending the differential adhesion hypothesis in embryonic cell sorting. Science 338 (6104), 212–215.

[10] Ananthakrishnan, R., Ehrlicher, A., 2007. The forces behind cell movement. International journal of biological sciences 3 (5), 303.

[11] Anklesaria, P., Teixido, J., Laiho, M., Pierce, J. H., Greenberger, J. S., Massague, J., 1990. Cell-cell adhesion mediated by binding of membrane-anchored transforming growth factor alpha to epidermal growth factor receptors promotes cell proliferation. Proceedings of the National Academy of Sciences 87 (9), 3289–3293.

[12] Artavanis-Tsakonas, S., Matsuno, K., Fortini, M. E., 1995. Notch signaling. Science 268 (5208), 225–232.

[13] Artavanis-Tsakonas, S., Rand, M. D., Lake, R. J., 1999. Notch signaling: cell fate control and signal integration in development. Science 284 (5415), 770–776.

[14] Azeloglu, E. U., Iyengar, R., 2015. Signaling networks: information flow, computation, and decision making. Cold Spring Harbor perspectives in biology 7 (4), a005934.

[15] Bajpai, S., Prabhakar, R., Chelakkot, R., Inamdar, M. M., 2021. Role of cell polarity dynamics and motility in pattern formation due to contact-dependent signalling. Journal of The Royal Society Interface 18 (175), 20200825.

[16] Bao, S., 2014. Notch controls cell adhesion in the drosophila eye. PLoS Genet 10 (1), e1004087.

[17] Barton, D. L., Henkes, S., Weijer, C. J., Sknepnek, R., 2017. Active vertex model for cell-resolution description of epithelial tissue mechanics. PLoS Computational biology 13 (6), e1005569.

[18] Belmonte, J. M., Thomas, G. L., Brunnet, L. G., de Almeida, R. M., Chaté, H., 2008. Self-propelled particle model for cell-sorting phenomena. Physical Review Letters 100 (24), 248702.

[19] Bénazéraf, B., Francois, P., Baker, R., Little, C., Pourquié, O., 2009. A random cell motility gradient downstream of fgf controls elongation of amniote embryos.

[20] Benjamin, M., Hillen, B., 2003. Mechanical influences on cells, tissues and organs-'mechanical morphogenesis'. European journal of morphology 41 (1), 3–7.

[21] Bhalla, U. S., Iyengar, R., 1999. Emergent properties of networks of biological signaling pathways. Science 283 (5400), 381–387.

[22] Bi, D., Lopez, J., Schwarz, J. M., Manning, M. L., 2015. A density-independent rigidity transition in biological tissues. Nature Physics 11 (12), 1074–1079.

[23] Bi, D., Yang, X., Marchetti, M. C., Manning, M. L., 2016. Motility-driven glass and jamming transitions in biological tissues. Physical Review X 6 (2), 021011.

[24] Bi, D., Yang, X., Marchetti, M. C., Manning, M. L., 2016. Motility-driven glass and jamming transitions in biological tissues. Physical Review X 6 (2), 021011.

[25] Blanchoin, L., Boujemaa-Paterski, R., Sykes, C., Plastino, J., 2014. Actin dynamics, architecture, and mechanics in cell motility. Physiological reviews 94 (1), 235–263.

[26] Block, M., Schöll, E., Drasdo, D., 2007. Classifying the expansion kinetics and critical surface dynamics of growing cell populations. Physical review letters 99 (24), 248101.

[27] Boareto, M., Jolly, M. K., Goldman, A., Pietilä, M., Mani, S. A., Sengupta, S., Ben-Jacob, E., Levine, H., Onuchic, J., 2016. Notch-jagged signalling can give rise to clusters of cells exhibiting a hybrid epithelial/mesenchymal phenotype. Journal of the Royal Society Interface 13 (118), 20151106.

[28] Boareto, M., Jolly, M. K., Lu, M., Onuchic, J. N., Clementi, C., Ben-Jacob, E., 2015. Jagged–delta asymmetry in notch signaling can give rise to a sender/receiver hybrid phenotype. Proceedings of the National Academy of Sciences 112 (5), E402–E409.

[29] Bolós, V., Grego-Bessa, J., de la Pompa, J. L., 2007. Notch signaling in development and cancer. Endocrine reviews 28 (3), 339–363.

[30] Borggrefe, T., Giaimo, B. D., 2018. Molecular mechanisms of notch signaling. Springer.

[31] Borghi, N., Sorokina, M., Shcherbakova, O. G., Weis, W. I., Pruitt, B. L., Nelson, W. J., Dunn, A. R., 2012. E-cadherin is under constitutive actomyosin-generated tension that is increased at cell–cell contacts upon externally applied stretch. Proceedings of the National Academy of Sciences 109 (31), 12568–12573.

[32] Brodland, G. W., 2002. The differential interfacial tension hypothesis (dith): a comprehensive theory for the self-rearrangement of embryonic cells and tissues. J. Biomech. Eng. 124 (2), 188–197.

[33] Brodland, G. W., Chen, H. H., 2000. The mechanics of heterotypic cell aggregates: insights from computer simulations. J. Biomech. Eng. 122 (4), 402–407.

[34] Brosnan, C. F., John, G. R., et al., 2009. Revisiting notch in remyelination of multiple sclerosis lesions. The Journal of clinical investigation 119 (1), 10–13.

[35] Butler, M. T., Wallingford, J. B., 2017. Planar cell polarity in development and disease. Nature reviews Molecular cell biology 18 (6), 375–388.

[36] Camley, B. A., Rappel, W.-J., 2017. Physical models of collective cell motility: from cell to tissue. Journal of Physics D: Applied Physics 50 (11), 113002.

[37] Capuana, L., Boström, A., Etienne-Manneville, S., 2020. Multicellular scale front-to-rear polarity in collective migration. Current Opinion in Cell Biology 62, 114–122.

[38] Chabab, S., Lescroart, F., Rulands, S., Mathiah, N., Simons, B. D., Blanpain, C., 2016. Uncovering the number and clonal dynamics of mesp1 progenitors during heart morphogenesis. Cell reports 14 (1), 1–10.

[39] Chen, J., Imanaka, N., Griffin, J., 2010. Hypoxia potentiates notch signaling in breast cancer leading to decreased e-cadherin expression and increased cell migration and invasion. British journal of cancer 102 (2), 351–360.

[40] Cheng, D., Yan, X., Qiu, G., Zhang, J., Wang, H., Feng, T., Tian, Y., Xu, H., Wang, M., He, W., et al., 2018. Contraction of basal filopodia controls periodic feather branching via notch and fgf signaling. Nature communications 9 (1), 1–11.

[41] Chigurupati, S., Arumugam, T. V., Son, T. G., Lathia, J. D., Jameel, S., Mughal, M. R., Tang, S.-C., Jo, D.-G., Camandola, S., Giunta, M., et al., 2007. Involvement of Notch signaling in wound healing. PloS One 2 (11), e1167.

[42] Chirat, R., Moulton, D. E., Goriely, A., 2013. Mechanical basis of morphogenesis and convergent evolution of spiny seashells. Proceedings of the National Academy of Sciences 110 (15), 6015–6020.

[43] Chitnis, A., Henrique, D., Lewis, J., Ish-Horowicz, D., Kintner, C., 1995. Primary neurogenesis in xenopus embryos regulated by a homologue of the drosophila neurogenic gene delta. Nature 375 (6534), 761–766.

[44] Cohen, M., Georgiou, M., Stevenson, N. L., Miodownik, M., Baum, B., 2010. Dynamic filopodia transmit intermittent delta-notch signaling to drive pattern refinement during lateral inhibition. Developmental Cell 19 (1), 78–89.

[45] Cohen, M., Georgiou, M., Stevenson, N. L., Miodownik, M., Baum, B., 2010. Dynamic Filopodia Transmit Intermittent Delta-Notch Signaling to Drive Pattern Refinement during Lateral Inhibition. Developmental Cell 19 (1), 78–89.

[46] Cohen, R., Amir-Zilberstein, L., Hersch, M., Woland, S., Loza, O., Taiber, S., Matsuzaki, F., Bergmann, S., Avraham, K. B., Sprinzak, D., 2020. Mechanical forces drive ordered patterning of hair cells in the mammalian inner ear. Nature communications 11 (1), 1–12.

[47] Collier, J. R., Monk, N. A., Maini, P. K., Lewis, J. H., 1996. Pattern formation by lateral inhibition with feedback: a mathematical model of delta-notch intercellular signalling. Journal of Theoretical Biology 183 (4), 429–446.

[48] Collier, J. R., Monk, N. A., Maini, P. K., Lewis, J. H., 1996. Pattern formation by lateral inhibition with feedback: a mathematical model of delta-notch intercellular signalling. Journal of theoretical Biology 183 (4), 429–446.

[49] Cooper, G., 2000. Signaling molecules and their receptors. Cell Mol. Approach.

[50] Corson, F., Couturier, L., Rouault, H., Mazouni, K., Schweisguth, F., 2017. Self-organized notch dynamics generate stereotyped sensory organ patterns in Drosophila. Science 356 (6337).

[51] Cuschieri, A., Bannister, L. H., 1975. The development of the olfactory mucosa in the mouse: electron microscopy. Journal of anatomy 119 (Pt 3), 471.

[52] Daley, W. P., Gulfo, K. M., Sequeira, S. J., Larsen, M., 2009. Identification of a mechanochemical checkpoint and negative feedback loop regulating branching morphogenesis. Developmental biology 336 (2), 169–182.

[53] Das, G., Reynolds-Kenneally, J., Mlodzik, M., 2002. The atypical cadherin flamingo links frizzled and notch signaling in planar polarity establishment in the drosophila eye. Developmental cell 2 (5), 655–666.

[54] Davies, J., 2013. Mechanisms of morphogenesis. Academic Press.

[55] De Joussineau, C., Soule, J., Martin, M., Anguille, C., Montcourrier, P., Alexandre, D., 2003. Delta-promoted filopodia mediate long-range lateral inhibition in drosophila. Nature 426 (6966), 555–559.

[56] De Smet, F., Segura, I., De Bock, K., Hohensinner, P. J., Carmeliet, P., 2009. Mechanisms of vessel branching: filopodia on endothelial tip cells lead the way. Arteriosclerosis, thrombosis, and vascular biology 29 (5), 639–649.

[57] Delfini, M.-C., Dubrulle, J., Malapert, P., Chal, J., Pourquié, O., 2005. Control of the segmentation process by graded mapk/erk activation in the chick embryo. Proceedings of the National Academy of Sciences 102 (32), 11343–11348.

[58] Derivery, E., Seum, C., Daeden, A., Loubéry, S., Holtzer, L., Jülicher, F., Gonzalez-Gaitan, M., 2015. Polarized endosome dynamics by spindle asymmetry during asymmetric cell division. Nature 528 (7581), 280–285.

[59] Dhillon, A. S., Hagan, S., Rath, O., Kolch, W., 2007. Map kinase signalling pathways in cancer. Oncogene 26 (22), 3279–3290.

[60] Downes, K. A., Goldblum, J. R., Montgomery, E. A., Fisher, C., 2001. Pleomorphic liposarcoma: a clinicopathologic analysis of 19 cases. Modern Pathology 14 (3), 179–184.

[61] Dreher, D., Pasakarnis, L., Brunner, D., 2016. Snapshot: mechanical forces in development ii. Cell 165 (4), 1028–1028.

[62] Dufraine, J., Funahashi, Y., Kitajewski, J., 2008. Notch signaling regulates tumor angiogenesis by diverse mechanisms. Oncogene 27 (38), 5132–5137.

[63] Ehebauer, M., Hayward, P., Martinez-Arias, A., 2006. Notch signaling pathway. Science's STKE 2006 (364), cm7–cm7.

[64] El-Naggar, A. K., Chan, J. K., Grandis, J. R., Takata, T., Slootweg, P. J., 2017. WHO classification of head and neck tumours. International Agency for Research on Cancer.

[65] Eom, D. S., Bain, E. J., Patterson, L. B., Grout, M. E., Parichy, D. M., 2015. Long-distance communication by specialized cellular projections during pigment pattern development and evolution. Elife 4, e12401.

[66] Erban, R., Chapman, J., Maini, P., 2007. A practical guide to stochastic simulations of reaction-diffusion processes. arXiv preprint arXiv:0704.1908.

[67] Ermentrout, G. B., Edelstein-Keshet, L., 1993. Cellular automata approaches to biological modeling. Journal of theoretical Biology 160 (1), 97–133.

[68] Ester, M., Kriegel, H. P., Sander, J., Xu, X., 1996. Proceedings of the second international conference on knowledge discovery and data mining (kdd-96).

[69] Etournay, R., Popović, M., Merkel, M., Nandi, A., Blasse, C., Aigouy, B., Brandl, H., Myers, G., Salbreux, G., Jülicher, F., et al., 2015. Interplay of cell dynamics and epithelial tension during morphogenesis of the drosophila pupal wing. Elife 4, e07090.

[70] Farhadifar, R., Röper, J.-C., Aigouy, B., Eaton, S., Jülicher, F., 2007. The influence of cell mechanics, cell-cell interactions, and proliferation on epithelial packing. Current Biology 17 (24), 2095–2104.

[71] Fehon, R. G., Kooh, P. J., Rebay, I., Regan, C. L., Xu, T., Muskavitch, M. A., Artavanis-Tsakonas, S., 1990. Molecular interactions between the protein products of the neurogenic loci notch and delta, two egf-homologous genes in drosophila. Cell 61 (3), 523–534.

[72] Ferreira, A. C., Suriano, G., Mendes, N., Gomes, B., Wen, X., Carneiro, F., Seruca, R., Machado, J. C., 2012. E-cadherin impairment increases cell survival through notch-dependent upregulation of bcl-2. Human molecular genetics 21 (2), 334–343.

[73] Fletcher, A. G., Osborne, J. M., Maini, P. K., Gavaghan, D. J., 2013. Implementing vertex dynamics models of cell populations in biology within a consistent computational framework. Progress in biophysics and molecular biology 113 (2), 299–326.

[74] Fletcher, A. G., Osterfield, M., Baker, R. E., Shvartsman, S. Y., 2014. Vertex models of epithelial morphogenesis. Biophysical journal 106 (11), 2291–2304.

[75] Fletcher, D. A., Mullins, R. D., 2010. Cell mechanics and the cytoskeleton. Nature 463 (7280), 485–492.

[76] Forgacs, G., Newman, S. A., 2005. Biological physics of the developing embryo. Cambridge University Press.

[77] Foty, R. A., Steinberg, M. S., 2004. Cadherin-mediated cell-cell adhesion and tissue segregation in relation to malignancy. International Journal of Developmental Biology 48 (5-6), 397–409.

[78] Foty, R. A., Steinberg, M. S., 2005. The differential adhesion hypothesis: a direct evaluation. Developmental biology 278 (1), 255–263.

[79] Freed, D., Stevens, E. L., Pevsner, J., 2014. Somatic mosaicism in the human genome. Genes 5 (4), 1064–1094.

[80] Friedl, P., Gilmour, D., 2009. Collective cell migration in morphogenesis, regeneration and cancer. Nature reviews Molecular cell biology 10 (7), 445–457.

[81] Galbraith, M., Bocci, F., Onuchic, J. N., 2022. Stochastic fluctuations promote ordered pattern formation of cells in the notch-delta signaling pathway. arXiv preprint arXiv:2202.00763.

[82] Garber, K., 2007. Notch emerges as new cancer drug target.

[83] Garraway, L. A., Sellers, W. R., 2006. Lineage dependency and lineage-survival oncogenes in human cancer. Nature Reviews Cancer 6 (8), 593–602.

[84] George, J., Lim, J. S., Jang, S. J., Cun, Y., Ozretić, L., Kong, G., Leenders, F., Lu, X., Fernández-Cuesta, L., Bosco, G., et al., 2015. Comprehensive genomic profiles of small cell lung cancer. Nature 524 (7563), 47–53.

[85] Ghabrial, A. S., Krasnow, M. A., 2006. Social interactions among epithelial cells during tracheal branching morphogenesis. Nature 441 (7094), 746–749.

[86] Ghysen, A., Dambly-Chaudiere, C., 2004. Development of the zebrafish lateral line. Current opinion in neurobiology 14 (1), 67–73.

[87] Ginzberg, M. B., Kafri, R., Kirschner, M., 2015. On being the right (cell) size. Science 348 (6236).

[88] Glazier, J. A., Graner, F., 1993. Simulation of the differential adhesion driven rearrangement of biological cells. Physical Review E 47 (3), 2128.

[89] Gordon, W. R., Zimmerman, B., He, L., Miles, L. J., Huang, J., Tiyanont, K., McArthur, D. G., Aster, J. C., Perrimon, N., Loparo, J. J., et al., 2015. Mechanical allostery: evidence for a force requirement in the proteolytic activation of notch. Developmental cell 33 (6), 729–736.

[90] Goriely, A., Dumont, N., Dambly-Chaudiere, C., Ghysen, A., 1991. The determination of sense organs in drosophila: effect of the neurogenic mutations in the embryo. Development 113 (4), 1395–1404.

[91] Graner, F., Glazier, J. A., 1992. Simulation of biological cell sorting using a two-dimensional extended potts model. Physical review letters 69 (13), 2013.

[92] Green, J. B., Sharpe, J., 2015. Positional information and reaction-diffusion: two big ideas in developmental biology combine. Development 142 (7), 1203–1211.

[93] Gregor, T., Wieschaus, E. F., McGregor, A. P., Bialek, W., Tank, D. W., 2007. Stability and nuclear dynamics of the bicoid morphogen gradient. Cell 130 (1), 141–152.

[94] Gross, P., Kumar, K. V., Grill, S. W., 2017. How active mechanics and regulatory biochemistry combine to form patterns in development. Annual Review of Biophysics 46, 337–356.

[95] Gross, P., Kumar, K. V., Grill, S. W., 2017. How active mechanics and regulatory biochemistry combine to form patterns in development. Annual review of biophysics 46, 337–356.

[96] Guisoni, N., Martinez-Corral, R., Garcia-Ojalvo, J., de Navascués, J., 2017. Diversity of fate outcomes in cell pairs under lateral inhibition. Development 144 (7), 1177–1186.

[97] Gumbiner, B. M., 2005. Regulation of cadherin-mediated adhesion in morphogenesis. Nature reviews Molecular cell biology 6 (8), 622–634.

[98] Gupta, R. C., 2015. Handbook of toxicology of chemical warfare agents. Academic Press.

[99] Hadjivasiliou, Z., Hunter, G. L., Baum, B., 2016. A new mechanism for spatial pattern formation via lateral and protrusion-mediated lateral signalling. Journal of the Royal Society Interface 13 (124), 20160484.

[100] Hakim, V., Silberzan, P., 2017. Collective cell migration: a physics perspective. Reports on Progress in Physics 80 (7), 076601.

[101] Hamada, H., Watanabe, M., Lau, H. E., Nishida, T., Hasegawa, T., Parichy, D. M., Kondo, S., 2014. Involvement of delta/notch signaling in zebrafish adult pigment stripe patterning. Development 141 (2), 318–324.

[102] Hannezo, E., Heisenberg, C.-P., 2019. Mechanochemical feedback loops in development and disease. Cell 178 (1), 12–25.

[103] Hansson, E. M., Lendahl, U., Chapman, G., 2004. Notch signaling in development and disease. In: Seminars in cancer biology. Vol. 14. Elsevier, pp. 320–328.

[104] Hatakeyama, J., Wakamatsu, Y., Nagafuchi, A., Kageyama, R., Shigemoto, R., Shimamura, K., 2014. Cadherin-based adhesions in the apical endfoot are required for active notch signaling to control neurogenesis in vertebrates. Development 141 (8), 1671–1682.

[105] Hecht, I., Rappel, W.-J., Levine, H., 2009. Determining the scale of the bicoid morphogen gradient. Proceedings of the National Academy of Sciences 106 (6), 1710–1715.

[106] Heitzler, P., Simpson, P., 1991. The choice of cell fate in the epidermis of drosophila. Cell 64 (6), 1083–1092.

[107] Henrique, D., Adam, J., Myat, A., Chitnis, A., Lewis, J., Ish-Horowicz, D., 1995. Expression of a delta homologue in prospective neurons in the chick. Nature 375 (6534), 787–790.

[108] Henrique, D., Schweisguth, F., 2019. Mechanisms of notch signaling: a simple logic deployed in time and space. Development 146 (3).

[109] Hodkinson, P. S., Elliott, P. A., Lad, Y., McHugh, B. J., MacKinnon, A. C., Haslett, C., Sethi, T., 2007. Mammalian notch-1 activates β1 integrins via the small gtpase r-ras. Journal of Biological Chemistry 282 (39), 28991–29001.

[110] Hoffman, B. D., Crocker, J. C., 2009. Cell mechanics: dissecting the physical responses of cells to force. Annual review of biomedical engineering 11, 259–288.

[111] Hogan, B. L., 1999. Morphogenesis. Cell 96 (2), 225–233.

[112] Hogeweg, P., 2000. Evolving mechanisms of morphogenesis: on the interplay between differential adhesion and cell differentiation. Journal of theoretical biology 203 (4), 317–333.

[113] Holley, S. A., Geisler, R., Nüsslein-Volhard, C., 2000. Control of her1 expression during zebrafish somitogenesis by a delta-dependent oscillator and an independent wave-front activity. Genes & Development 14 (13), 1678–1690.

[114] Honda, H., Eguchi, G., 1980. How much does the cell boundary contract in a monolayered cell sheet? Journal of theoretical biology 84 (3), 575–588.

[115] Honda, H., Nagai, T., Tanemura, M., 2008. Two different mechanisms of planar cell intercalation leading to tissue elongation. Developmental dynamics: an official publication of the American Association of Anatomists 237 (7), 1826–1836.

[116] Hori, K., Sen, A., Artavanis-Tsakonas, S., 2013. Notch signaling at a glance. Journal of cell science 126 (10), 2135–2140.

[117] Howard, J., Grill, S. W., Bois, J. S., 2011. Turing's next steps: the mechanochemical basis of morphogenesis. Nature Reviews Molecular Cell Biology 12 (6), 392–398.

[118] Howard, J., et al., 2001. Mechanics of motor proteins and the cytoskeleton.

[119] Huang, X., Zhang, L., Yang, S., Zhang, Y., Wu, M., Chen, P., 2020. Hes5. 9 coordinate fgf and notch signaling to modulate gastrulation via regulating cell fate specification and cell migration in xenopus tropicalis. Genes 11 (11), 1363.

[120] Hunter, G. L., Hadjivasiliou, Z., Bonin, H., He, L., Perrimon, N., Charras, G., Baum, B., 2016. Coordinated control of notch/delta signalling and cell cycle progression drives lateral inhibition-mediated tissue patterning. Development 143 (13), 2305–2310.

[121] Inaba, M., Yamanaka, H., Kondo, S., 2012. Pigment pattern formation by contact-dependent depolarization. Science 335 (6069), 677–677.

[122] Jolly, M. K., Boareto, M., Lu, M., Jose'N, O., Clementi, C., Ben-Jacob, E., 2015. Operating principles of notch–delta–jagged module of cell–cell communication. New Journal of Physics 17 (5), 055021.

[123] Kageyama, R., Niwa, Y., Shimojo, H., Kobayashi, T., Ohtsuka, T., 2010. Ultradian oscillations in notch signaling regulate dynamic biological events. Current topics in developmental biology 92, 311–331.

[124] Katsunuma, S., Honda, H., Shinoda, T., Ishimoto, Y., Miyata, T., Kiyonari, H., Abe, T., Nibu, K.-i., Takai, Y., Togashi, H., 2016. Synergistic action of nectins and cadherins generates the mosaic cellular pattern of the olfactory epithelium. Journal of Cell Biology 212 (5), 561–575.

[125] Kelley, M. W., 2006. Regulation of cell fate in the sensory epithelia of the inner ear. Nature Reviews Neuroscience 7 (11), 837–849.

[126] Kimmel, C. B., Ballard, W. W., Kimmel, S. R., Ullmann, B., Schilling, T. F., 1995. Stages of embryonic development of the zebrafish. Developmental dynamics 203 (3), 253–310.

[127] King, T. C., King, T. C., 2007. 3—tissue homeostasis, damage, and repair. Elsevier's integrated pathology. Philadelphia: Mosby, 59–88.

[128] Kondo, S., 2009. How animals get their skin patterns: fish pigment pattern as a live turing wave. Systems Biology, 37–46.

[129] Kopan, R., Ilagan, M. X. G., 2009. The canonical notch signaling pathway: unfolding the activation mechanism. Cell 137 (2), 216–233.

[130] Kouzak, S. S., Mendes, M. S. T., Costa, I. M. C., 2013. Cutaneous mosaicisms: concepts, patterns and classifications. Anais Brasileiros de Dermatologia 88 (4), 507–517.

[131] Kressmann, S., Campos, C., Castanon, I., Fürthauer, M., González-Gaitán, M., 2015. Directional notch trafficking in sara endosomes during asymmetric cell division in the spinal cord. Nature Cell Biology 17 (3), 333–339.

[132] Lai, E. C., 2004. Notch signaling: control of cell communication and cell fate.

[133] Lawton, A. K., Nandi, A., Stulberg, M. J., Dray, N., Sneddon, M. W., Pontius, W., Emonet, T., Holley, S. A., 2013. Regulated tissue fluidity steers zebrafish body elongation. Development 140 (3), 573–582.

[134] Lebreton, G., Casanova, J., 2014. Specification of leading and trailing cell features during collective migration in the drosophila trachea. Journal of Cell Science 127 (2), 465–474.

[135] Lecuit, T., Lenne, P.-F., 2007. Cell surface mechanics and the control of cell shape, tissue patterns and morphogenesis. Nature reviews Molecular cell biology 8 (8), 633–644.

[136] Lecuit, T., Mahadevan, L., 2017. Morphogenesis one century after on growth and form.

[137] Leduc, C., Etienne-Manneville, S., 2017. Regulation of microtubule-associated motors drives intermediate filament network polarization. Journal of Cell Biology 216 (6), 1689–1703.

[138] Lehmann, R., Jiménez, F., Dietrich, U., Campos-Ortega, J. A., 1983. On the phenotype and development of mutants of early neurogenesis indrosophila melanogaster. Wilhelm Roux's Archives of Developmental Biology 192 (2), 62–74.

[139] Leong, K. G., Niessen, K., Kulic, I., Raouf, A., Eaves, C., Pollet, I., Karsan, A., 2007. Jagged1-mediated notch activation induces epithelial-to-mesenchymal transition through slug-induced repression of e-cadherin. The Journal of experimental medicine 204 (12), 2935–2948.

[140] Li, F., Lan, Y., Wang, Y., Wang, J., Yang, G., Meng, F., Han, H., Meng, A., Wang, Y., Yang, X., 2011. Endothelial smad4 maintains cerebrovascular integrity by activating n-cadherin through cooperation with notch. Developmental cell 20 (3), 291–302.

[141] Li, J., Yue, Y., Dong, X., Jia, W., Li, K., Liang, D., Dong, Z., Wang, X., Nan, X., Zhang, Q., et al., 2015. Zebrafish foxc1a plays a crucial role in early somitogenesis by restricting the expression of aldh1a2 directly. Journal of Biological Chemistry 290 (16), 10216–10228.

[142] Liu, C., Peng, G., Jing, N., 2018. Tgf-β signaling pathway in early mouse development and embryonic stem cells. Acta biochimica et biophysica Sinica 50 (1), 68–73.

[143] Lobry, C., Oh, P., Mansour, M. R., Look, A. T., Aifantis, I., 2014. Notch signaling: switching an oncogene to a tumor suppressor. Blood, The Journal of the American Society of Hematology 123 (16), 2451–2459.

[144] Logan, C. Y., Nusse, R., 2004. The wnt signaling pathway in development and disease. Annu. Rev. Cell Dev. Biol. 20, 781–810.

[145] Lowell, S., Watt, F. M., 2001. Delta regulates keratinocyte spreading and motility independently of differentiation. Mechanisms of Development 107 (1-2), 133–140.

[146] Lowell, S., Watt, F. M., 2001. Delta regulates keratinocyte spreading and motility independently of differentiation. Mechanisms of development 107 (1-2), 133–140.

[147] Luiken, S., Fraas, A., Bieg, M., Sugiyanto, R., Goeppert, B., Singer, S., Ploeger, C., Warsow, G., Marquardt, J. U., Sticht, C., et al., 2020. Notch target gene hes5 mediates oncogenic and tumor suppressive functions in hepatocarcinogenesis. Oncogene 39 (15), 3128–3144.

[148] Lupski, J. R., 2013. Genome mosaicism—one human, multiple genomes. Science 341 (6144), 358–359.

[149] Maître, J.-L., Heisenberg, C.-P., 2013. Three functions of cadherins in cell adhesion. Current Biology 23 (14), R626–R633.

[150] Majidinia, M., Alizadeh, E., Yousefi, B., Akbarzadeh, M., Zarghami, N., 2016. Downregulation of notch signaling pathway as an effective chemosensitizer for cancer treatment. Drug research 66 (11), 571–579.

[151] Mammoto, T., Ingber, D. E., 2010. Mechanical control of tissue and organ development. Development 137 (9), 1407–1420.

[152] Mao, X., Xu, N., Lubensky, T., 2010. Soft modes and elasticity of nearly isostatic lattices: Randomness and dissipation. Physical review letters 104 (8), 085504.

[153] Mara, A., Schroeder, J., Chalouni, C., Holley, S. A., 2007. Priming, initiation and synchronization of the segmentation clock by deltad and deltac. Nature cell biology 9 (5), 523–530.

[154] Marchetti, M. C., Joanny, J.-F., Ramaswamy, S., Liverpool, T. B., Prost, J., Rao, M., Simha, R. A., 2013. Hydrodynamics of soft active matter. Reviews of Modern Physics 85 (3), 1143.

[155] Marchetti, M. C., Joanny, J. F., Ramaswamy, S., Liverpool, T. B., Prost, J., Rao, M., Simha, R. A., 2013. Hydrodynamics of soft active matter. Reviews of Modern Physics 85, 1143–1189.

[156] Marcon, L., Sharpe, J., 2012. Turing patterns in development: what about the horse part? Current opinion in genetics & development 22 (6), 578–584.

[157] Martin, P., 1997. Wound healing–aiming for perfect skin regeneration. Science 276 (5309), 75–81.

[158] Martin-Belmonte, F., Bernascone, I., Galvez-Santisteban, M., 2016. Cell polarity. In: Bradshaw, R. A., Stahl, P. D. (Eds.), Encyclopedia of Cell Biology. Academic Press, Waltham, pp. 741–750.

[159] Martín-Gómez, A., Levis, D., Díaz-Guilera, A., Pagonabarraga, I., 2018. Collective motion of active brownian particles with polar alignment. Soft Matter 14 (14), 2610–2618.

[160] Martín-Gómez, A., Levis, D., Díaz-Guilera, A., Pagonabarraga, I., 2018. Collective motion of active brownian particles with polar alignment. Soft Matter 14 (14), 2610–2618.

[161] Martins, G. G., Rifes, P., Amândio, R., Rodrigues, G., Palmeirim, I., Thorsteinsdóttir, S., 2009. Dynamic 3d cell rearrangements guided by a fibronectin matrix underlie somitogenesis. PLoS One 4 (10), e7429.

[162] Mayer, M., Depken, M., Bois, J. S., Jülicher, F., Grill, S. W., 2010. Anisotropies in cortical tension reveal the physical basis of polarizing cortical flows. Nature 467 (7315), 617–621.

[163] Mazur, P. K., Grüner, B. M., Nakhai, H., Sipos, B., Zimber-Strobl, U., Strobl, L. J., Radtke, F., Schmid, R. M., Siveke, J. T., 2010. Identification of epidermal pdx1 expression discloses different roles of notch1 and notch2 in murine kras g12d-induced skin carcinogenesis in vivo. PloS one 5 (10), e13578.

[164] McCaffrey, L. M., Macara, I. G., 2012. Signaling pathways in cell polarity. Cold Spring Harbor perspectives in biology 4 (6), a009654.

[165] McClure, M. J., Ramey, A. N., Rashid, M., Boyan, B. D., Schwartz, Z., 2019. Integrin-α7 signaling regulates connexin 43, m-cadherin, and myoblast fusion. American Journal of Physiology-Cell Physiology 316 (6), C876–C887.

[166] McDaniell, R., Warthen, D. M., Sanchez-Lara, P. A., Pai, A., Krantz, I. D., Piccoli, D. A., Spinner, N. B., 2006. Notch2 mutations cause alagille syndrome, a heterogeneous disorder of the notch signaling pathway. The American Journal of Human Genetics 79 (1), 169–173.

[167] Meinhardt, H., 2003. Models of biological pattern formation: common mechanism in plant and animal development. International Journal of Developmental Biology 40 (1), 123–134.

[168] Meinhardt, H., 2008. Models of biological pattern formation: from elementary steps to the organization of embryonic axes. Current topics in developmental biology 81, 1–63.

[169] Meloty-Kapella, L., Shergill, B., Kuon, J., Botvinick, E., Weinmaster, G., 2012. Notch ligand endocytosis generates mechanical pulling force dependent on dynamin, epsins, and actin. Developmental Cell 22 (6), 1299–1312.

[170] Merkel, M., Sagner, A., Gruber, F. S., Etournay, R., Blasse, C., Myers, E., Eaton, S., Jülicher, F., 2014. The balance of prickle/spiny-legs isoforms controls the amount of coupling between core and fat pcp systems. Current Biology 24 (18), 2111–2123.

[171] Meyen, D., Tarbashevich, K., Banisch, T. U., Wittwer, C., Reichman-Fried, M., Maugis, B., Grimaldi, C., Messerschmidt, E.-M., Raz, E., 2015. Dynamic filopodia are required for chemokine-dependent intracellular polarization during guided cell migration in vivo. Elife 4, e05279.

[172] Mirams, G. R., Arthurs, C. J., Bernabeu, M. O., Bordas, R., Cooper, J., Corrias, A., Davit, Y., Dunn, S.-J., Fletcher, A. G., Harvey, D. G., et al., 2013. Chaste: an open source c++ library for computational physiology and biology. PLoS Comput Biol 9 (3), e1002970.

[173] Miyamoto, Y., Maitra, A., Ghosh, B., Zechner, U., Argani, P., Iacobuzio-Donahue, C. A., Sriuranpong, V., Iso, T., Meszoely, I. M., Wolfe, M. S., et al., 2003. Notch mediates tgfα-induced changes in epithelial differentiation during pancreatic tumorigenesis. Cancer cell 3 (6), 565–576.

[174] Montagne, C., Gonzalez-Gaitan, M., 2014. Sara endosomes and the asymmetric division of intestinal stem cells. Development 141 (10), 2014–2023.

[175] Montell, D. J., 2003. Border-cell migration: the race is on. Nature reviews Molecular cell biology 4 (1), 13–24.

[176] Murata, A., Hayashi, S.-I., 2016. Notch-mediated cell adhesion. Biology 5 (1), 5.

[177] Murisic, N., Hakim, V., Kevrekidis, I. G., Shvartsman, S. Y., Audoly, B., 2015. From discrete to continuum models of three-dimensional deformations in epithelial sheets. Biophysical journal 109 (1), 154–163.

[178] Murray, J. D., Maini, P. K., Tranquillo, R. T., 1988. Mechanochemical models for generating biological pattern and form in development. Physics Reports 171 (2), 59–84.

[179] Muskavitch, M. A., 1994. Delta-notch signaling and drosophila cell fate choice. Developmental biology 166 (2), 415–430.

[180] Nagai, T., Honda, H., 2001. A dynamic cell model for the formation of epithelial tissues. Philosophical Magazine B 81 (7), 699–719.

[181] Nagai, T., Honda, H., 2006. Wound healing mechanism in epithelial tissues cell adhesion to basal lamina. WSEAS Transactions on Biology and Biomedicine 3 (6), 389.

[182] Nelson, B. R., Hodge, R. D., Bedogni, F., Hevner, R. F., 2013. Dynamic interactions between intermediate neurogenic progenitors and radial glia in embryonic mouse neocortex: potential role in dll1-notch signaling. Journal of Neuroscience 33 (21), 9122–9139.

[183] Nelson, W. J., 2008. Regulation of cell–cell adhesion by the cadherin–catenin complex. Biochemical Society Transactions 36 (2), 149–155.

[184] Nicolas, M., Wolfer, A., Raj, K., Kummer, J. A., Mill, P., van Noort, M., Hui, C.-c., Clevers, H., Dotto, G. P., Radtke, F., 2003. Notch1 functions as a tumor suppressor in mouse skin. Nature genetics 33 (3), 416–421.

[185] Nourhani, A., Lammert, P. E., Borhan, A., Crespi, V. H., 2014. Kinematic matrix theory and universalities in self-propellers and active swimmers. Physical Review E 89 (6), 062304.

[186] Ntziachristos, P., Lim, J. S., Sage, J., Aifantis, I., 2014. From fly wings to targeted cancer therapies: a centennial for notch signaling. Cancer cell 25 (3), 318–334.

[187] Oates, A. C., Morelli, L. G., Ares, S., 2012. Patterning embryos with oscillations: structure, function and dynamics of the vertebrate segmentation clock. Development 139 (4), 625–639.

[188] Odell, G. M., Oster, G., Alberch, P., Burnside, B., 1981. The mechanical basis of morphogenesis: I. epithelial folding and invagination. Developmental biology 85 (2), 446–462.

[189] O'Keefe, D. D., Prober, D. A., Moyle, P. S., Rickoll, W. L., Edgar, B. A., 2007. Egfr/ras signaling regulates de-cadherin/shotgun localization to control vein morphogenesis in the drosophila wing. Developmental biology 311 (1), 25–39.

[190] Owen, M. R., Sherratt, J. A., Wearing, H. J., 2000. Lateral induction by juxtacrine signaling is a new mechanism for pattern formation. Developmental biology 217 (1), 54–61.

[191] O'Dea, R. D., King, J. R., 2011. Multiscale analysis of pattern formation via intercellular signalling. Mathematical Biosciences 231 (2), 172–185.

[192] Pasakarnis, L., Dreher, D., Brunner, D., 2016. Snapshot: mechanical forces in development i. Cell 165 (3), 754–754.

[193] Peck, D., Isacke, C. M., 1998. Hyaluronan-dependent cell migration can be blocked by a cd44 cytoplasmic domain peptide containing a phosphoserine at position 325. Journal of Cell Science 111 (11), 1595–1601.

[194] Pettigrew, C. A., Asp, E., Emerson Jr, C. P., 2014. A new role for hedgehogs in juxtacrine signaling. Mechanisms of Development 131, 137–149.

[195] Podgorski, G. J., Bansal, M., Flann, N. S., 2007. Regular mosaic pattern development: a study of the interplay between lateral inhibition, apoptosis and differential adhesion. Theoretical Biology and Medical Modelling 4 (1), 1–19.

[196] Popović, M., Nandi, A., Merkel, M., Etournay, R., Eaton, S., Jülicher, F., Salbreux, G., 2017. Active dynamics of tissue shear flow. New Journal of Physics 19 (3), 033006.

[197] Pourquié, O., 2011. Vertebrate segmentation: from cyclic gene networks to scoliosis. Cell 145 (5), 650–663.

[198] Price, S. R., Garcia, N. V. D. M., Ranscht, B., Jessell, T. M., 2002. Regulation of motor neuron pool sorting by differential expression of type ii cadherins. Cell 109 (2), 205–216.

[199] Puliafito, A., Primo, L., Celani, A., 2017. Cell-size distribution in epithelial tissue formation and homeostasis. Journal of The Royal Society Interface 14 (128), 20170032.

[200] Radice, G. L., Rayburn, H., Matsunami, H., Knudsen, K. A., Takeichi, M., Hynes, R. O., 1997. Developmental defects in mouse embryos lacking n-cadherin. Developmental biology 181 (1), 64–78.

[201] Radtke, F., Raj, K., 2003. The role of notch in tumorigenesis: oncogene or tumour suppressor? Nature Reviews Cancer 3 (10), 756–767.

[202] Ramanathan, S. P., Krajnc, M., Gibson, M. C., 2019. Cell-size pleomorphism drives aberrant clone dispersal in proliferating epithelia. Developmental cell 51 (1), 49–61.

[203] Raymond, P. A., Colvin, S. M., Jabeen, Z., Nagashima, M., Barthel, L. K., Hadidjojo, J., Popova, L., Pejaver, V. R., Lubensky, D. K., 2014. Patterning the cone mosaic array in zebrafish retina requires specification of ultraviolet-sensitive cones. PLoS One 9 (1), e85325.

[204] Reymann, A.-C., Staniscia, F., Erzberger, A., Salbreux, G., Grill, S. W., 2016. Cortical flow aligns actin filaments to form a furrow. eLife 5, e17807.

[205] Rho, S.-S., Kobayashi, I., Oguri-Nakamura, E., Ando, K., Fujiwara, M., Kamimura, N., Hirata, H., Iida, A., Iwai, Y., Mochizuki, N., et al., 2019. Rap1b promotes notch-signal-mediated hematopoietic stem cell development by enhancing integrin-mediated cell adhesion. Developmental cell 49 (5), 681–696.

[206] Riahi, R., Sun, J., Wang, S., Long, M., Zhang, D. D., Wong, P. K., 2015. Notch1–dll4 signalling and mechanical force regulate leader cell formation during collective cell migration. Nature Communications 6 (1), 1–11.

[207] Rogers, A. W., 1983. Cells and Tissues. Academic Press London, New York.

[208] Romanczuk, P., Bär, M., Ebeling, W., Lindner, B., Schimansky-Geier, L., 2012. Active brownian particles. The European Physical Journal Special Topics 202 (1), 1–162.

[209] Ross, D. A., Kadesch, T., 2004. Consequences of notch-mediated induction of jagged1. Experimental cell research 296 (2), 173–182.

[210] Roy, S., Hsiung, F., Kornberg, T. B., 2011. Specificity of Drosophila cytonemes for distinct signaling pathways. Science 332 (6027), 354–358.

[211] Rulands, S., Lescroart, F., Chabab, S., Hindley, C. J., Prior, N., Sznurkowska, M. K., Huch, M., Philpott, A., Blanpain, C., Simons, B. D., 2018. Universality of clone dynamics during tissue development. Nature physics 14 (5), 469–474.

[212] Sanders, T. A., Llagostera, E., Barna, M., 2013. Specialized filopodia direct long-range transport of shh during vertebrate tissue patterning. Nature 497 (7451), 628–632.

[213] Schaller, G., Meyer-Hermann, M., 2005. Multicellular tumor spheroid in an off-lattice voronoi-delaunay cell model. Physical Review E 71 (5), 051910.

[214] Scheppke, L., Murphy, E. A., Zarpellon, A., Hofmann, J. J., Merkulova, A., Shields, D. J., Weis, S. M., Byzova, T. V., Ruggeri, Z. M., Iruela-Arispe, M. L., et al., 2012. Notch promotes vascular maturation by inducing integrin-mediated smooth muscle cell adhesion to the endothelial basement membrane. Blood, The Journal of the American Society of Hematology 119 (9), 2149–2158.

[215] Schweisguth, F., 2015. Asymmetric cell division in the drosophila bristle lineage: from the polarization of sensory organ precursor cells to notch-mediated binary fate decision. Wiley Interdisciplinary Reviews: Developmental Biology 4 (3), 299–309.

[216] Schweisguth, F., Corson, F., 2019. Self-organization in pattern formation. Developmental Cell 49 (5), 659–677.

[217] Shah, G., Thierbach, K., Schmid, B., Waschke, J., Reade, A., Hlawitschka, M., Roeder, I., Scherf, N., Huisken, J., 2019. Multi-scale imaging and analysis identify pan-embryo cell dynamics of germlayer formation in zebrafish. Nature Communications 10 (1), 1–12.

[218] Shapiro, L., Fannon, A. M., Kwong, P. D., Thompson, A., Lehmann, M. S., Grübel, G., Legrand, J.-F., Als-Nielsen, J., Colman, D. R., Hendrickson, W. A., 1995. Structural basis of cell-cell adhesion by cadherins. Nature 374 (6520), 327–337.

[219] Shaya, O., Binshtok, U., Hersch, M., Rivkin, D., Weinreb, S., Amir-Zilberstein, L., Khamaisi, B., Oppenheim, O., Desai, R. A., Goodyear, R. J., et al., 2017. Cell-cell contact area affects notch signaling and notch-dependent patterning. Developmental cell 40 (5), 505–511.

[220] Shaya, O., Binshtok, U., Hersch, M., Rivkin, D., Weinreb, S., Amir-Zilberstein, L., Khamaisi, B., Oppenheim, O., Desai, R. A., Goodyear, R. J., et al., 2017. Cell-cell contact area affects notch signaling and notch-dependent patterning. Developmental cell 40 (5), 505–511.

[221] Siebel, C., Lendahl, U., 2017. Notch signaling in development, tissue homeostasis, and disease. Physiological reviews 97 (4), 1235–1294.

[222] Simpson, P., 1990. Lateral inhibition and the development of the sensory bristles of the adult peripheral nervous system of drosophila. Development 109 (3), 509–519.

[223] Singh, A. B., Harris, R. C., 2005. Autocrine, paracrine and juxtacrine signaling by egfr ligands. Cellular signalling 17 (10), 1183–1193.

[224] Sjöqvist, M., Andersson, E. R., 2019. Do as i say, not (ch) as i do: Lateral control of cell fate. Developmental biology 447 (1), 58–70.

[225] Small, J. V., Rottner, K., Kaverina, I., Anderson, K., 1998. Assembling an actin cytoskeleton for cell attachment and movement. Biochimica Et Biophysica Acta (BBA)-Molecular Cell Research 1404 (3), 271–281.

[226] Sprinzak, D., Lakhanpal, A., LeBon, L., Garcia-Ojalvo, J., Elowitz, M. B., 2011. Mutual inactivation of notch receptors and ligands facilitates developmental patterning. PLoS Comput Biol 7 (6), e1002069.

[227] Sprinzak, D., Lakhanpal, A., Lebon, L., Santat, L. A., Fontes, M. E., Anderson, G. A., Garcia-Ojalvo, J., Elowitz, M. B., 2010. Cis-interactions between Notch and Delta generate mutually exclusive signalling states. Nature 465 (7294), 86–90.

[228] St Johnston, D., Sanson, B., 2011. Epithelial polarity and morphogenesis. Current opinion in cell biology 23 (5), 540–546.

[229] Staple, D. B., Farhadifar, R., Röper, J.-C., Aigouy, B., Eaton, S., Jülicher, F., 2010. Mechanics and remodelling of cell packings in epithelia. The European Physical Journal E 33 (2), 117–127.

[230] Steinberg, M. S., 1970. Does differential adhesion govern self-assembly processes in histogenesis? equilibrium configurations and the emergence of a hierarchy among populations of embryonic cells. Journal of Experimental Zoology 173 (4), 395–433.

[231] Steinberg, M. S., 1978. Cell-cell recognition in multicellular assembly: levels of specificity. In: Symposia of the Society for Experimental Biology. Vol. 32. pp. 25–49.

[232] Steinke, A., Meier-Stiegen, S., Drenckhahn, D., Asan, E., 2008. Molecular composition of tight and adherens junctions in the rat olfactory epithelium and fila. Histochemistry and cell biology 130 (2), 339.

[233] Suh, Y., 2002. Cell signaling in aging and apoptosis. Mechanisms of ageing and development 123 (8), 881–890.

[234] Sussman, D. M., 2017. cellgpu: Massively parallel simulations of dynamic vertex models. Computer Physics Communications 219, 400–406.

[235] Szabó, A., Ünnep, R., Méhes, E., Twal, W., Argraves, W., Cao, Y., Czirók, A., 2010. Collective cell motion in endothelial monolayers. Physical biology 7 (4), 046007.

[236] Takeichi, M., 1988. The cadherins: cell-cell adhesion molecules controlling animal morphogenesis. Development 102 (4), 639–655.

[237] Taylor, W. R., Morley, R., Krasavin, A., Gregory, L., Wilkinson, D. G., Poliakov, A., 2012. A mechanical model of cell segregation driven by differential adhesion.

[238] Teddy, J. M., Kulesa, P. M., 2004. In vivo evidence for short-and long-range cell communication in cranial neural crest cells.

[239] Teimouri, H., Kolomeisky, A. B., 2016. Mechanisms of the formation of biological signaling profiles. Journal of Physics A: Mathematical and Theoretical 49 (48), 483001.

[240] Teng, X., Qin, L., Le Borgne, R., Toyama, Y., 2017. Remodeling of adhesion and modulation of mechanical tensile forces during apoptosis in drosophila epithelium. Development 144 (1), 95–105.

[241] Thompson, D. W., Thompson, D. W., 1942. On growth and form. Vol. 2. Cambridge university press Cambridge.

[242] Togashi, H., 2016. Differential and cooperative cell adhesion regulates cellular pattern in sensory epithelia. Frontiers in cell and developmental biology 4, 104.

[243] Togashi, H., Katsunuma, S., 2017. Cellular recognition and patterning in sensory systems. Experimental Cell Research 358 (1), 52–57.

[244] Togashi, H., Kominami, K., Waseda, M., Komura, H., Miyoshi, J., Takeichi, M., Takai, Y., 2011. Nectins establish a checkerboard-like cellular pattern in the auditory epithelium. Science 333 (6046), 1144–1147.

[245] Townes, P. L., Holtfreter, J., 1955. Directed movements and selective adhesion of embryonic amphibian cells. Journal of experimental zoology 128 (1), 53–120.

[246] Travis, W. D., Brambilla, E., Burke, A. P., Marx, A., Nicholson, A. G., 2015. Introduction to the 2015 world health organization classification of tumors of the lung, pleura, thymus, and heart. Journal of Thoracic Oncology 10 (9), 1240–1242.

[247] Trembley, A., 1744. X. translation of a letter from mr. abraham trembley, frs to the president, with observations upon several newly discover'd species of fresh-water polypi. Philosophical Transactions of the Royal Society of London 43 (474), 169–183.

[248] Turing, A. M., 1990. The chemical basis of morphogenesis. Bulletin of Mathematical Biology 52 (1-2), 153–197.

[249] Uriu, K., Ares, S., Oates, A. C., Morelli, L. G., 2012. Optimal cellular mobility for synchronization arising from the gradual recovery of intercellular interactions. Physical Biology 9 (3), 036006.

[250] Uriu, K., Morelli, L. G., 2014. Collective cell movement promotes synchronization of coupled genetic oscillators. Biophysical Journal 107 (2), 514–526.

[251] Uriu, K., Morishita, Y., Iwasa, Y., 2010. Random cell movement promotes synchronization of the segmentation clock. Proceedings of the National Academy of Sciences 107 (11), 4979–4984.

[252] Van Liedekerke, P., Buttenschön, A., Drasdo, D., 2018. Off-lattice agent-based models for cell and tumor growth: numerical methods, implementation, and applications. In: Numerical methods and advanced simulation in biomechanics and biological processes. Elsevier, pp. 245–267.

[253] Van Roy, F., Berx, G., 2008. The cell-cell adhesion molecule e-cadherin. Cellular and molecular life sciences 65 (23), 3756–3788.

[254] Vanderleest, T. E., Smits, C. M., Xie, Y., Jewett, C. E., Blankenship, J. T., Loerke, D., 2018. Vertex sliding drives intercalation by radial coupling of adhesion and actomyosin networks during drosophila germband extension. Elife 7, e34586.

[255] Vasilopoulos, G., Painter, K. J., 2016. Pattern formation in discrete cell tissues under long range filopodia-based direct cell to cell contact. Mathematical Biosciences 273, 1–15.

[256] Vasilyev, A., Liu, Y., Mudumana, S., Mangos, S., Lam, P.-Y., Majumdar, A., Zhao, J., Poon, K.-L., Kondrychyn, I., Korzh, V., et al., 2009. Collective cell migration drives morphogenesis of the kidney nephron. PLoS biology 7 (1), e1000009.

[257] Vedula, S. R. K., Ravasio, A., Lim, C. T., Ladoux, B., 2013. Collective cell migration: a mechanistic perspective. Physiology 28 (6), 370–379.

[258] Venkei, Z. G., Yamashita, Y. M., 2018. Emerging mechanisms of asymmetric stem cell division. Journal of Cell Biology 217 (11), 3785–3795.

[259] Vicsek, T., Czirók, A., Ben-Jacob, E., Cohen, I., Shochet, O., 1995. Novel type of phase transition in a system of self-driven particles. Physical review letters 75 (6), 1226.

[260] Vicsek, T., Zafeiris, A., 2012. Collective motion. Physics reports 517 (3-4), 71–140.

[261] Waclaw, B., Bozic, I., Pittman, M. E., Hruban, R. H., Vogelstein, B., Nowak, M. A., 2015. A spatial model predicts that dispersal and cell turnover limit intratumour heterogeneity. Nature 525 (7568), 261–264.

[262] Wang, W., Wang, L., Mizokami, A., Shi, J., Zou, C., Dai, J., Keller, E. T., Lu, Y., Zhang, J., 2017. Down-regulation of e-cadherin enhances prostate cancer chemoresistance via notch signaling. Chinese journal of cancer 36 (1), 1–13.

[263] Wang, Z., Li, Y., Ahmad, A., Azmi, A. S., Banerjee, S., Kong, D., Sarkar, F. H., 2010. Targeting notch signaling pathway to overcome drug resistance for cancer therapy. Biochimica et Biophysica Acta (BBA)-Reviews on Cancer 1806 (2), 258–267.

[264] Warga, R. M., Kimmel, C. B., 1990. Cell movements during epiboly and gastrulation in zebrafish. Development 108 (4), 569–580.

[265] Wartlick, O., Kicheva, A., González-Gaitán, M., 2009. Morphogen gradient formation. Cold Spring Harbor perspectives in biology 1 (3), a001255.

[266] Watt, F. M., Estrach, S., Ambler, C. A., 2008. Epidermal notch signalling: differentiation, cancer and adhesion. Current opinion in cell biology 20 (2), 171–179.

[267] Weijer, C. J., 2009. Collective cell migration in development. Journal of cell science 122 (18), 3215–3223.

[268] Weng, A. P., Ferrando, A. A., Lee, W., Morris, J. P., Silverman, L. B., Sanchez-Irizarry, C., Blacklow, S. C., Look, A. T., Aster, J. C., 2004. Activating mutations of notch1 in human t cell acute lymphoblastic leukemia. Science 306 (5694), 269–271.

[269] Wolpert, L., Beddington, R., Brockes, J., Jessell, T., Lawrence, P., et al., 1998. Principles of development oxford university press. New York.

[270] Wyczalkowski, M. A., Chen, Z., Filas, B. A., Varner, V. D., Taber, L. A., 2012. Computational models for mechanics of morphogenesis. Birth defects research part C: Embryo today: Reviews 96 (2), 132–152.

[271] Xia, P., Gütl, D., Zheden, V., Heisenberg, C.-P., 2019. Lateral inhibition in cell specification mediated by mechanical signals modulating taz activity. Cell 176 (6), 1379–1392.

[272] Yaron, T., Cordova, Y., Sprinzak, D., 2014. Juxtacrine signaling is inherently noisy. Biophysical journal 107 (10), 2417–2424.

[273] Zaidel-Bar, R., 2013. Cadherin adhesome at a glance. Journal of cell science 126 (2), 373–378.

[274] Zhang, S., Chung, W., Xu, K., 2016. Lunatic fringe is a potent tumor suppressor in kras-initiated pancreatic cancer. Oncogene 35 (19), 2485–2495.

[275] Zhang, Y., Thomas, G. L., Swat, M., Shirinifard, A., Glazier, J. A., 2011. Computer simulations of cell sorting due to differential adhesion. PloS one 6 (10), e24999.